



National Library  
of Canada

Bibliothèque nationale  
du Canada

Canadian Theses Service

Services des thèses canadiennes

Ottawa, Canada  
K1A 0N4

## CANADIAN THESES

## THÈSES CANADIENNES

### NOTICE

The quality of this microfiche is heavily dependent upon the quality of the original thesis submitted for microfilming. Every effort has been made to ensure the highest quality of reproduction possible.

If pages are missing, contact the university which granted the degree.

Some pages may have indistinct print especially if the original pages were typed with a poor typewriter ribbon or if the university sent us an inferior photocopy.

Previously copyrighted materials (journal articles, published tests, etc.) are not filmed.

Reproduction in full or in part of this film is governed by the Canadian Copyright Act, R.S.C. 1970, c. C-30.

**THIS DISSERTATION  
HAS BEEN MICROFILMED  
EXACTLY AS RECEIVED**

### AVIS

La qualité de cette microfiche dépend grandement de la qualité de la thèse soumise au microfilmage. Nous avons tout fait pour assurer une qualité supérieure de reproduction.

S'il manque des pages, veuillez communiquer avec l'université qui a conféré le grade.

La qualité d'impression de certaines pages peut laisser à désirer, surtout si les pages originales ont été dactylographiées à l'aide d'un ruban usé ou si l'université nous a fait parvenir une photocopie de qualité inférieure.

Les documents qui font déjà l'objet d'un droit d'auteur (articles de revue, examens publiés, etc.) ne sont pas microfilmés.

La reproduction, même partielle, de ce microfilm est soumise à la Loi canadienne sur le droit d'auteur, SRC 1970, c. C-30.

**LA THÈSE A ÉTÉ  
MICROFILMÉE TELLE QUE  
NOUS L'AVONS REÇUE**

THE UNIVERSITY OF ALBERTA

FLOW OF FINES AND SAND PRODUCTION IN  
UNCONSOLIDATED POROUS MEDIA

by

RAWYA J. SELBY

A THESIS

SUBMITTED TO THE FACULTY OF GRADUATE STUDIES AND RESEARCH  
IN PARTIAL FULFILMENT OF THE REQUIREMENTS FOR THE DEGREE OF  
MASTER OF SCIENCE

IN

PETROLEUM ENGINEERING

DEPARTMENT OF MINING, METALLURGICAL AND PETROLEUM ENGINEERING

EDMONTON, ALBERTA

SPRING, 1987

Permission has been granted to the National Library of Canada to microfilm this thesis and to lend or sell copies of the film.

The author (copyright owner) has reserved other publication rights, and neither the thesis nor extensive extracts from it may be printed or otherwise reproduced without his/her written permission.

L'autorisation a été accordée à la Bibliothèque nationale du Canada de microfilmer cette thèse et de prêter ou de vendre des exemplaires du film.

L'auteur (titulaire du droit d'auteur) se réserve les autres droits de publication; ni la thèse ni de longs extraits de celle-ci ne doivent être imprimés ou autrement reproduits sans son autorisation écrite.

ISBN 0-315-37798-4

THE UNIVERSITY OF ALBERTA

RELEASE FORM

NAME OF AUTHOR: RAWYA J. SELBY

TITLE OF THESIS: FLOW OF FINES AND SAND PRODUCTION  
IN UNCONSOLIDATED POROUS MEDIA

DEGREE: MASTER OF SCIENCE

YEAR THIS DEGREE GRANTED: SPRING, 1987

Permission is hereby granted to THE UNIVERSITY OF ALBERTA LIBRARY to reproduce single copies of this thesis and to lend or sell such copies for private, scholarly or scientific research purposes only.

The author reserves other publication rights, and neither the thesis nor extensive extracts from it may be printed or otherwise reproduced without the author's written permission.

(SIGNED) *R. Selby*.....

PERMANENT ADDRESS:

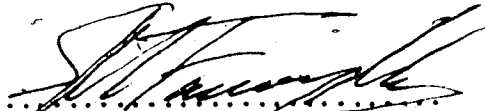
\*204 8509-106 A STREET  
EDMONTON, ALBERTA  
T6E 4J8 CANADA

DATED APRIL 13 1987

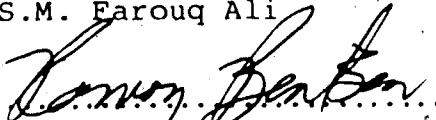
THE UNIVERSITY OF ALBERTA

FACULTY OF GRADUATE STUDIES AND RESEARCH

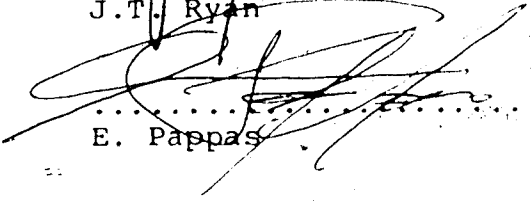
The undersigned certify that they have read, and recommend to the Faculty of Graduate Studies and Research, for acceptance, a thesis entitled FLOW OF FINES AND SAND PRODUCTION IN UNCONSOLIDATED POROUS MEDIA submitted by RAWYA J. SELBY in partial fulfilment of the requirements for the degree of MASTER OF SCIENCE in PETROLEUM ENGINEERING.

  
.....  
Supervisor

S.M. Farouq Ali

  
.....  
R.G. Bentsen

  
.....  
J.T. Ryan

  
.....  
E. Pappas

Date Nov. 12, 87.....

To Myron, Riad and Sami

## ABSTRACT

The flow of fines in porous media was studied by conducting linear flow experiments in two different size porous packs. In all the tests, the core holder was packed with unconsolidated sand through which distilled water was flowed. Effluent samples were collected and analyzed to determine their fines content.

The movement of fines in porous media was found to be dependent on the initial amount of fines present, the fluid flow rate, the size and shape of sand grains, and the size and density of fines. The amount of fines in the effluent was found to increase as the flow rate and the initial amount of fines in the porous medium were increased. The concentration of fines at the outlet was higher for large, spherical grain packs than for small, angular grain packs. Fines entrainment was negligible in the case of particles of high density.

In the second part of this study, sand production was investigated by carrying out radial flow experiments in a model simulating a wellbore and surroundings under various overburden loads. Distilled water was injected into the cell, which was packed with unconsolidated sand, and the volume of sand in the effluent was measured.

It was observed that increasing the fluid flow rate and the overburden pressure applied on the sand pack led to an increase in the volume of sand produced. In addition, a larger sand production

occurred for spherical, small-grained sandpacks than for angular, large-grained packs. More sand was produced from well tubings with large slots than from tubings with small perforations.

The effect of migration of fines on relative permeability was examined by conducting a two-phase flow experiment in a Berea sandstone core containing naturally occurring migrating clays. The experiment consisted of a sequence of four fluid displacement steps. In the first step, the two phases were Hamilton Lake crude and 2% (w) brine. In the second step, Hamilton Lake crude and 30% (w) brine were employed. The third and fourth steps were a repeat of the first and second steps, respectively.

The relative permeabilities to oil and brine were found to decrease in Steps 2 and 4, as the salt concentration in the brine was increased from 2% NaCl to 30% NaCl. The relative permeabilities increased in Step 3 to values lower than the initial values obtained in Step 1, as the concentration was changed from 30% NaCl to 2% NaCl. The absolute permeability of the core was noted to decrease from an initial value of  $0.661 \mu\text{m}^2$  to a value of  $0.247 \mu\text{m}^2$  at the end of the experiment.



## ACKNOWLEDGEMENTS

The author wishes to express her sincere gratitude to her supervisor, Dr. Farouq Ali, for his guidance and encouragement throughout this study.

The author also thanks Mrs. Sara Thomas for her assistance in the experimental work and the graph reproductions.

Appreciation is extended to Dr. Jim Ryan, Mr. Ernie Pappas, and Dr. Hans Vaziri for their comments and suggestions regarding the experimental results.

Thanks are due to Mr. Bob Smith for his help in setting up the experimental apparatus, and to Mrs. Vivian Spak and Mr. Kacheong Yeung for typing the manuscript.

The financial support for this research provided by the Natural Sciences and Engineering Research Council (NSERC) is gratefully acknowledged.

## TABLE OF CONTENTS

CHAPTER	PAGE
1. INTRODUCTION . . . . .	1
2. LITERATURE REVIEW . . . . .	3
2.1. GENERAL DESCRIPTION OF THE PROBLEM . . . . .	3
2.1.1. Flow of Fines . . . . .	3
2.1.2. Sand Production . . . . .	3
2.2. EXPERIMENTAL STUDIES OF FLOW OF FINES . . . . .	4
2.2.1. Clarification Experiments . . . . .	4
2.2.1.1. Physical Studies . . . . .	4
2.2.1.2. Chemical Studies . . . . .	5
2.2.2. Experiments in Porous Media . . . . .	6
2.2.2.1. Physical Studies . . . . .	6
2.2.2.2. Chemical Studies . . . . .	9
2.3. THEORETICAL DEVELOPMENT OF FLOW OF FINES . . . . .	10
2.3.1. Clarification Studies . . . . .	10
2.3.2. Investigations in Porous Media . . . . .	13
2.4. EXPERIMENTAL STUDIES OF SAND PRODUCTION . . . . .	18
2.5. THEORETICAL DEVELOPMENT OF SAND PRODUCTION . . . . .	21
2.6. FIELD EXPERIENCE . . . . .	24
2.6.1. Mechanical Sand Control Methods . . . . .	24
2.6.2. Chemical Sand Control Methods . . . . .	25
2.6.3. Other Sand Control Methods . . . . .	27

CHAPTER	PAGE
3. STATEMENT OF THE PROBLEM . . . . .	29
4. EXPERIMENTAL EQUIPMENT, MATERIALS AND PROCEDURE . . . . .	31
4.1. DESCRIPTION OF THE MODELS DESIGNED . . . . .	31
4.1.1. Linear Models . . . . .	31
4.1.2. Radial Model . . . . .	31
4.2. DESCRIPTION OF THE APPARATUS AND EXPERIMENTAL PROCEDURE . . . . .	32
4.2.1. Flow of Fines . . . . .	32
4.2.2. Sand Production . . . . .	35
4.2.3. Two-Phase Flow . . . . .	35
4.3. MATERIALS USED . . . . .	38
4.4. PREPARATION OF FINES . . . . .	39
4.5. PACKING THE MODELS WITH SAND OR GLASS BEADS . . . . .	40
4.5.1. Packing the Linear Model . . . . .	40
4.5.2. Packing the Radial Model . . . . .	41
4.6. ANALYTICAL METHODS EMPLOYED . . . . .	41
4.6.1. Porosity Determinations . . . . .	41
4.6.2. Determination of Absolute Permeability . . . . .	46
4.6.3. Determination of Relative Permeability . . . . .	46
4.7. ANALYSIS OF EFFLUENT SAMPLES . . . . .	48
5. DISCUSSION OF RESULTS . . . . .	49
5.1. PRESENTATION OF THE EXPERIMENTAL RESULTS . . . . .	49
5.2. CHARACTERISTICS OF GLASS BEADS, OTTAWA SAND AND FINES .	49

CHAPTER	PAGE
5.3. LINEAR FLOW TESTS . . . . .	52
5.3.1. Small Core Experiments . . . . .	60
5.3.2. Small Core Results . . . . .	65
5.3.3. Large Core Experiments . . . . .	70
5.3.4. Large Core Results . . . . .	74
5.3.5. Reproducibility of Experiments . . . . .	82
5.3.6. Discussion of Fines Flow Results . . . . .	86
5.3.6.1. Effect of Flow Rate . . . . .	87
5.3.6.2. Effect of Initial Amount of Fines Present . . . . .	88
5.3.6.3. Effect of Sand Grain Size . . . . .	89
5.3.6.4. Flow of Fines Equation . . . . .	90
5.3.6.5. Fines Concentration Versus Cumulative Volume Curve . . . . .	92
5.3.7. Discussion of Fines Flow Mechanisms . . . . .	95
5.4. RADIAL FLOW TESTS . . . . .	97
5.4.1. Radial Flow Experiments . . . . .	97
5.4.2. Radial Flow Results . . . . .	101
5.4.3. Discussion of Sand Production Results . . . . .	117
5.4.4. Discussion of Sand Production Mechanisms . . . . .	128
5.5. TWO-PHASE FLOW TESTS . . . . .	130
6. CONCLUSIONS . . . . .	137
7. RECOMMENDATIONS . . . . .	139

	PAGE
REFERENCES . . . . .	140
APPENDIX A. EXPERIMENTAL EQUIPMENT SPECIFICATIONS . . . . .	144
APPENDIX B. SAMPLE CALCULATIONS . . . . .	147
APPENDIX C. EXPERIMENTAL DATA . . . . .	158

## LIST OF TABLES

Table	Description of Table	Page
1	Properties of Materials Used at 23°C	38
2	Sieve Openings in Metric Units	40
3	Porosity of Radial Model Sand Packs	42
4	Properties of Linear Flow Sand Packs	47
5	Summary of Linear Flow Tests	61
6	Effect of Interstitial Velocity	88
7	Effect of Mass of Fines	88
8	Effect of Grain Size	90
9	Experimental Values of the Proportionality Constant	92
10	Ratio of Darcy Velocity Over Particle Size	94
11	Lloydminster Sand Sieve Analysis	96
12	Summary of Radial Flow Tests	98
13	Well Tubing Specifications	101
14	Factors Affecting Sand Production	131
B1	Dimensions of Barite Particles	149
B2	Waterflooding Data	151
B3	Intermediate Steps Results	154
B4	Final Steps Results	156
C1	Small Core Linear Flow Run #1	159
C2	Small Core Linear Flow Run #2	160
C3	Small Core Linear Flow Run #3	161
C4	Small Core Linear Flow Run #4	162
C5	Small Core Linear Flow Run #5	163

Table	Description of Table	Page
C6	Small Core Linear Flow Run #6	164
C7	Small Core Linear Flow Run #7	165
C8	Small Core Linear Flow Run #8	166
C9	Small Core Linear Flow Run #9	167
C10	Small Core Linear Flow Run #10	168
C11	Large Core Linear Flow Run #1	169
C12	Large Core Linear Flow Run #2	170
C13	Large Core Linear Flow Run #3	171
C14	Large Core Linear Flow Run #4	172
C15	Large Core Linear Flow Run #5	173
C16	Large Core Linear Flow Run #6	174
C17	Large Core Linear Flow Run #7	175
C18	Large Core Linear Flow Run #8	176
C19	Large Core Linear Flow Run #9	177
C20	Large Core Linear Flow Run #10	178
C21	Large Core Linear Flow Run #11	179
C22	Large Core Linear Flow Run #12	180
C23	Large Core Linear Flow Run #13	181
C24	Large Core Linear Flow Run #14	182
C25	Large Core Linear Flow Run #15	183
C26	Large Core Linear Flow Run #16	184
C27	Radial Flow Run #1	185
C28	Radial Flow Run #2	186
C29	Radial Flow Run #3	187

Table	Description of Table	Page
C30	Radial Flow Run #4	188
C31	Radial Flow Run #5	189
C32	Radial Flow Run #6	190
C33	Radial Flow Run #7	191
C34	Radial Flow Run #8	192
C35	Radial Flow Run #9	193
C36	Radial Flow Run #10	194
C37	Radial Flow Run #11	195
C38	Radial Flow Run #12	196
C39	Radial Flow Run #13	197
C40	Radial Flow Run #14	198
C41	Radial Flow Run #15	199
C42	Radial Flow Run #16	200
C43	Radial Flow Run #17	201
C44	Radial Flow Run #18	202
C45	Radial Flow Run #19	203
C46	Radial Flow Run #20	204
C47	Radial Flow Run #21	205
C48	Two-Phase Flow Step #1	206
C49	Two-Phase Flow Step #2	207
C50	Two-Phase Flow Step #3	208
C51	Two-Phase Flow Step #4	209



## LIST OF FIGURES

Figure	Description of Figure	Page
1	Diagram of Radial Model	33
2	Schematic of Flow of Fines Apparatus	34
3	Schematic of Sand Production Apparatus	36
4	Change of Refractive Index Due to Change in Brine Concentration	43
5(a)	Determination of Pore Volume by Miscible Displacement of A by B	44
5(b)	Determination of Pore Volume by Miscible Displacement of B by A	44
6(a)	Determination of Pore Volume by Miscible Displacement of A by B	45
6(b)	Determination of Pore Volume by Miscible Displacement of B by A	45
7(a)	SEM Photomicrograph of Calcium Carbonate Fines	50
7(b)	SEM Photomicrograph of Barite Fines	50
7(c)	SEM Photomicrograph of Glass Beads Fines	51
8(a)	SEM Photomicrograph of Ottawa Sand 50-100 Mesh	53
8(b)	SEM Photomicrograph of Glass Beads 100-325 Mesh	53
8(c)	SEM Photomicrograph of Silica 40-70 Mesh	54
9(a)	SEM Photomicrograph of Ottawa Sand 70-140 Mesh	55
9(b)	SEM Photomicrograph of Ottawa Sand 70-140 Mesh Produced at 1731.3 kPa	55
10(a)	Size Distribution of Barite Fines	56
10(b)	Size Distribution of Glass Beads Fines	56

Figures	Description of Figure	Page
11(a)	Size Distribution of Ottawa Sand 50-100 Mesh	57
11(b)	Size Distribution of Glass Beads 100-325 Mesh	57
11(c)	Size Distribution of Silica 40-70 Mesh	58
12(a)	Size Distribution of Ottawa Sand 70-140 Mesh	59
12(b)	Size Distribution of Ottawa Sand 70-140 Mesh Produced at 1731.3 kPa	59
13	Effect of Mass of Glass Fines	64
14	Effect of Flow Rate	65
15	Effect of Grain Size	67
16	Effect of Absence of Fines	68
17	Effect of Packing Method	69
18	Reproducibility of Small Grain Size	71
19	Reproducibility of Large Grain Size	72
20	Reproducibility of Dry Packing Method	73
21	Effect of Mass of Glass Fines	75
22	Effect of Flow Rate	76
23	Effect of Grain Size	77
24	Effect of Grain Shape	79
25	Effect of Fines Density	80
26	Effect of Fines Size	81
27	Effect of Absence of Fines	83
28	Reproducibility of Ottawa Sand 50-100 Mesh	84
29	Reproducibility of Silica 40-70 Mesh	85
30	Effect of Overburden Pressure (Angular Sand)	102
31	Effect of Overburden Pressure (Spherical Sand)	103

Figure	Description of Figure	Page
32	Effect of Flow Rate (No Overburden Pressure)	105
33	Effect of Flow Rate (High Overburden Pressure)	106
34	Effect of Grain Size (Angular Sand, No Overburden Pressure)	107
35	Effect of Grain Size (Angular Sand, High Overburden Pressure)	108
36	Effect of Grain Size (Spherical Sand)	109
37	Effect of Sand Shape	111
38	Effect of Tubing Perforations	112
39	Reproducibility of Ottawa Sand 70-140 Mesh (No Overburden Pressure)	113
40	Reproducibility of Ottawa Sand 70-140 Mesh (High Overburden Pressure)	114
41	Reproducibility of Glass Beads 80-120 Mesh	115
42	Reproducibility of Silica 40-70 Mesh	116
43	Sand Flux Versus Time Curve For Stable Sand Arches	119
44	Sand Flux Versus Time Curve For Unstable Sand Arches	120
45	Sand Flux Versus Time Curve For Absence of Sand Arches	121
46	Effect of Overburden Pressure (Slotted Tubing Perforations)	122
47	Effect of Flow Rate (Slotted Tubing Perforations)	123
48	Effect of Grain Size (Slotted Tubing Perforations)	124
49	Effect of Grain Size and Shape (Round Tubing Perforations)	125

Figure	Description of Figure	Page
50(a)	Relative Permeability of Hamilton Lake Crude and 2% NaCl Brine - Step 1	134
50(b)	Relative Permeability of Hamilton Lake Crude and 30% NaCl Brine - Step 2	134
50(c)	Relative Permeability of Hamilton Lake Crude and 2% NaCl Brine - Step 3	134
50(d)	Relative Permeability of Hamilton Lake Crude and 30% NaCl Brine - Step 4	134
C1	Conversion Chart of Calcium Carbonate Fines	210
C2	Conversion Chart of Barite Fines	211
C3	Conversion Chart of Glass Bead Fines	212

## NOMENCLATURE

- $a$  = Release Coefficient ( $s^{-1}$ )
- $a_0$  = Constant (ml/min)
- $a_1$  = Constant (ml/min<sup>2</sup>)
- $a_2$  = Constant (ml/min<sup>3</sup>)
- $b$  = Capture Coefficient ( $s^{-1}$ )
- $c$  = Constant ( $s/cm^2$ )
- $C$  = Concentration ( $cm^3/cm^3$  or  $g/cm^3$ )
- $d$  = Constant ( $cm^{-1}$ )
- $d'$  = Constant ( $cm^{-1}$ )
- $D$  = Average Sand Grain Diameter ( $\mu m$  or  $cm$ )
- $D_p$  = Average Particle Diameter ( $\mu m$  or  $cm$ )
- $f_o$  = Fractional Flow of Oil
- $f_w$  = Fractional Flow of Water
- $F_i$  = Inertial Force (dyne)
- $FI$  = Initial Fines In-Place (% of Total Pore Volume)
- $FP$  = Fines Produced (% of Initial Fines In-Place)
- $h$  = Height (m)
- $k$  = Permeability ( $m^2$ )
- $k_r$  = Relative Permeability
- $K$  = Constant
- $L$  = Measured Particle Length (mm)
- $m$  = Mass of Particle (g)
- $V_p$  = Volume of Oil Produced ( $cm^3$  or ml)
- $q$  = Flow Rate ( $m^3/s$  or  $cm^3/hr$ )

$\dot{Q}$  = Rate of Dry Sand Produced (ml/min)  
 $r$  = Radius (m or  $\mu\text{m}$ )  
 $r_c$  = Rate of Capture ( $\text{g}/\text{cm}^3 \text{ s}$ )  
 $r_r$  = Rate of Release ( $\text{g}/\text{cm}^3 \text{ s}$ )  
 $R$  = Equivalent Particle Radius (mm)  
 $S_{co}$  = Cohesive Strength (Pa)  
 $S_o$  = Initial Specific Surface ( $\text{cm}^{-1}$ )  
 $S_w$  = Water Saturation  
 $t$  = Time (s or min)  
 $T$  = Parameter Dependent on Failure Angle  
 $v$  = Approach Velocity ( $\text{cm}/\text{s}$ )  
 $V$  = Sphere Volume ( $\mu\text{m}^3$ )  
 $V_p$  = Core Pore Volume ( $\text{cm}^3$  or ml)  
 $V_s$  = Volume of Dry Sand Produced (ml)  
 $W$  = Measured Particle Width (mm)  
 $x$  = Depth (cm)  
 $\alpha$  = Constant ( $\text{cm}^{-1}$ )  
 $\beta$  = Constant ( $\text{s}^{-1}$ )  
 $\gamma$  = Volume of Fines per Unit Pore Volume ( $\text{cm}^3/\text{cm}^3$ )  
 $\delta$  = Constant ( $\text{cm}^{-1}$ )  
 $\Delta P$  = Pressure Drop ( $\text{g}/\text{cm s}^2$  or kPa)  
 $\theta$  = Failure Angle  
 $\lambda$  = Clarification Coefficient ( $\text{cm}^{-1}$ )  
 $\lambda^{-1}$  = Effective Viscosity (mPa.s)  
 $\mu$  = Viscosity ( $\text{g}/\text{cm s}$ , mPa.s or Pa.s)  
 $\rho$  = Constant ( $\text{cm}^{-1}$ )

$\sigma$  = Specific Deposit ( $\text{cm}^3/\text{cm}^3$ )

$\sigma_1$  = Concentration of Particles on Pore Wall ( $\text{g}/\text{cm}^3$ )

$\phi$  = Porosity

## 1. INTRODUCTION

Formation damage is a problem frequently encountered when producing from reservoirs containing significant amounts of clays and fines. Fines have been defined by Muecke (1979) as small loose solid particles present in the pore spaces of consolidated or unconsolidated formations. These fines are able to migrate through the pores, causing large reductions in permeability. Permeability reduction has also been attributed to the presence of clay particles in the formation, which can cause formation damage either by swelling upon contact with fresh water, or by migrating through the pores along with the fluids flowing in the reservoir.

Sand production usually occurs when producing from wells completed in shallow, unconsolidated formations, and can lead to several complications, such as reduced production, wellbore plugging, and equipment damage. This is particularly a problem in Saskatchewan reservoirs. Several sand control methods have been designed and implemented with only marginal success.

In order to devise efficient sand control methods and avoid permeability impairment when producing from problem-prone formations, the mechanics of the movement of fines in the reservoir and the flow of sand into the wellbore should be thoroughly understood. The purpose of this investigation, which is experimental in nature, is not to devise sand control methods; rather it is to study the mechanics of flow of fines and sand production in the context of Saskatchewan reservoirs, and to examine fines migration in a Berea sandstone.



In particular, the conditions which lead to the production of fines or sand were examined in order to determine the governing factors causing sand production and formation damage. Three types of experiments were conducted: linear flow experiments to study the flow of fines, radial flow experiments to investigate sand production, and two-phase flow experiments to examine the effect of fines migration on relative permeability. The linear flow experiments were carried out to study the flow of fines in sand packs having a grain size distribution which is comparable to that found in Saskatchewan reservoirs. However, the amount of fines reaching the outlet in these experiments was too low to cause sand production problems such as those existing in Saskatchewan reservoirs. A radial model was therefore designed to study the factors affecting sand production from sand packs of different grain size distributions, subjected to various axial loads. Because no change in permeability due to the flow of fines was detected in the tests conducted in the linear, unconsolidated packs, two-phase flow experiments were carried out in a Berea sandstone to obtain a preliminary idea on the effect of fines movement on the relative permeability of a consolidated sandstone core.

## 2. LITERATURE REVIEW

### 2.1. GENERAL DESCRIPTION OF THE PROBLEM

There are two aspects of the subject of this research: flow of fines in a porous medium, and sand production in a producing well. These two phenomena will now be discussed at length.

#### 2.1.1. Flow of Fines

The flow of fines in porous media was initially investigated in the field of water clarification. Water carrying solid suspensions is filtered by passing it through a sand filter bed. Clarification studies investigated the various sand bed parameters as well as water and suspension characteristics that led to the concept of optimum filter performance.

Particle transport and deposition was more recently studied from a reservoir engineering perspective. Several factors that may lead to formation damage have been identified. These include the presence of clay fines in the porous medium, the physical properties of fluids, the flow rate, the flowing phases involved, and the characteristics of the porous medium.

#### 2.1.2. Sand Production

Sand production is a problem commonly encountered in shallow, poorly consolidated formations. From experimental investigations and mathematical models, several factors that influence sand production have been recognized. Among these, production rates, formation stresses around the wellbore, and the ability of the sand to form stable arches, have been found to have a dominant effect on sand production.

## 2.2. EXPERIMENTAL STUDIES OF FLOW OF FINES

### 2.2.1. Clarification Experiments

#### 2.2.1.1. Physical Studies

The experimental studies conducted by Eliassen (1941) are among the earlier investigations in the field of sand filtration. The experiments consisted of flowing raw water through a multi-layer filter at a constant flowrate, while monitoring the pressure and the amount of suspended solids in the water corresponding to each filter layer. The experimental results showed a linear increase in pressure drop with time in each filter layer. The removal of suspended solids in the top sand layer, closest to the flow inlet, started at its highest level and decreased steadily thereafter. Removal in subsequent layers began at a lower level than previous ones, and increased as previous layers became saturated with suspensions. Removal of solids in the bottom layer was negligible for the duration of the run. It was concluded that at the beginning of the runs, the filter layers closest to the inlet carried most of the suspended particles. However, as these layers became clogged, removal of solid matter occurred in subsequent layers, and almost no contribution from the first layers was apparent at the end of the runs.

Maroudas and Eisenklam (1965) conducted clarification experiments in three different types of porous media: a transparent two-dimensional model, a packed bed of glass spheres, and a sintered disc. Studies on the two-dimensional visual model led to two observations: (1) It was noted that a critical interstitial velocity existed, above which no deposition occurred. (2) Two deposition modes were apparent: a constricting

mode and a blocking mode. In the constricting mode, the particles gradually plugged the flow paths until the interstitial velocity increased to its critical value, at which point no further deposition occurred. In the blocking mode, some channels became totally blocked due to a decrease in the interstitial velocity, while others remained unobstructed because in these flow paths the velocity was higher than the critical value. Furthermore, the number of blocked flowpaths was found to be largest near the inlet. This finding agrees with Eliassen's experimental results, where the top layers of the filter bed became clogged before the remaining layers. Maroudas and Eisenklam also showed that the pressure drop increased with time for every run. However, because their investigations included both angular and spherical suspensions, they discerned a lower pressure drop in the case of spherical particles than that for angular particles. For the particle size chosen, the spherical particles led to a constricting mode of deposition, while the angular particles resulted in the blocking mode. Similar results were obtained in the case of the packed bed and the sintered disc.

#### 2.2.1.2. Chemical Studies

In addition to the studies investigating filter performance in terms of physical variables, other works aimed at investigating the chemical characteristics that affect particle deposition. O'Melia and Crapps (1964) stated that the theories of clarification based on physical considerations such as sand size, particle size and density, and flowrate, were inadequate. Their experimental work was directed at identifying the chemical properties in the water/suspension system

that improved filtration. In their experiments, O'Melia and Crapps varied the chemical composition of the carrier liquid by varying the type of dissolved anions. Increasingly negative zeta potential and high pH level in the system were found to reduce particle deposition. Although their data showed that bed penetration varied with the type of anion used, the correlation between anion type and bed penetration was not successfully attributed to specific chemical properties of flocs.

The influence of pH level and type of anion dissolved on solids removal was also demonstrated by O'Melia and Stumm (1967). In their research, the chemical factors contributing to removal of hydrolyzed iron from the carrier liquid were investigated. An optimum pH level of 7 was obtained, above and below which iron removal decreased. The removal of iron dispersions at pH levels higher than 5 was altered when the suspensions were aged by stirring for a certain time period before starting the run. In addition, removal was improved at a pH 5 level when sulfate ions were present at a concentration of  $10^{-3}$ M. The authors suggested that filtration is controlled by two mechanisms; particle transport which is influenced by physical parameters, and particle attachment which is dominated by chemical properties.

## 2.2.2. Experiments in Porous Media

### 2.2.2.1. Physical Studies

The experimental methods used in clarification studies were slightly altered in order to investigate the flow of fines in porous media. Donaldson et al. (Donaldson, Baker and Carroll, 1977) considered the effect of pore size and particle size distribution on the flow of fines. Analysis of particle size distribution in the effluent led to

the suggestion that larger particles were captured first in the medium. A pressure increase with time was noted; however, this increase was not significant until many pore volumes of slurry were passed. Cake buildup on the core surface was found to consist of the larger particles. In the experiments where the cake was removed and the run continued, the pressure decreased significantly. It was concluded that the core became only partially plugged at the end of the run, and that the pressure increase was mostly due to cake buildup for the particle size distributions and pore size distributions studied.

A significant contribution to the study of movement of fines in a porous medium was provided by Muecke (1979). His research included an analysis of fines encountered in unconsolidated formations, visual experiments in a micromodel to discern the impact of single and multi-phase flow, and linear experiments in sandpacks. The fines, defined as particles smaller than  $37\mu\text{m}$  (400 mesh), represented 2 to 15 wt% of the formation particles. Analysis of their composition showed that the mineral present in highest concentrations was quartz (39 wt%), while clays were present in much smaller quantities (11 wt%). Muecke suggested that any process designed to treat fines movement in the reservoir should apply not only to clays, but also to the other minerals constituting the fines. From the visual model, it was observed that when a single liquid phase was present, particles flowed with the liquid unless they bridged at pore constrictions. The bridges were more stable when formed at high velocities than when formed at low velocities, and could be broken by flow reversals or pressure disturbances. Different mechanisms controlled fines movement in the case of multi-phase

flow. Wettability of fines and surface and interfacial forces were dominant in this case. When oil was used to displace water, the water-wet fines were swept by the interface. At connate water saturation, the fines were retained in the water phase and did not move. Muecke concluded that these multi-phase mechanisms dominate fines movement in the reservoir: that permeability reduction and fines production in unconsolidated sands is greatly increased when water production begins, and permeability is restored when fluid flow is reversed by injecting fluids into the formation.

Gruesbeck and Collins (1982) investigated particle deposition and entrainment separately by conducting two types of experiments. To study deposition, a fluid carrying suspension was passed through sandpacks that were initially free of fines. The other experiment type, representing entrainment, involved flowing a clean liquid through sandpacks that contained fines. Their results were in agreement with those of Maroudas and Eisenklam in that a critical velocity was discerned, below which no fines were entrained. Depending on the ratio of pore diameter to particle diameter, either plugging or surface deposition and entrainment occurred. It was noted that at ratios above 6.0, surface deposition and entrainment were dominant. Experiments depicting both plugging and surface deposition indicated that after flowing a certain amount of suspension-laden fluid, the sandpack became non-retaining. Earlier, Maroudas and Eisenklam had also noted that effect in the blocking mode of deposition. Maroudas and Eisenklam reported that the non-retaining state occurred also in surface deposition (constricting mode); however, this result was not evident in the surface

deposition experiments of Gruesbeck and Collins. Experiments carried out on Berea sandstone cores resulted in a decrease in permeability at higher flowrates, while permeability remained unchanged at lower flowrates. Flow reversal was found to restore original core permeability, a finding that agrees with Muecke's results.

#### 2.2.2.2. Chemical Studies

Both physical and chemical mechanisms were investigated by Gabriel and Inamdar (1983). The presence of a critical flowrate, which was reported by various investigators, was noted in this study to occur when flowing a wetting fluid such as brine. No critical flowrate was established for the flow of oil at connate water saturation. From a chemical viewpoint, permeability was affected by the type of cations present. Flowing fresh water through a core that was initially contacted with potassium chloride or sodium chloride resulted in severe permeability reduction, regardless of flow rate. However, when the core initially contained calcium chloride, the permeability declined only when the fresh water flowrate was higher than critical. Reduction of KCl concentration in the flow also led to permeability reduction. Gabriel and Inamdar concluded that the major chemical variables affecting permeability were the relative change in fluid salinity and type of cations present in the fluid.

The dependence of permeability on salt concentration has also been demonstrated by Khilar (1981). Experiments conducted on Berea sandstones containing only non-swelling clays (mostly kaolinite) indicated that a critical salt concentration existed, above which no reduction in permeability occurred when fluid salinity in the core was



changed. The critical salt concentration was strongly dependent on temperature and nature of cations present. No critical salt concentration was reached when bivalent salt solutions, such as  $\text{CaCl}_2$  or  $\text{MgCl}_2$ , were used to saturate the core. In addition, the rate at which salt concentration was decreased had a significant effect on permeability reduction. A critical value of the rate of decrease was noted, below which core permeability was hardly reduced, and that value decreased with decreasing flow rates.

Investigations similar to those of O'Melia and Stumm have been carried out by Potter and Dibble (1985) to obtain a better understanding of formation damage. These studies considered mainly the effect of pH and anion type on formation plugging by ferric oxyhydroxide colloids. The research showed that permeability reduction at each pH level investigated varied with the type of anion present. While the presence of some anions led to a substantial permeability reduction at low pH levels, the same anions did not affect the permeability at high pH levels. Two different mechanisms were believed to contribute to formation plugging: a flocculation of ferric oxyhydroxide colloids that led to filter cake formation at the sandpack inlet, and a colloid/quartz surface interaction that resulted in a uniform buildup of colloid throughout the sandpack.

### 2.3. THEORETICAL DEVELOPMENT OF FLOW OF FINES

#### 2.3.1. Clarification Studies

The first efforts to represent particle movement by mathematical models were directed towards applications in the water clarification

area. Iwasaki (1937) presented three basic formulae governing the flow of fines in sand filters. The first equation states that the rate of fines deposition is proportional to their concentration at the sand filter inlet:

$$\frac{\delta C}{\delta x} = -\lambda C$$

where  $C$  is the concentration of particles in  $\text{cm}^3/\text{cm}^3$

$x$  is the sand bed depth in  $\text{cm}$

and  $\lambda$  is the clarification coefficient in  $\text{cm}^{-1}$ .

The clarification coefficient varies with the filter bed conditions:

$$\lambda = \lambda_0 + d\sigma$$

where  $\lambda_0$  is the initial clarification coefficient in  $\text{cm}^{-1}$

$\sigma$  is the volume of particles deposited per unit  
volume of bed in  $\text{cm}^3/\text{cm}^3$

and  $d$  is a constant in  $\text{cm}^{-1}$ .

The third equation represents a mass balance of particles in the system, and is given by:

$$\frac{\delta \sigma}{\delta t} = -v \frac{\delta C}{\delta x}$$

where  $t$  is the time in  $\text{s}$

and  $v$  is the approach velocity in  $\text{cm/s}$ .

While some investigators (Iwasaki, 1937; Stein, 1940) assumed that the clarification coefficient increased with increasing specific deposit  $\sigma$ , others (Ornatskii, 1955; Maroudas and Eisenklam, 1965) suggested that

the coefficient decreased with increasing specific deposit. Ives (1962) proposed that the filter coefficient increased initially because of the increase in the surface area available for deposition, and decreased thereafter due to an increase in interstitial velocity. The filter coefficient is then governed by the equation:

$$\lambda = \lambda_0 + d\sigma - \frac{d'\sigma^2}{(\phi_0 - \sigma)}$$

where  $\phi_0$  is the initial bed porosity

and  $d'$  is a constant in  $\text{cm}^{-1}$ .

In order to predict filter behaviour, the parameters  $\lambda_0$ ,  $d$  and  $d'$  have to be determined from experimental runs. An expression for the pressure drop increase across the bed was derived from the Kozeny equation:

$$\frac{\Delta P_0}{x} = \frac{K\mu v S_0^2}{\phi^3}$$

where  $\Delta P_0$  is the initial pressure drop in  $\text{g/cm s}^2$

$\mu$  is the dynamic viscosity in  $\text{g/cm s}$

$K$  is a constant

and  $S_0$  is the initial surface of filter grains per unit filter volume in  $\text{cm}^{-1}$ .

The pressure drop equation presented by Ives also contained parameters that needed to be evaluated experimentally.

Maroudas and Eisenklam obtained expressions for the concentration of suspensions in the fluid and the pressure drop across the filter bed based on the blocking mode of deposition observed experimentally. The equations presented were more efficient than those of previous authors in that the parameters involved could be estimated without resorting to experimental runs, and theoretical results were found to agree well with their experimental data.

In an extensive review of the literature on clarification, Herzig et al. (Herzig, LeClerc and Le Goff, 1970) examined the mechanisms of clogging and the models of filtration considered by various investigators in their filtration analysis. Because different systems were characterized by different mechanisms, experimental investigations were recommended to determine which mechanisms play a dominant role. Two types of filtration were noted: a mechanical filtration in the case of particles larger than  $30\mu\text{m}$ , and a physicochemical filtration for small particles ( $\leq 1\mu\text{m}$ ).

### 2.3.2. Investigations in Porous Media

The equations describing filtration phenomena were based on the assumption that both suspensions and filter bed grains consisted of unisize and homogeneous particles. Donaldson et al. (Donaldson, Baker and Carroll, 1977) presented a mathematical model based on a statistical analysis that included the effects of pore size and particle size distributions. The porous medium, a sandstone core, was represented by a number of capillaries of different diameters. The probability of a particle entering a capillary depended on the magnitude of flow in that capillary and the relative size of the particle with respect to that

of the capillary. The statistical model was developed using Poiseuille's flow equation, a random number generator, and the probability of particle passage through a capillary. The values of pressure, pore size distribution and particle size distribution obtained experimentally were compared with those calculated using the model. The authors did not present measured and calculated data on the same graph to allow for easy quantitative comparison. They did however report good qualitative agreement for pressure and output particle size distribution. The calculated values of pore size distribution and input particle size distribution were noted to have a lower range than the experimental values.

Gruesbeck and Collins (1982) accounted for particle and pore size distribution by considering that the porous medium consisted of plugging and non-plugging pathways. In the plugging pathways, the pore sizes were taken to be small, and plugging deposition occurred. The non-plugging pathways contained larger pores, and yielded surface deposition. Local laws of surface entrainment and deposition were developed first, and then modified to apply to both surface and plugging conditions. For surface deposition, the material balance equation is expressed as:

$$\frac{\delta}{\delta t} (\phi C + \phi_0 \gamma) + v \frac{\delta C}{\delta x} = 0$$

where  $\gamma$  is the volume of fines deposited per unit original pore volume in  $\text{cm}^3/\text{cm}^3$ .

If  $\phi$  and  $C$  are assumed to be constant, the equation becomes:

$$\phi_0 \frac{\delta \gamma}{\delta t} = -v \frac{\delta C}{\delta x}$$

which is similar to the continuity equation presented by Iwasaki.

The rate of deposition of fines is assumed to be proportional to the fines concentration, and is given by:

$$\frac{\delta \gamma}{\delta t} = \beta C$$

where  $\beta$  is a constant determined experimentally in  $s^{-1}$ .

Because no entrainment occurs at velocities lower than the critical, the equation representing entrainment is:

$$\frac{\delta \gamma}{\delta t} = \alpha \gamma (v - v_c) \quad \text{for } v > v_c$$

$$\frac{\delta \gamma}{\delta t} = 0 \quad \text{for } v < v_c$$

where  $\alpha$  is a constant in  $cm^{-1}$ ,

and  $v_c$  is the critical velocity in cm/s.

For the more general case, where both surface and plugging conditions apply, the material balance equation is modified by substituting  $\phi_0(1 - \gamma)$  for  $\phi$ , and assuming that  $\gamma$  and  $C$  are negligible. The volume of the porous medium is assumed to consist of two parts: a fraction  $f$  of the volume that has pluggable pathways and a fraction  $(1 - f)$  containing non-pluggable pathways.

In the non-pluggable channels, the equations developed for surface deposition and entrainment apply:

$$\frac{\delta \gamma_{np}}{\delta t} = -\alpha(v_{np} - v_c)\gamma_{np} + BC \quad \text{for } v > v_c$$

and

$$\frac{\delta \gamma_{np}}{\delta t} = BC \quad \text{for } v < v_c.$$

Here,  $\gamma_{np}$  is the volume of fines deposited in non-pluggable pathways per unit original pore volume in  $\text{cm}^3/\text{cm}^3$

and  $v_{np}$  is the fluid velocity in nonpluggable pathways in  $\text{cm}/\text{sec}$ .

In the pluggable channels, the governing equation is postulated to be:

$$\frac{\delta \gamma_p}{\delta t} = (\delta + \rho \gamma_p) v_p C$$

where the subscript  $p$  refers to pluggable pathways and  $\delta$  and  $\rho$  are constants in  $\text{cm}^{-1}$ .

The drawback of this model is that the constants in these equations have to be either assumed or determined from experimental data. Values of deposits and effluent concentrations were calculated using the model and compared with experimental data. The authors concluded that in spite of its simplicity, the model reproduced experimental results quite adequately.

In developing a model to represent the water sensitivity of sandstones, Khilar (1981) suggested that the porous medium could be partitioned into thin sections. Each section contained many pores or

unit cells having a length similar to that of the section. It was assumed that pores within the same section were not interconnected, although they could be connected to those of adjacent sections. Clay particles, initially attached to pore walls, were released when the salt concentration in the fluid fell below the critical salt concentration. These particles then travelled with the fluid until they reached pore constrictions and were captured, resulting in a permeability decrease. A material balance on particles in a unit cell yielded:

$$\frac{dC}{dt} = r_r - r_c$$

where  $C$  is the concentration of particles in the fluid in  $\text{g/cm}^3$

$r_r$  is the rate of release of clay particles from the pore wall in  $\text{g/cm}^3\text{s}$

and  $r_c$  is the rate of capture of particles in  $\text{g/cm}^3\text{s}$

The rate of release,  $r_r$ , depended on both physical and chemical variables. However, if the chemical conditions were kept constant, the rate of release could then be considered to be proportional to the concentration of clay particles on the pore walls.

$$r_r = a\sigma_1$$

where  $\sigma_1$  is the concentration of clay particles on the pore wall in  $\text{g/cm}^3$

and  $a$  is the release coefficient, which becomes zero at salt concentrations higher than the CSC, in  $\text{s}^{-1}$



The rate of capture  $r_c$  was given by:

$$r_c = bC$$

where  $b$  is the capture coefficient, obtained by carrying an analysis of particle deposition based on spherical collectors, in  $s^{-1}$ .

The release and capture coefficients must be determined experimentally. Khilar recognized this disadvantage and suggested that once the values of the coefficients are measured at a certain flow rate, values at other flow rates could be readily determined, because these coefficients were proportional to flow rate for Berea Sandstone.

#### 2.4. EXPERIMENTAL STUDIES OF SAND PRODUCTION

Although numerous studies of sand control have been reported in the literature, few investigations have been oriented towards the mechanics of sand production and the variables that influence it. Hall and Harrisberger (1970) pointed out that sand production occurs when the sand around the well bore fails to form stable arches. They conducted triaxial tests to determine sand failure mechanisms and arching tests to identify the conditions leading to formation of stable arches. In the triaxial experiments, sand samples were packed in a rubber tube placed inside a cell, and subjected to various confining stresses and axial loads. Low confining stresses resulted in a sharper failure indication than high confining stresses, and grain crushing occurred in the high confining stress range. Rounder and coarser mesh sands exhibited lower shear resistance than angular and finer mesh sands. In the arching experiments, sand samples were compacted in a cell with

a trap door at the bottom that could be removed easily to determine whether arching was occurring over the opening. Various axial loads were applied, and in some runs fluids were flowed through the samples. The tests indicated that angular sands arched more readily than round sands. A small load (500 psi) improved arch stability in angular sand, while a large load (2000 psi) led to arching failure because sand crushing occurred. Round sand failed to arch at all axial loads unless some restraint was induced on the grains by moistening the sand or flowing air into the opening. Although this research was qualitative in nature, it served to identify the major factors affecting arching stability, namely restraint on sand grains and sand crushing at sufficiently high loads.

The effect of flow rate on arch formation and stability was examined by Tippie and Kohlhaas (1973). A semi-cylindrical cell with a simulated casing attached to its flat side was packed with sand, and arching behaviour over the casing perforation was observed. Radial flow was achieved by installing a screen inlet in the circular section of the cell. In most runs, fluid flow was started at a low rate, and was gradually increased until sand production occurred. The experiments showed that sand-free fluids were produced when stable arches formed over the perforation. Larger initial arch sizes corresponded to larger initial flowrates. Smaller arches were found to be more stable and allowed a high fluid velocity to be reached before failure. As flowrates were increased, stable arches were broken, and newer larger arches were formed. While a gradual increase in flowrate to a certain value still allowed a stable arch to exist, a sudden increase in the

rate to that value resulted in arch failure and sand production. Experimental data indicated that a permeability reduction was associated with arch failure. The authors suggested that fines were migrating through the sand and bridging on the arch, resulting in high pressure gradients and arch failure.

Cleary and colleagues (Cleary, Melvan and Kohlhaas, 1979) investigated the stability of sand arches when subjected to various stress levels and hydrocarbon fluids. Their experimental apparatus consisted of a sand cell containing a semicircular casing with two perforations where arches could be formed. Visual observation of the arches was made possible by placing plexiglass viewing ports over the perforations. Fluids were injected through inlets located across the perforations. It was noted that the shape of the sand arch depended on the direction of the principal stresses, and that arch size decreased with increasing confining pressure. Two hydrocarbons, kerosene and mineral spirits, were used in the experiments. Kerosene was found to exhibit stronger cohesive forces on the arches than mineral spirits, and led to the formation of more stable arches. Arch stability also increased with increasing horizontal and vertical stresses, however the most stable arches were obtained when the horizontal (confining) stress was at the maximum, and the vertical stress at the minimum.

## 2.5. THEORETICAL DEVELOPMENT OF SAND PRODUCTION

A large number of articles offering various techniques to handle sand-producing formations have appeared in the literature. A method for estimating the maximum production rate that can be applied without resorting to sand control measures was suggested by Stein and Hilchie (1972). The method proposed involved estimating formation strength from density and acoustic velocity logs, and determining the maximum sand-free production rate of a sand with known strength in the same area. That method was later modified to apply to different well completion geometries (Stein, Odeh and Jones, 1974). Techniques have also been developed to identify the sand-producing intervals in multi-completion gas wells (Stein, Kelly, Baldwin and McNeely, 1972), and the formations that are strong enough to sustain high production rates with no sand control measures (Tixier, Loveless and Anderson, 1975; Stein, 1976).

A theoretical model describing sand stresses and sand failure was presented by Bratli and Risnes (1981). To simplify their analysis of the stresses in the sand, the porous material was represented by a spherical shell, and axial loading was not considered. The analysis included, however, the effect of pore-fluid pressure. The porous material was assumed to behave elastically until a Coulomb failure was reached in which the material would be in a plastic state. Expressions for the stresses were given for the elastic state and the plastic state. Two modes of failure due to fluid flow were deduced from the model: total collapse of the material, given by

$$\frac{\mu q}{4\pi k r_1} = \frac{T+1}{T} 4 S_{co} \tan \theta$$

and collapse of the inner shell, expressed by

$$\frac{\mu q}{4\pi k r_1} = \frac{T+1}{T} 4 S_{co} \tan \theta \cdot \frac{1}{1 + \frac{1}{T} \left(\frac{r_1}{r_s}\right)^{T+1}}$$

In these equations,  $\mu$  is the fluid viscosity in Pa.s

$q$  is the flowrate in  $m^3/s$

$k$  is the permeability in  $m^2$

$T$  is a parameter depending on failure angle

$\theta$  is the failure angle

$S_{co}$  is the cohesive strength in Pa

$r_1$  is the inner surface radius in m

and  $r_s$  is the radius of the new arch at shell collapse in m.

In a theoretical analysis similar to that of stresses behind a perforation opening suggested by Bratli and Risnes, the stresses around a wellbore were studied by Risnes and colleagues (Risnes, Bratli and Horsrud, 1982). The model used was a disc of sand with a central cylindrical hole. The rock was assumed to be homogeneous and isotropic, and steady state fluid flow conditions were assumed close to the wellbore. Expressions for stresses in the elastic state and plastic state were obtained, and a stability criterion was determined to be:

$$\frac{\mu q}{2\pi k h} = 2 S_{co} \tan \theta$$

where  $h$  is the height of the producing layer in m.

The equation above characterized total collapse of the formation which was the only failure mode detected when permeability was assumed to be constant. Collapse of the inner shell was deemed possible only in the case of variable permeability.

Stresses around wells subjected to steam injection were investigated by Reeves (1985). Reeves noted that steam injection into unconsolidated reservoirs leads to high pore pressures, and could result in reservoir fluidization. He suggested that "pipes" or channels could form between injectors and producers due to the fluidization process. A theoretical model was developed assuming radial, steady-state flow in a homogeneous, isotropic porous medium. While the model of Risnes et al. (Risnes, Bratli and Horsrud, 1982) was based on Darcian flow and used Coulomb's failure criterion, Reeves' model allowed for non-Darcy flow and included the Griffith-Murrell plastic yield criterion. It was observed that although the expression for reservoir stresses obtained could be used to predict reservoir heaving and subsidence, and pipes formation, experimental values of mechanical properties were needed to provide a quantitative analysis.

An investigation of stresses present in oil sands was carried out by Vaziri (Byrne and Vaziri, 1985; Vaziri, 1986). A theoretical model representing time-dependent sand stresses, deformation, and flow was developed using a finite element method of analysis. The model was reported to yield good reservoir behaviour predictions because it included the effect of dissolved gas in the bitumen, the varying permeability and compressibility of pore fluids, non-linear sand stresses and non-linear fluid flow.

## 2.6. FIELD EXPERIENCE

Many problems have been associated with sand production and movement of fines in producing unconsolidated formations. The flow of fines in these formations was recognized to lead to pore plugging and to result in permeability loss and formation damage. Sand flow into the wellbore was found to cause complications, such as production loss due to bridging of sand in casing and tubing, equipment failure, and reservoir subsidence (Suman, 1975).

In a handbook on sand control, Suman (1975) discussed the problems commonly associated with sand production, and presented the measures to be taken to minimize sanding problems. A description of sand control methods was also included in the handbook. Sand control techniques were reported to be of two types: mechanical and chemical.

### 2.6.1. Mechanical Sand Control Methods

In mechanical methods, the main process preventing sand flow is bridging of sand grains using sand retention devices such as gravel packs, slotted liners and screens. Gravel packing allows fluids to be produced while retaining solid particles. A survey conducted by Schwartz (1969) showed that several crucial factors should be considered to attain proper gravel pack performance: formation sand size distribution should be determined accurately, the gravel-to-sand ratio should be chosen carefully to avoid permeability impairment, and gravel sizing should be designed to withstand high fluid velocities which could otherwise destroy pack stability. Other factors affecting gravel pack success include presence of contaminants in the gravel and the fluids, properties of the gravel, and gravel pack thickness. Methven and

Kemick (1969) suggested the use of an oil base fluid for drilling and gravel packing. Such a fluid would eliminate formation damage due to clay swelling and particle migration. Gravel packing was reported to be successful in several field applications (Mantooth and Williams, 1980; Sawolo, Krueger and Maly, 1983; Likwartz, 1976).

For instance, in the Teak Field of Trinidad, gravel packs combined with single wrap screens improved well performance and reduced sand production (Likwartz, 1976). In spite of the reported successes of gravel packing, some disadvantages became apparent. These include loss of productivity, difficulty of installation in directional or multi-completion wells, and poor performance in wells with plugged perforation holes and in poorly completed wells (Rike, 1975). Slotted liners and wire screens are used either with or without gravel packs. Common problems encountered with these devices are productivity loss, corrosion and erosion.

#### 2.6.2. Chemical Sand Control Methods

Chemical methods involve the injection of consolidating materials into the formation to cement the sand grains. Several types of chemicals such as Epoxy, Furan, Phenol-formaldehyde and Phenol resin are used for this purpose. With consolidation methods, special attention should be given to adequate well completion. For instance, formation damage around the wellbore due to drilling should be minimized, loss of treatment fluids should be avoided by proper cement application, and completion fluids should be kept free of solids and debris (Suman, 1975). For viscous, low-gravity oil reservoirs, a consolidation method was proposed which would circumvent the low productivity problems ensuing



from conventional sand control measures (Terwilliger, Smith and Goodwin, 1964). The technique consisted of injecting heated air into the formation to oxidize the crude and form an insoluble resin. The resin or coke would then bind the sand grains together. Air injection and temperature increase rates should be monitored closely to prevent spontaneous ignition of the crude. It was reported that the warm-air soaking method yielded sand-free production from the shallow, unconsolidated sand reservoirs tested. When consolidation is sought by injecting organic chemicals into the formation, the resins injected should have some essential characteristics. Resin viscosity should be sufficiently low to allow injection at pressures lower than fracturing pressures, but not so low as to impede polymerization. They should have a compressive strength high enough to withstand formation stress, good adherence properties, a short hardening time, and a high resistance to chemical reaction with well fluids (Rogers, 1971). Field applications of a sand consolidation process developed by Treadway et al. (Treadway, Brandt and Parker, 1966) in the Gulf Coast and California were reported to be quite successful. The process involved the injection of epoxy resin into the formation, followed by diesel oil injection to reduce the resin saturation to its residual value and thus establish formation permeability. An activator flush is then injected to polymerize the resin. The attractive features of this technique were the establishment of permeability prior to polymerization, the removal of time dependence of the resin polymerization process, and the rapid hardening of the resin regardless of formation temperature due to high activator concentrations. Common shortcomings of sand consolidation methods are loss

of productivity due to plugged perforations, deterioration of the resins in the formation with time and continued production, uneven resin coating in heterogeneous sands, and poor adherence to sand grains in formations with high clay content due to leaching of plastic by clay particles (Rike, 1975).

### 2.6.3. Other Sand Control Methods

Combination methods that use both mechanical devices and chemical consolidation, have also been investigated. Rike (1975) proposed a combination technique that consisted of injecting resin into the formation prior to gravel packing. Such a technique would remove the limitations associated with applying either method alone. Another combination method was tested that involved coating sand or gravel with resin (Sinclair and Graham, 1977). The technique required formation temperatures above 130°F to cure the resin. Field applications in two different areas showed that generally productivity was improved and sand production curtailed, although failure occurred in some wells.

Field experience in two areas exhibiting fines and sand production problems has been described and published by various authors. The oil fields, located in Lloydminster on the Alberta/Saskatchewan border, and in Santa Maria Valley, California, are both operated by Husky Oil. The Lloydminster reservoirs consist of fine-grained, clean, unconsolidated sands that contain a crude characterized by a high viscosity (950 to 6500 mPa.s) and a low gravity (13 to 17°API). The average oil production is 23 BOPD, with a sand cut that varies from 15% in new wells to 1% in wells that have been producing for some time (Adams, 1981). The Cat Canyon reservoirs of California are also fine-grained

and unconsolidated. They contain a higher viscosity (2000 - 45,000 mPa.s) and lower gravity (4-12°API) crude than those of Lloydminster.

Production rates vary from 35 to 350 BOPD with sand cuts up to 70% (Gurel, 1979). In both areas, conventional sand control techniques have been tried. In Lloydminster, gravel packing and sand consolidating reduced sand production; however, the already low oil production rate was also reduced to uneconomical levels. In California, well completion with gravel packed liners resulted in oil production rates as low as 10 BOPD (Vonde, 1980). It was decided that for these fields, sand production was best handled through special pumping and surface equipment. Because of the high viscosity of the crude and excessive amount of sand present, the downhole pumps were designed to reduce rod fall problems and withstand sand erosion. The downhole pumps that showed the most improved performance have two tubing strings: a power string where sucker rods and pump plungers are operated, and a production string where fluids are produced (Vonde, 1980; Gurel, 1979).

More recently, a new sand control device was designed to remedy sand production problems encountered in the Athabasca oil sands of Alberta. Fine-grained unconsolidated formations, high bitumen viscosity, and thermal recovery processes contributed to the sanding complications. Sand control measures such as gravel packs, wire-wrapped screens and consolidated sand packs had been employed with little success. The new filter consisted of stainless steel wool and coarse steel cloth. It was tested at Texaco's Fort McMurray Pilot, and satisfactory results were reported (Toma, Livesey and Heidrick, 1986).

### 3. STATEMENT OF THE PROBLEM

This investigation was undertaken to study two phenomena: flow of existing fines in a porous pack under various flow conditions, and sand production in a radial flow model simulating a wellbore. Specifically, the following objectives were set out for this study:

#### Experimental Apparatus Design

1. Design a flow system and analytical methods for studying the flow of fines in linear porous packs, without axial loading.
2. Design and build a radial flow system, simulating a wellbore and surroundings, with overburden simulation.

#### Experiments To Be Conducted

1. Carry out single-phase flow experiments in the linear porous pack, using different size sand and glass beads, with predetermined amounts of fines, at various flow rates and fines contents.
2. Carry out single-phase flow experiments in the radial model for a number of overburden pressures and flow rates, and determine sand production in each case.
3. Carry out selected two-phase flow experiments in a sandstone to determine the effect of fines on relative permeabilities.

The overall purpose of this investigation is to lay the groundwork for studies of flow of fines, and in particular, develop the operating criteria for the wellbore model, which is the unique feature

of this work. The radial model was designed following linear experiments to study flow of fines, when the quantity of fines produced was too small to explain sand production in Lloydminster oil sands.

## 4. EXPERIMENTAL EQUIPMENT, MATERIALS AND PROCEDURE

### 4.1. DESCRIPTION OF THE MODELS DESIGNED

#### 4.1.1. Linear Models

Experiments in the linear models were designed to investigate the factors affecting the flow of fine particles in porous packs, under various operating conditions. The flow of fines experiments were conducted in two different stainless steel core holders packed with unconsolidated sand or glass beads. A small core holder 25.4 cm in length and 2.4 cm in diameter was used to develop the experimental technique and to obtain qualitative information on the flow of fines. Quantitative data was obtained from subsequent linear runs which were carried out using a larger core holder, 47.5 cm in length and 3.8 cm in diameter. In both core holders, a sintered disc was attached to the inlet flange for flow distribution, and a 45  $\mu\text{m}$  (325 mesh) screen was attached to the outlet flange. The 45  $\mu\text{m}$  screen served to prevent the flow of bulk sand bodies through the outlet, thus allowing for the study of fine particles behaviour.

#### 4.1.2. Radial Model

Experiments in the radial model were designed to study the flow of sand into the well bore. The sand production experiments were carried out using a radial model that consisted of a stainless steel cylindrical cell, with a height of 17.7 cm and an inside diameter of 20.0 cm. The flow inlets were located on the outer walls of the cell, and radial flow was achieved by lining the inner cell walls with a ,

sintered sheet (see Figure 1). A hole drilled in the cell bottom served to hold a perforated stainless steel tubing 1.3 cm in diameter in the cell center. After packing the cell, a teflon disc 0.6 cm thick was inserted in the cell over the sand pack, and an aluminum cover 10.6 cm in height was placed over the disc. Bulk sand was produced because no screen was present to restrain large sand grains from flowing through the tubing perforations.

#### 4.2. DESCRIPTION OF THE APPARATUS AND EXPERIMENTAL PROCEDURE

##### 4.2.1. Flow of Fines

A schematic diagram of the experimental apparatus is shown in Figure 2. All experimental runs were conducted with distilled water as the flowing fluid. The displacement pump is a volumetric Ruska pump, with oil as the displacing fluid. The pump displaced distilled water from a 1 liter stainless steel cylinder into the sandpacked core holder. A millipore block filter with 8  $\mu\text{m}$  filter screens prevented solid particles that may have been present in the fluid from reaching the sandpack. For the experiments conducted in the large core holder, a pressure transducer located at the core holder inlet, and a digital multimeter, were used to obtain readings of the pressure drop across the pack. The pressure drop in the small core holder runs was not measured. The effluent was collected in centrifuge tubes fitted in an automatic sampler with a timer capable of providing 24 samples per cycle. Samples of effluent were analyzed for fines content using an optical turbidimeter. Equipment specifications are listed in Appendix A.

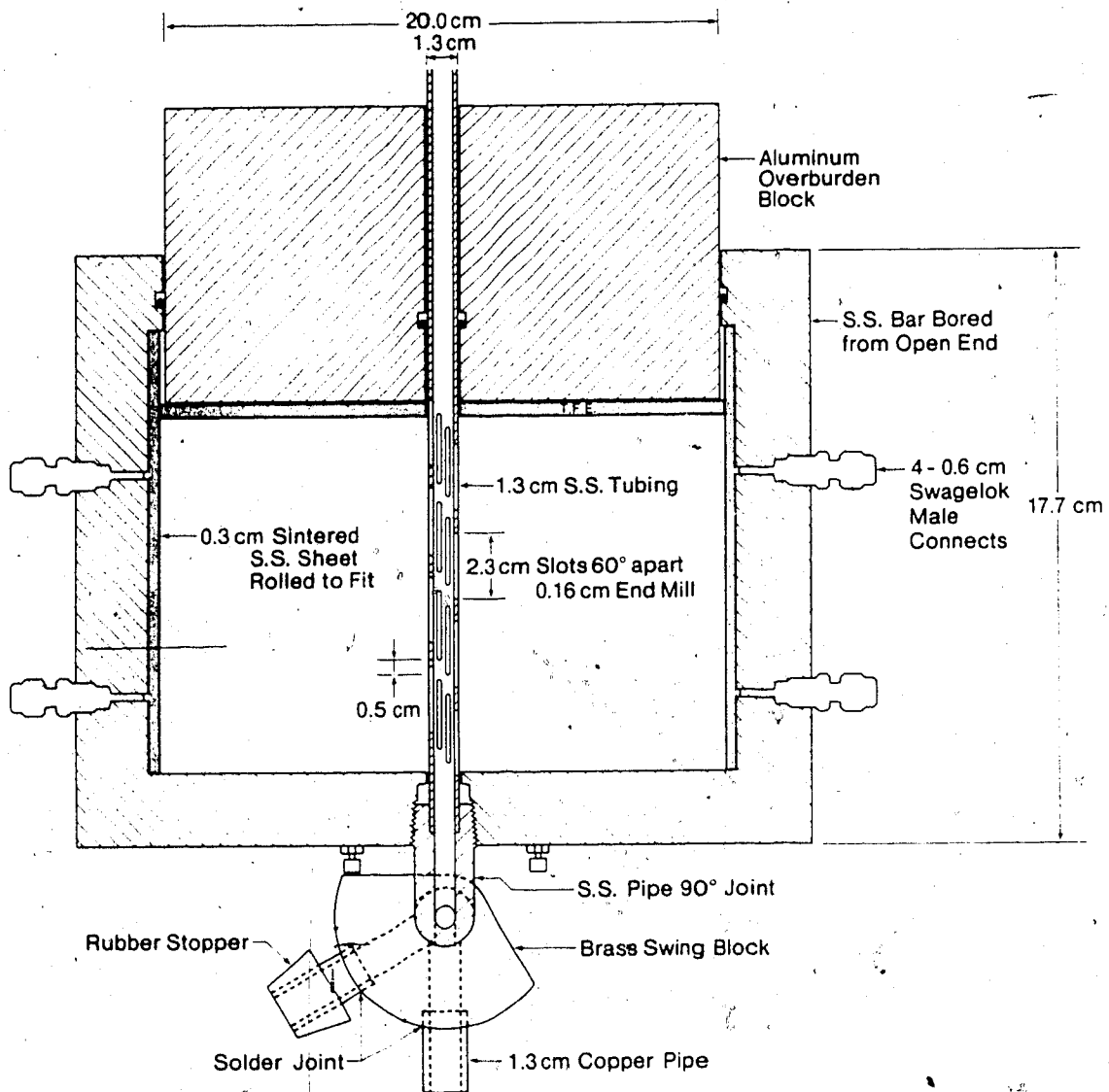


FIGURE 1: Diagram of Radial Model



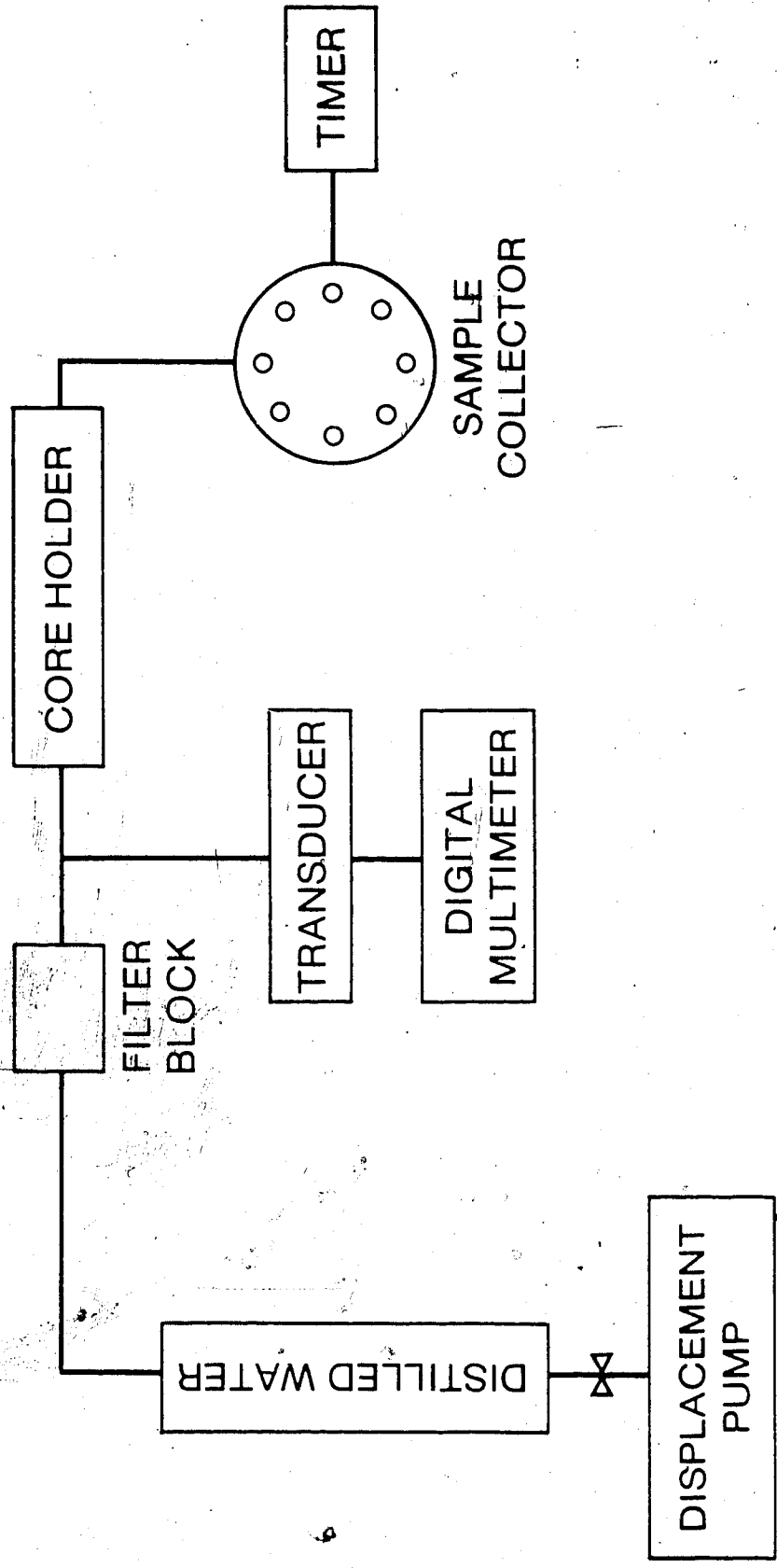


FIGURE 2: Schematic of Flow of Fines Apparatus

#### 4.2.2. Sand Production

A schematic diagram of the apparatus used for the sand production tests is shown in Figure 3. The Ruska pump was used to displace distilled water from the stainless steel cylinder into the radial cell. The sand or glass beads packs in the cell were subjected to various overburden loads using an Enerpac hydraulic press capable of applying loads up to 10,000 lbf with a ram 3.5 cm in diameter. The overburden pressure was kept to its initial value by adjusting the load with a manual air pump, as soon as a pressure decrease was noted. Samples of sand and water flowing through the tubing perforations were collected in centrifuge tubes. A total sand and water volume of 50 ml was collected in each tube, and the sand volume in each tube was measured and recorded.

#### 4.2.3. Two-Phase Flow

The two-phase flow test, designed to study the effect of fines migration on relative permeability, was conducted with a Berea sandstone as the porous medium. An x-ray analysis of the core to determine clay content revealed that clays constituted 1 to 3% of the total matrix. These clays consisted mostly of kaolinite and illite with trace amounts of chlorite. The core was painted with Phenoline 300 epoxy resin and allowed to dry at room temperature. The core was then baked in an oven at 100° F for two hours. After cooling to room temperature, a second coat of paint was applied and dried as before. The core was then placed in a core holder 61 cm in length and 5.0 cm in diameter, and was positioned with a three pin recessed disc at one end. The other end was centered using three pieces of rope placed

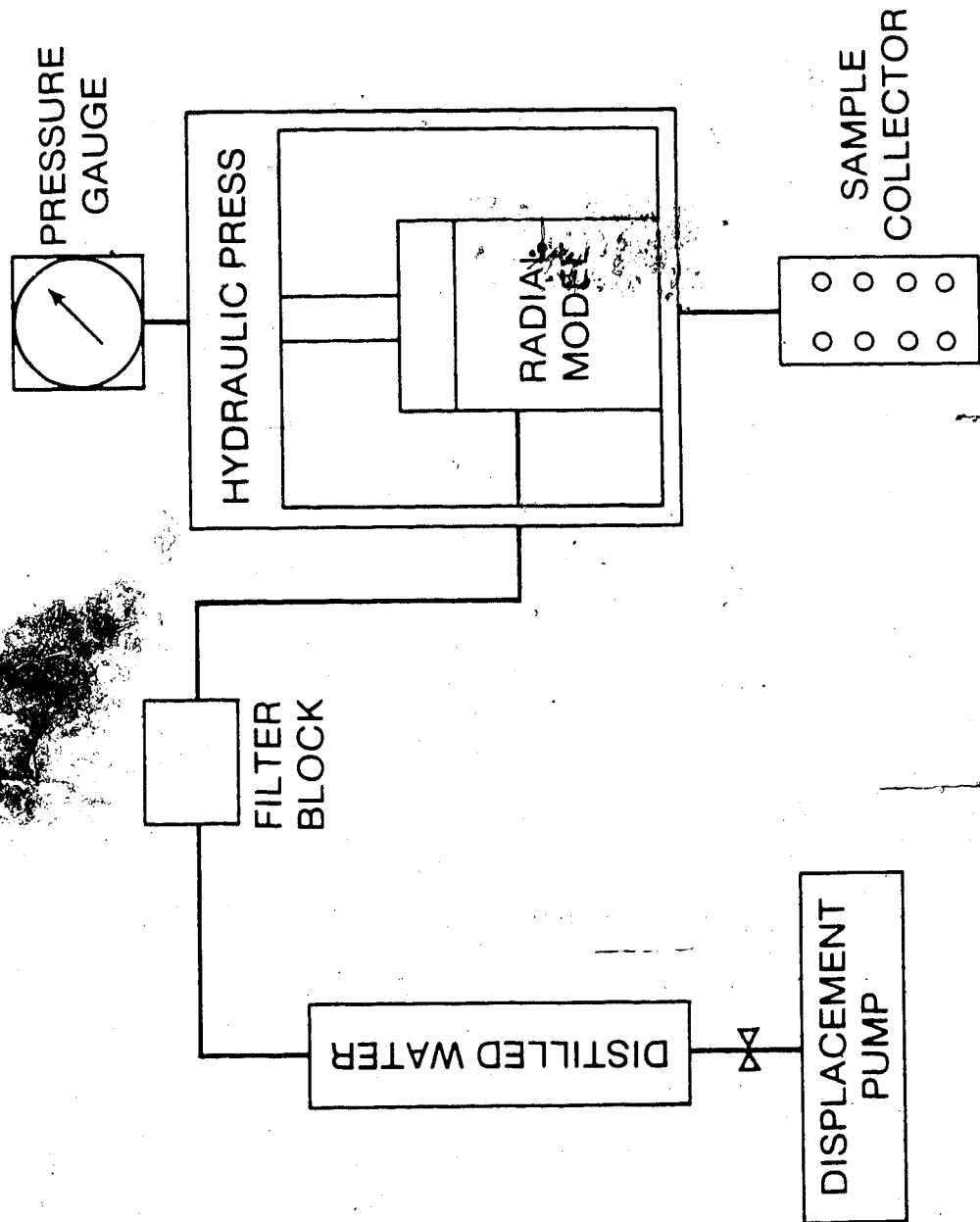


FIGURE 3: Schematic of Sand Production Apparatus

between the core and the core holder. Molten Cerrobend alloy was poured into the core holder, and the core was allowed to cool to room temperature. The ends of the core were then machined flush to the core holder and flanges fitted.

The experimental procedure consisted of four steps:

- Step 1: The core was saturated with 2% brine, and then was oil flooded with Hamilton Lake crude to irreducible water saturation. A 2% brine solution was then injected until residual oil saturation was reached. During this water-flooding stage, samples of effluent were collected to determine the outlet oil and water volumes, and the pressure drop was recorded at each sample collection. This data was used to calculate the relative permeability to the crude and to 2% brine.
- Step 2: The core was oil flooded with Hamilton Lake crude, then water flooded with 30% brine. The relative permeability to the crude and 30% brine was calculated.
- Step 3: The 30% brine solution was flushed out with 2% brine. The core was then oil flooded with Hamilton Lake crude, followed by water flooding with 2% brine. The relative permeability to the crude and 2% brine was then calculated.
- Step 4: The core was oil flooded with Hamilton Lake crude, then water flooded with 30% brine, and the relative permeability to the crude and 30% brine calculated.

#### 4.3. MATERIALS USED

Both sand production and flow of fines experiments were conducted with distilled water as the flowing fluid. The single-phase flow was chosen to simplify the problem, because with multiphase flow additional variables would be introduced. The unconsolidated packs were prepared using Ottawa sand, silica, or spherical glass beads. Both the Ottawa sand and silica consist of angular grains, with the silica grains being larger in size than the Ottawa sand grains. The materials used for fines were glass beads, barite, or calcium carbonate. The two-phase flow test was carried out in a Berea sandstone with a porosity of 21.23% and a permeability of  $0.6611 \mu\text{m}^2$ . The flowing fluids in this test were a 2% NaCl solution, a 30% NaCl solution and a Hamilton Lake crude. The measured properties of the materials used are listed in Table 1.

TABLE 1: Properties of Materials Used at 23°C

<u>Material</u>	<u>Density, g/cm<sup>3</sup></u>	<u>Viscosity, mPa.s</u>
Distilled Water	0.948	1.03
Hamilton Lake Crude	0.866	10.70
2% (w) Brine	1.014	1.07
30% (w) Brine	1.223	2.60
Silica	2.601	--
Ottawa Sand	2.634	--
Glass Beads < 283 $\mu\text{m}$	2.326	--
Calcium Carbonate	2.441	--
Barite	4.213	--
Glass Beads > 3327 $\mu\text{m}$	2.624	--

#### 4.4. PREPARATION OF FINES

In most of the experiments investigating the flow of fines in unconsolidated packs, the fines consisted of spherical glass beads smaller than 45  $\mu\text{m}$  (325 mesh). The glass beads were supplied in 22.7 kg bags having various nominal mesh size ranges. Dry sieving was initially applied to obtain glass fines. The dry sieving process involved placing small samples of beads on the top screen of several Tyler sieves, arranged in a decreasing screen opening order. Selected screen openings and their equivalent Tyler mesh size are shown in Table 2. The sieve series was then put in an automatic Ro-Tap shaker to facilitate the passage of beads through the screens. The fines consisted of the particles that passed through the bottom screen, which had the smallest openings (45  $\mu\text{m}$ ).

It became apparent, however, that a large portion of fines was not being recovered because they adhered to larger sized beads. To recover these fines and obtain a better sorting of the larger beads, wet sieving was employed. In this method, the samples were placed on a 325 mesh screen, and fines were collected in a receiver by pouring distilled water over the samples and lightly stirring the slurry. The beads remaining in the screen were then dried and sieved using the dry sieving method.

TABLE 2: Sieve Openings in Metric Units

<u>Mesh Size</u>	<u>Opening Size in <math>\mu\text{m}</math></u>
6	3327
20	833
50	283
70	187
100	147
140	111
230	67
270	53
325	44

#### 4.5. PACKING THE MODELS WITH SAND OR GLASS BEADS

##### 4.5.1. Packing the Linear Model

Before packing, the sand and beads were sieved and sorted into three size ranges: 40 to 70 mesh, 50 to 100 mesh, and 100 to 325 mesh. The fines were weighed using a Mettler scale, and thoroughly mixed with the sand in order to ensure a uniform fines distribution in the pack. A wet packing procedure was employed, which consisted of alternately pouring small amounts of distilled water and sand mixture in the linear model which was placed in a vertical position. A packing column was fitted to the top of the core holder to accommodate the excess sand mixture and water. The system was then vibrated overnight to obtain a tight pack. Before starting the experiments, the packing column

containing excess sand was removed, and the core holder was placed in a horizontal position.

#### 4.5.2. Packing the Radial Model

The objective of the radial model runs was to observe the production of sand under different operating conditions. Because the production of bulk sand rather than that of fines was of interest, sieving of the sand was not necessary. The radial model was packed using the sand or glass beads as supplied. The packing procedure involved gradually filling the cell with distilled water and sand, after fitting the perforated tubing in the cell. When the sand reached a specific height in the model, the excess water was emptied out, and the teflon disc and aluminum cover were placed over the sand. The hydraulic press was then used to apply the overburden pressure required, and the system was vibrated overnight at that pressure.

### 4.6. ANALYTICAL METHODS EMPLOYED

#### 4.6.1. Porosity Determinations

To determine the Berea sandstone porosity, the core was evacuated for 48 hours, and then allowed to imbibe 2.0% by weight brine. The volume of the brine imbibed into the pore space was assumed to be the pore volume.

The porosity in the radial model was determined for the 70 to 140 mesh Ottawa sand pack and the 40 to 70 mesh silica pack under two different overburden conditions. The procedure involved miscible displacement of 0.5% by weight brine by 2.0% brine. Samples of



effluent were collected and their refractive index measured using an Abbe refractometer. With the use of Figure 4, a plot of the percent displacing fluid in the effluent versus cumulative volume produced was made (see Figures 5 and 6). The areas above and below the S-shaped curve were balanced using a planimeter, and the pore volume determined. Having found the bulk volume by measuring the cell dimensions, the porosity was calculated. A sample calculation is provided in Appendix B, and the porosities obtained are shown in Table 3.

In the flow of fines experiments, porosity was determined for selected unconsolidated packs in the following manner: the mass of fines and sand packed in the core holder was measured, the total solids volume was obtained from the densities of materials used, and the porosity was calculated after determining the bulk volume of the core holder. A sample calculation is presented in Appendix B. The porosity of the remaining sand packs was estimated by using the value of porosity determined in packs consisting of similar grain type and size, and calculating the change in pore volume due to the change in the amount of fines present.

TABLE 3: Porosity of Radial Model Sand Packs

<u>Sand Pack Type</u>	<u>Overburden Pressure, kPa</u>	<u>Porosity, %</u>
Silica 40-70 Mesh	0	16.8
Silica 40-70 Mesh	1731.3	16.7
Ottawa Sand 70-140 Mesh	0	19.2
Ottawa Sand 70-140 Mesh	1731.3	20.8

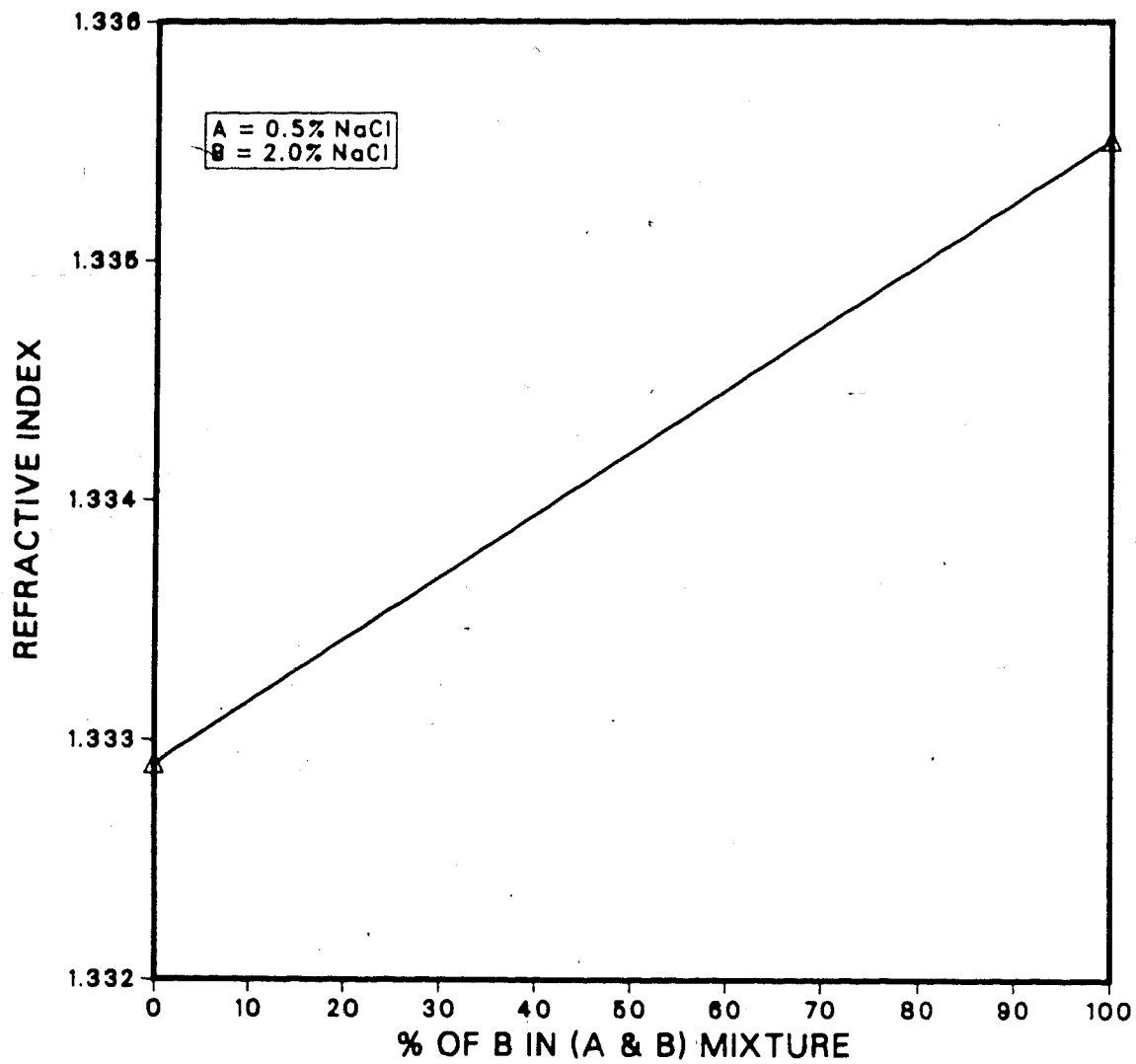


FIGURE 4 : Change of Refractive Index Due To Change in Brine Concentration

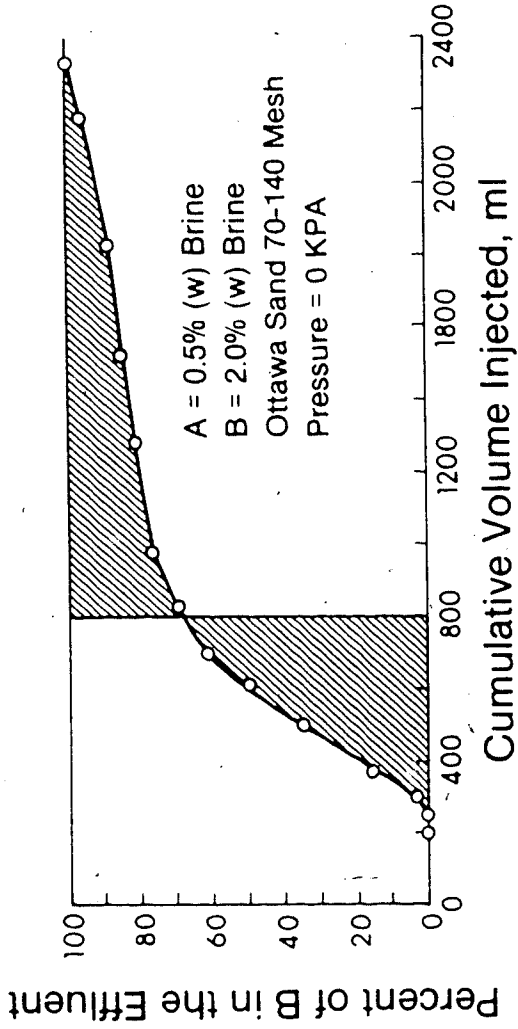


FIGURE 5(a): Determination of Pore Volume by Miscible Displacement of A by B.

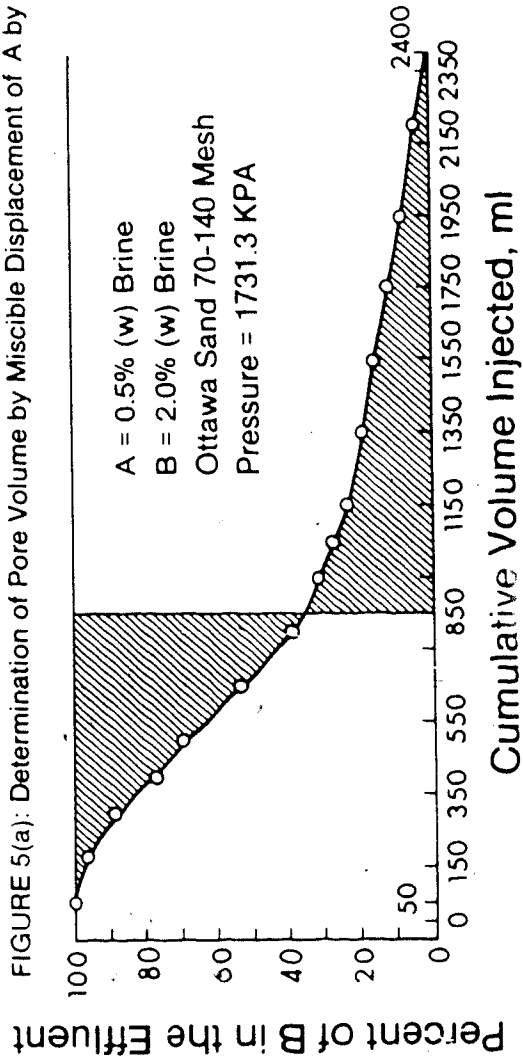


FIGURE 5(b): Determination of Pore Volume by Miscible Displacement of B by A.

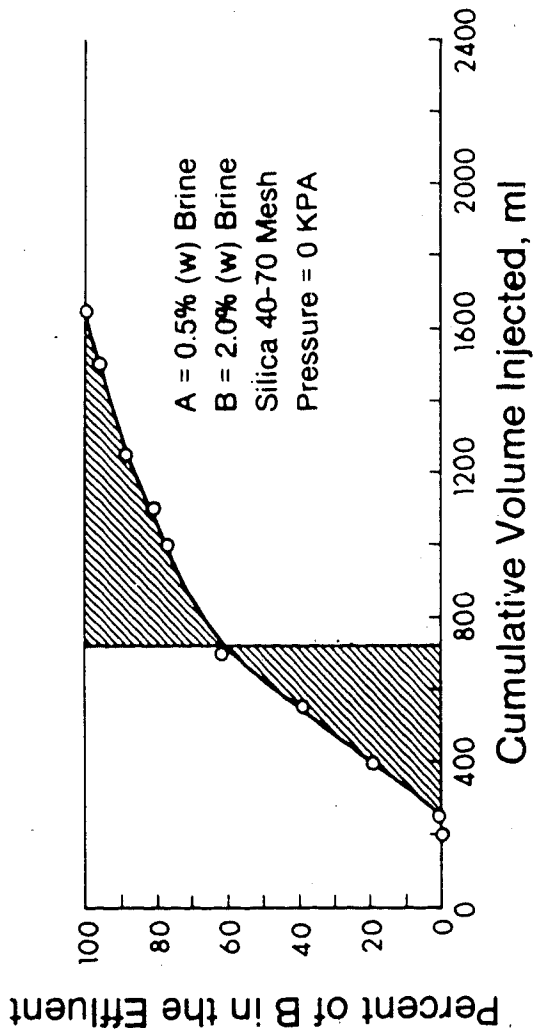


FIGURE 6(a): Determination of Pore Volume by Miscible Displacement of A by B.

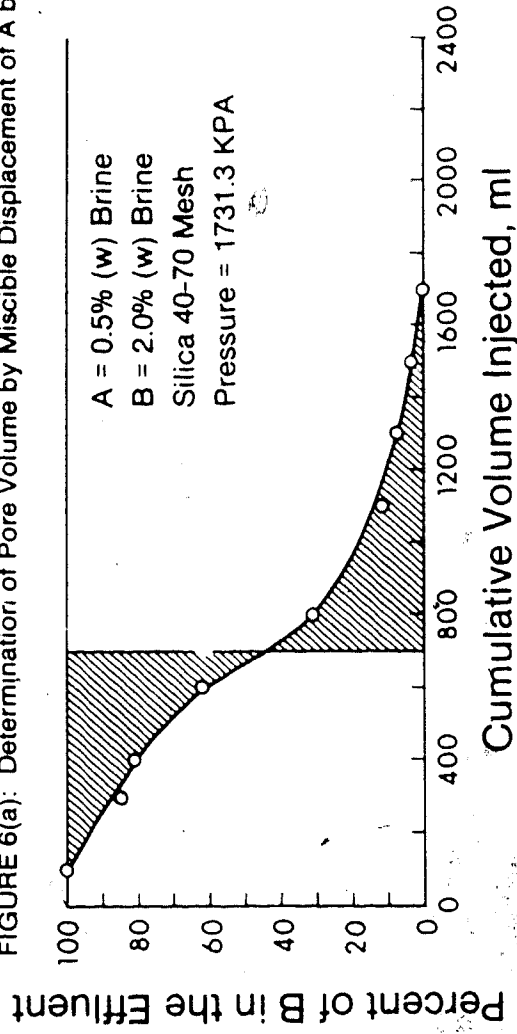


FIGURE 6(b): Determination of Pore Volume by Miscible Displacement of B by A.

#### 4.6.2. Determination of Absolute Permeability

The absolute permeability of the core was obtained by flowing 2.0% by weight brine at various rates and noting the pressure drop at each constant flow rate. Darcy's linear flow equation was then used to calculate the absolute permeability. For the linear sand packs, distilled water was used as the flowing fluid, and the permeability was evaluated on the basis of a single flow rate (see Table 4).

The absolute permeability of the radial model was estimated on the basis of the pressure drop across the cell which was very small, being approximately 0.125 kPa. Using Darcy's radial flow equation, the absolute permeability was determined to be of the order of  $3.5 \mu\text{m}^2$ .

#### 4.6.3. Determination of Relative Permeability

The relative permeability to Hamilton Lake crude and to brine was determined for each step in the two-phase flow test employing a graphical technique developed by Jones and Roszelle (1978). The experimental procedure consisted of saturating the core with brine, oil flooding to irreducible water saturation, then water flooding the core. During the water flooding stage, the effluents were collected, the amounts of water and oil measured, and the pressure drop and flow-rate recorded. The calculation details are presented in Appendix B.

Table 4: Properties of Linear Flow Sand Packs

Run#	Ave. Pres. Drop, kPa	Permeability, $\mu\text{m}^2$	Porosity, %
L1	4.757	11.570	29.0*
L2	9.515	5.787	20.9*
L3	10.894	5.054	20.9*
L4	23.856	2.308	13.9*
L5	29.510	1.866	11.7*
L6	11.445	8.001	20.9
L7	10.687	5.152	25.1
L8	17.995	3.060	16.2*
L9	2.896	19.013	20.9
L10	2.068	26.619	20.9*
L11	5.102	10.791	12.0*
L12	25.439	1.554	37.2*
L13	37.783	1.457	30.0
L14	5.998	9.179	24.2*
L15	36.956	1.490	16.7
L16	7.998	6.884	17.6
S1			42.0
S2			42.0*
S3			27.1*
S4			42.0*
S5			39.7
S6			39.7*
S7			39.7*
S8			49.5*
S9			39.8
S10			39.8

\*: Estimated Values  
 S: Small Core Holder Experiments  
 L: Large Core Holder Experiments

#### 4.7 ANALYSIS OF EFFLUENT SAMPLES

In the experiments investigating the movement of fines, samples of effluent were collected and analyzed to determine the concentration of suspended particles. Charts of concentration of fines in Nephelometric Turbidity Units (NTU) versus concentration in  $\text{g/cm}^3$  were developed for each type of fines used by preparing samples of known concentrations and measuring their corresponding NTU values. Each sample collected was poured into a special transparent vial and placed in the turbidimeter, which indicated the fines content of the sample in NTU. The NTU reading was then converted into  $\text{g/cm}^3$  using the appropriate conversion chart. The conversion graphs are shown in Appendix C.

The NTU reading was found to be dependent on the size of particles in suspension. For instance, at a particle concentration of  $0.0019 \text{ g/cm}^3$ , a turbidimeter reading of 48 NTU was obtained when the average particle size was  $95 \mu\text{m}$  and a reading of 88 NTU was obtained for particles smaller than  $44 \mu\text{m}$ . Similarly, at a particle concentration of  $0.0088 \text{ g/cm}^3$ , the turbidimeter reading was 300 NTU for particles having an average size of  $95 \mu\text{m}$  and 600 NTU for particles smaller than  $44 \mu\text{m}$ .

## 5. DISCUSSION OF RESULTS

### 5.1. PRESENTATION OF THE EXPERIMENTAL RESULTS

In this study, three types of experimental tests were carried out: linear flow tests, radial flow tests, and two-phase flow tests. Results of linear flow tests are presented in Figures 13 to 29, and the experimental data is given in Tables C1 to C26. Results of radial flow tests are presented in Figures 30 to 49, and the corresponding data is given in Tables C27 to C47. Two-phase flow results are shown in Figure 50, and the detailed experimental data are provided in Tables C48 to C51. All of the important run parameters are indicated in the figures and tables for convenience.

### 5.2. CHARACTERISTICS OF GLASS BEADS, OTTAWA SAND AND FINES

The materials used to represent unconsolidated porous media were Ottawa sand, glass beads and silica. The fines consisted of glass beads, barite, or calcium carbonate. The calcium carbonate was delivered in powder form, and did not require any sieving because particle sizes were already well below 325 mesh. The barite was sieved to yield fines smaller than 325 mesh. The glass fines were obtained by sieving spherical beads that were supplied in bags with nominal size ranges of 80 to 120 mesh, 120 to 200 mesh, and 170 to 325 mesh. Scanning electron microscope (SEM) photographs of the barite, glass beads, and calcium carbonate fines are shown in Figure 7. Figure 7(a) indicates that the  $\text{CaCO}_3$  fines were present in flocculated form. Individual particles were difficult to distinguish; however, the average particle diameter



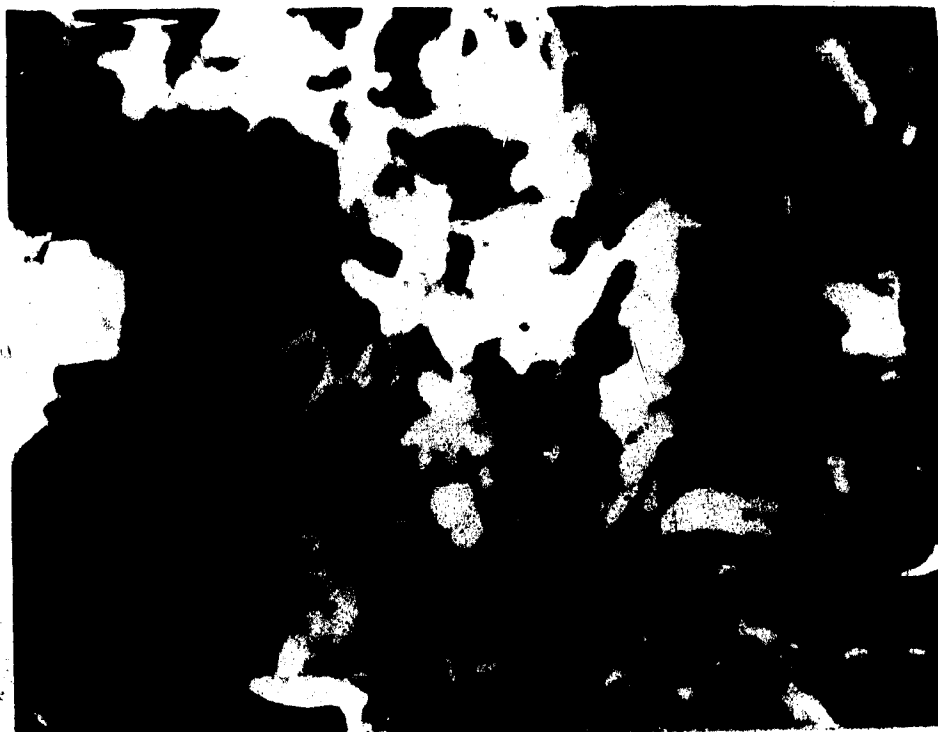


FIGURE 7(a): SEM Photomicrograph of Calcium Carbonate Fines  
Magnification: 6400x

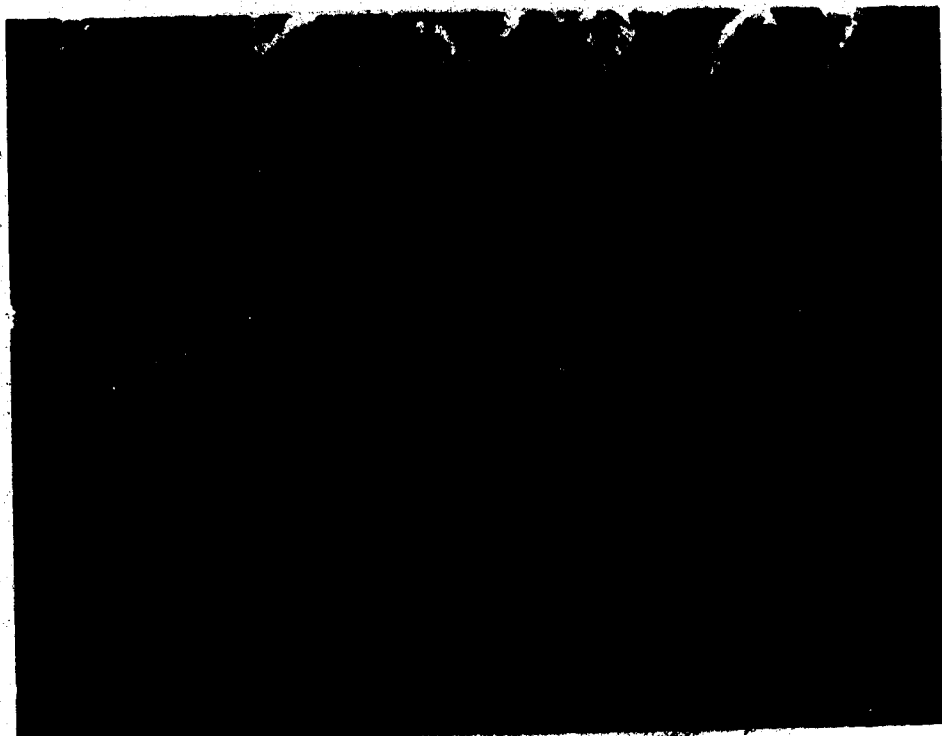


FIGURE 7(b): SEM Photomicrograph of Barite Fines  
Magnification: 2400x

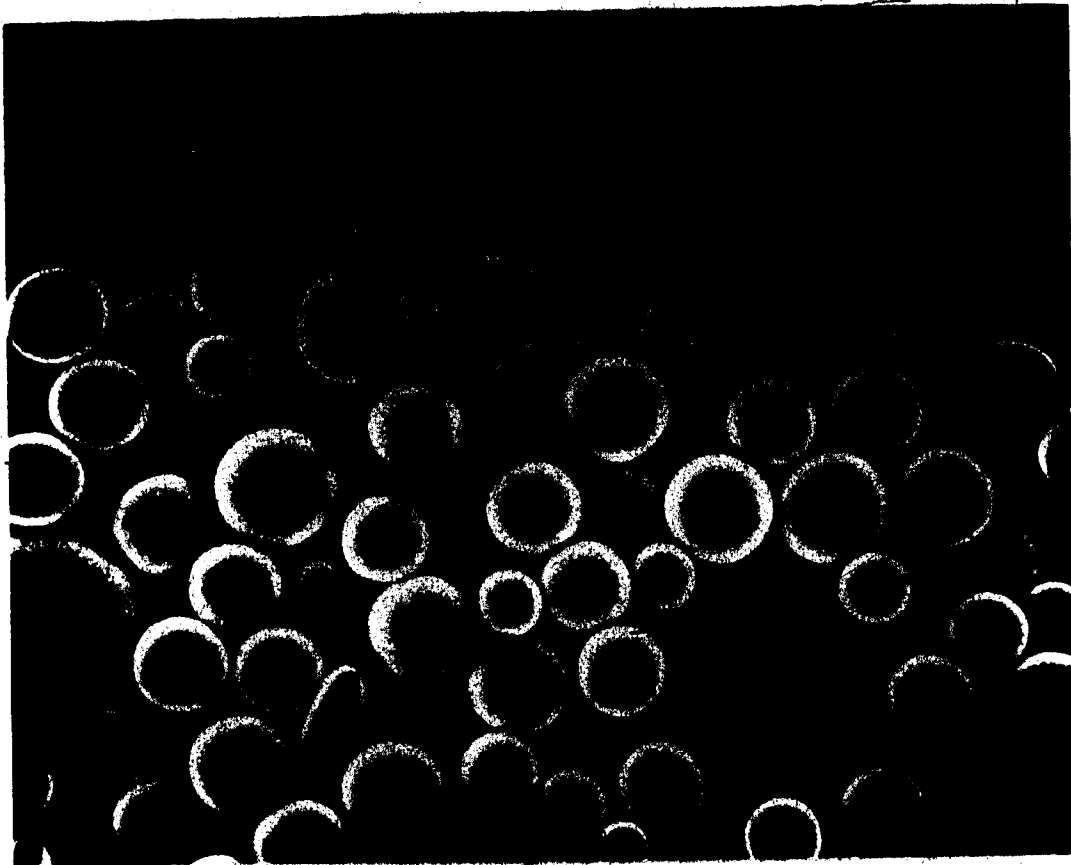


FIGURE 7(c): SEM Photomicrograph of Glass Beads Fines  
Magnification: 240×

was estimated to be about 1.4  $\mu\text{m}$ . Barite fines were angular and had a narrow particle size range, while glass fines were spherical and of a much wider size range. The particle size distribution was determined by measuring the dimensions of all particles in the forefront of the photograph, and determining the percent volume in each particle diameter range. A sample particle size distribution calculation is provided in Appendix B.

Ottawa sand and silica were delivered in bags with nominal size ranges of 70 to 140 mesh, and 40 to 70 mesh, respectively. While these materials were used as supplied in radial flow experiments, sieving of the sands was necessary for the linear experiments studying the flow of fines. SEM photomicrographs of sieved Ottawa sand 50 to 100 mesh, silica 40 to 70 mesh, and glass beads 100 to 325 mesh are shown in Figure 8.

In addition, SEM photomicrographs were taken of the Ottawa sand as supplied, and after being produced in a radial flow test at an overburden load of 1731.3 kPa (see Figure 9). The purpose of this SEM analysis was to find out if crushing of the sand grains was occurring at high overburden pressures. As indicated by the photographs and the size distribution plots, no apparent shift in particle size was discerned when the sand was produced under high overburden loads.

The particle size distribution curves, determined from SEM analysis of the photomicrographs, are plotted in Figures 10, 11 and 12.

### 5.3. LINEAR FLOW TESTS

Previous studies of the movement of fines in porous media revealed that, depending on the fine particles size, either physical or

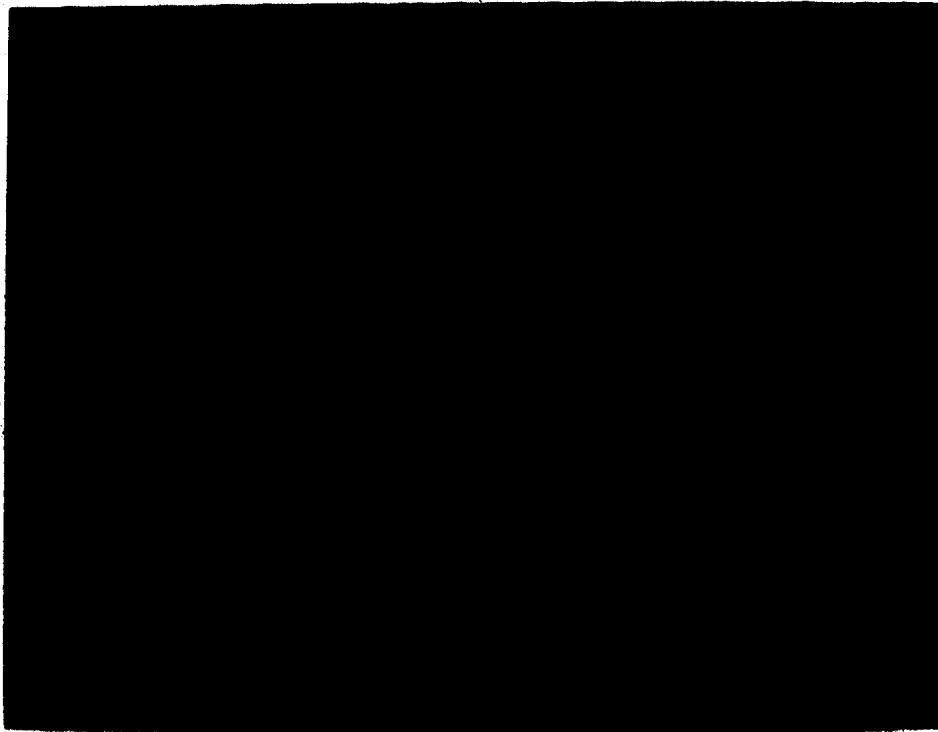


FIGURE 8(a): SEM Photomicrograph of Ottawa Sand 50 - 100 Mesh  
Magnification: 72x



FIGURE 8(b): SEM Photomicrograph of Glass Beads 100 - 325 Mesh  
Magnification: 240x



FIGURE 8(c): SEM Photomicrograph of Silica 40 - 70 Mesh  
Magnification: 72x

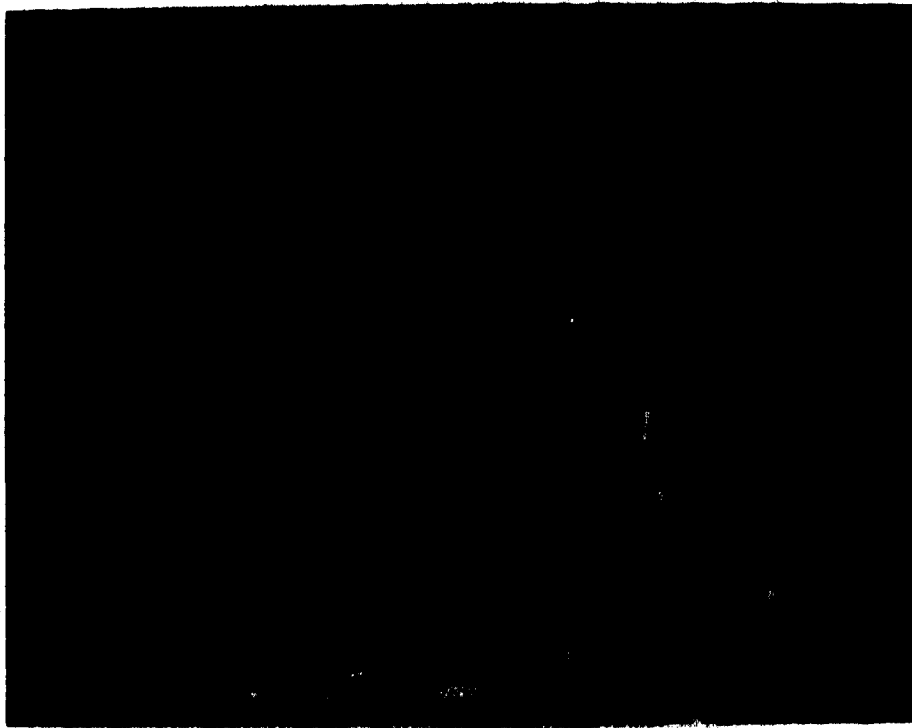


FIGURE 9(a): SEM Photomicrograph of Ottawa Sand 70 - 140 Mesh  
Magnification: 72x

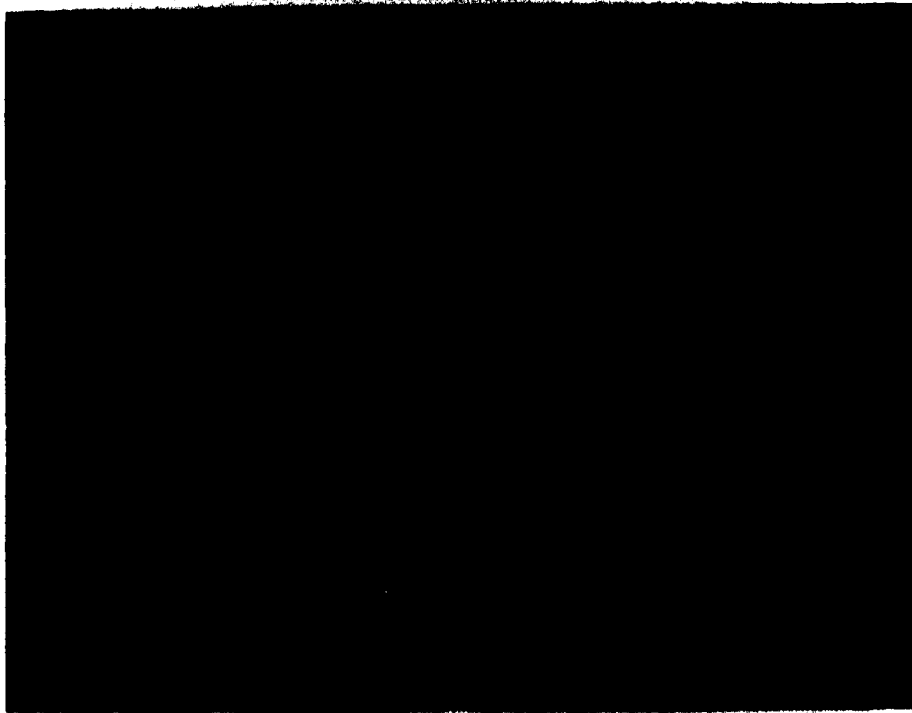


FIGURE 9(b): SEM Photomicrograph of Ottawa Sand 70 - 140 Mesh  
Produced at 1731.3 kPa - Magnification: 72x

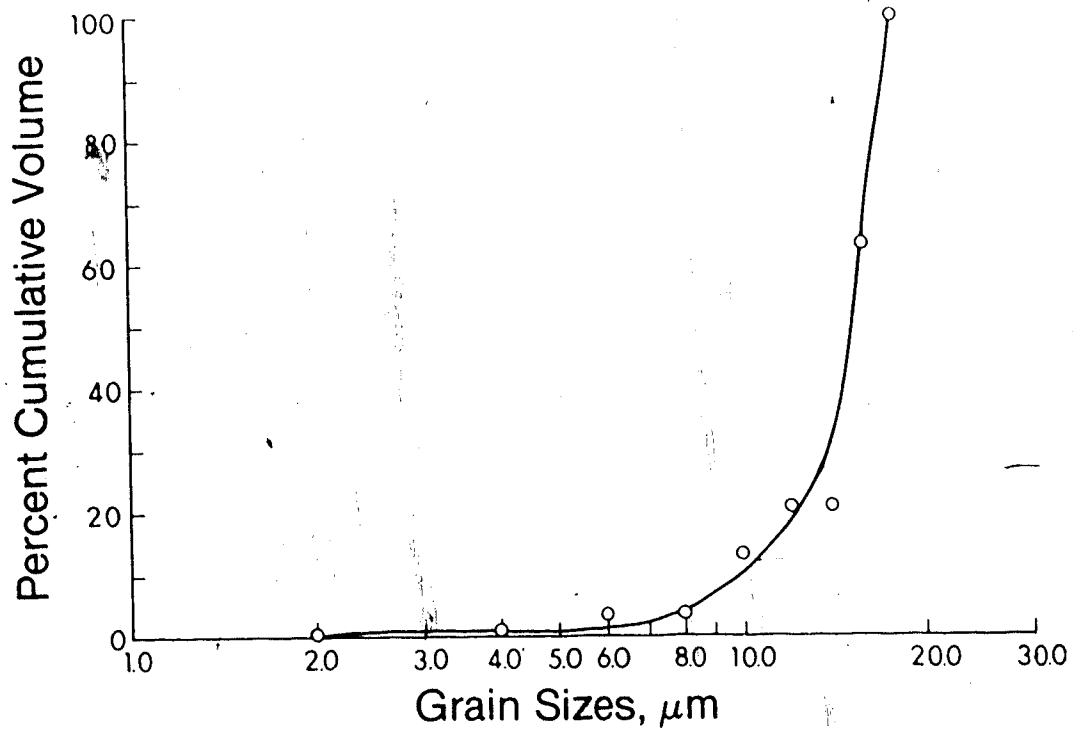


FIGURE 10(a): Size Distribution of Barite Fines

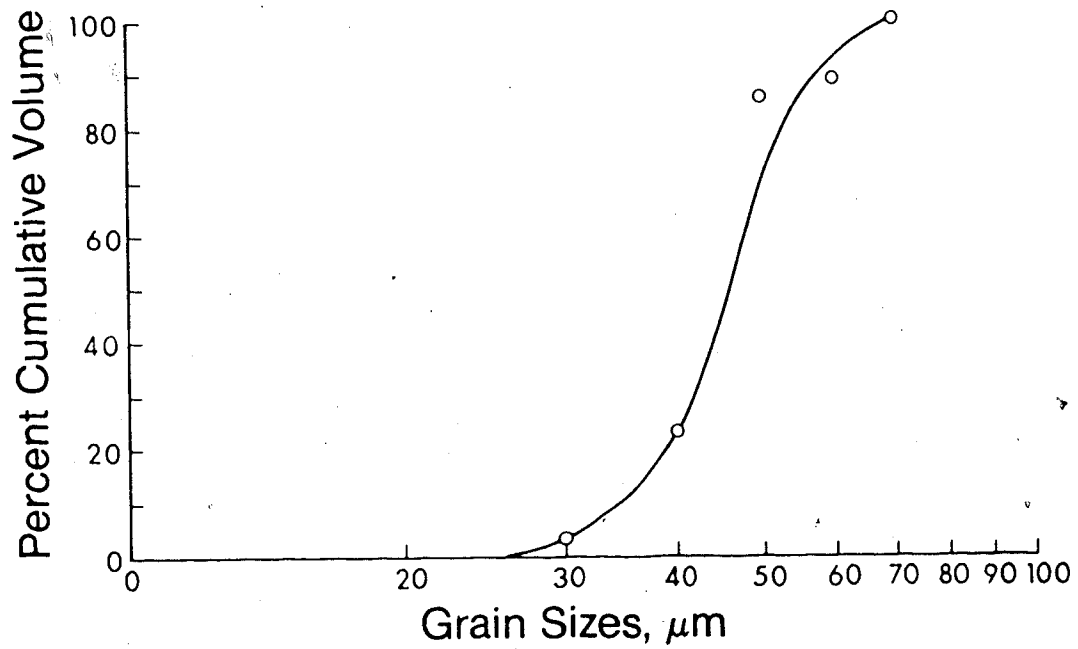


FIGURE 10(b): Size Distribution of Glass Beads Fines

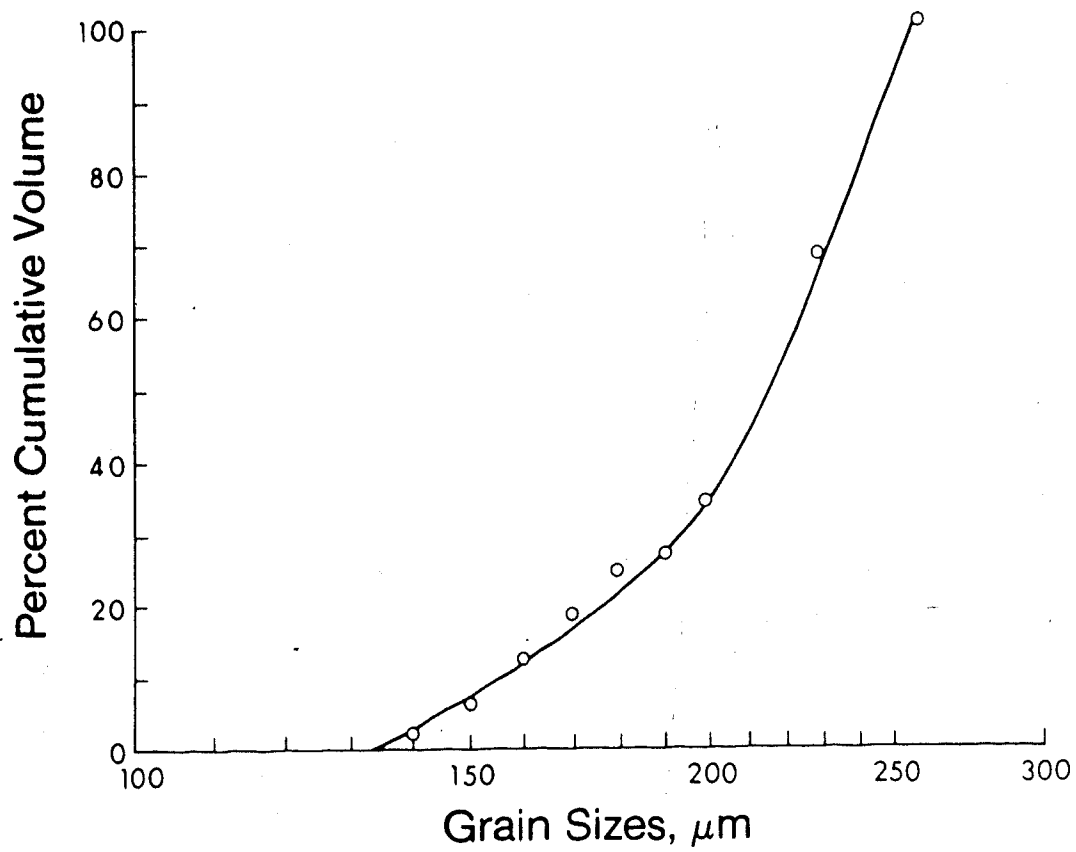


FIGURE 11(a): Size Distribution of Ottawa Sand 50-100 Mesh

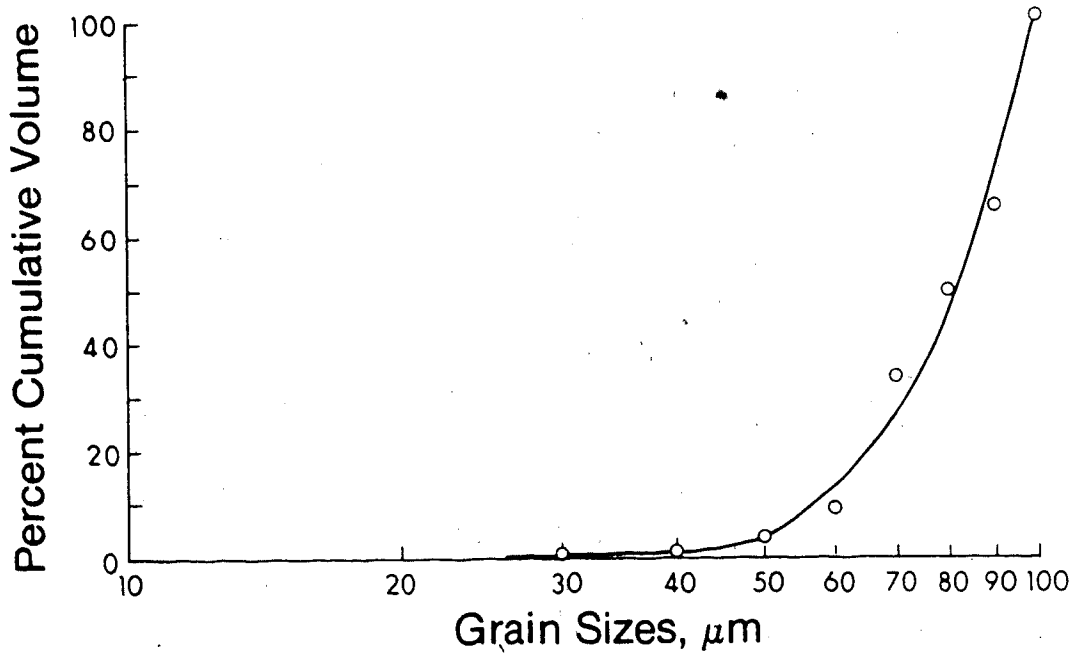


FIGURE 11(b): Size Distribution of Glass Beads 100-325 Mesh



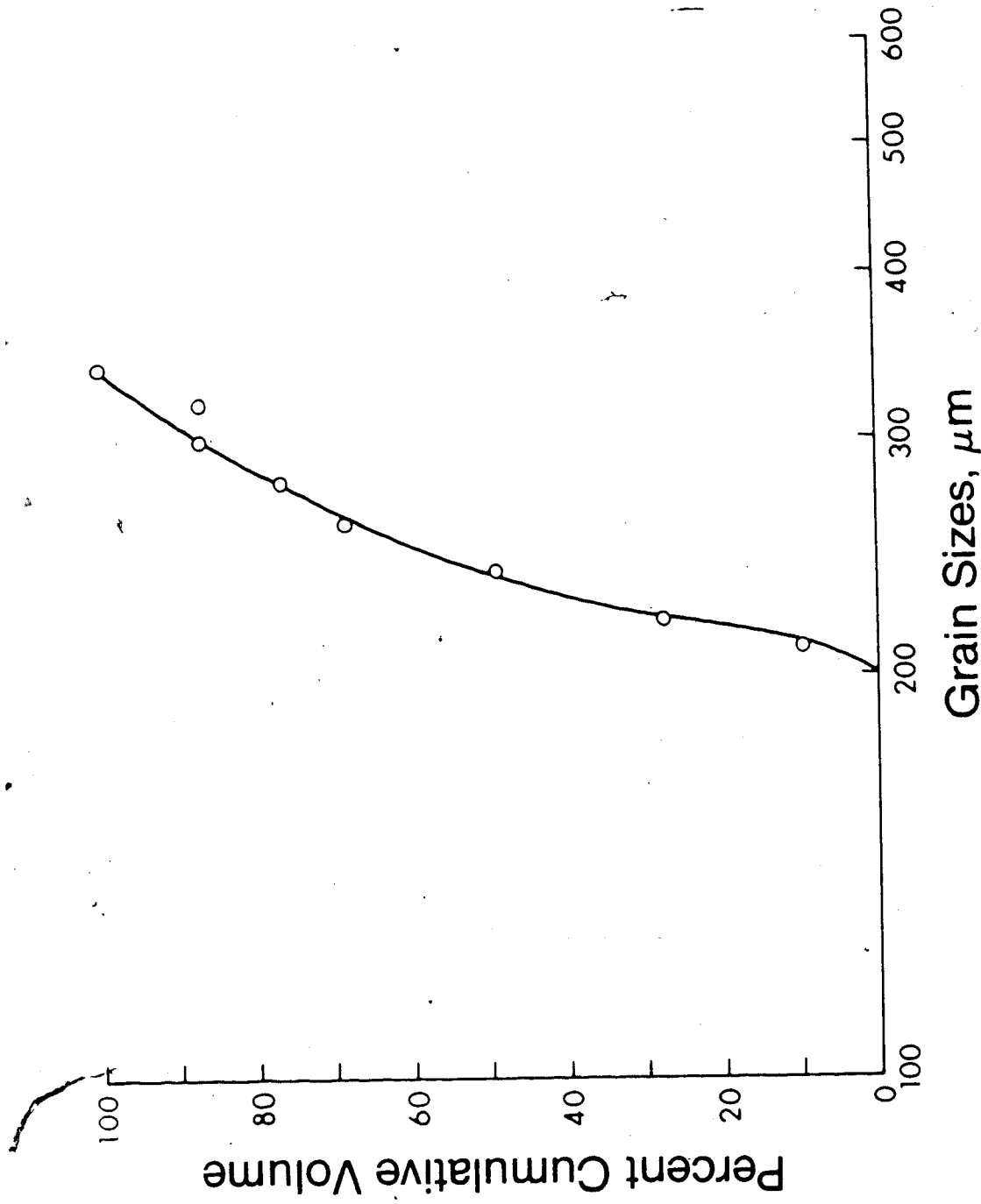


FIGURE 11(C): Size Distribution of Silica 40-70 Mesh

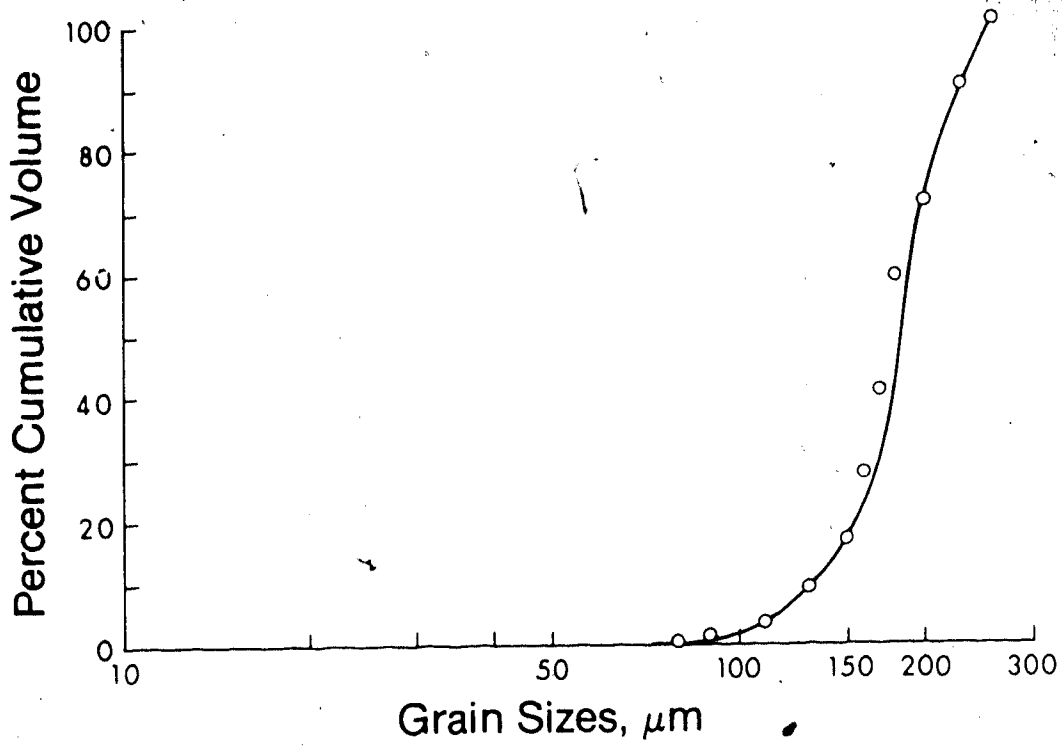


FIGURE 12(a): Size Distribution of Ottawa Sand 70-140 Mesh

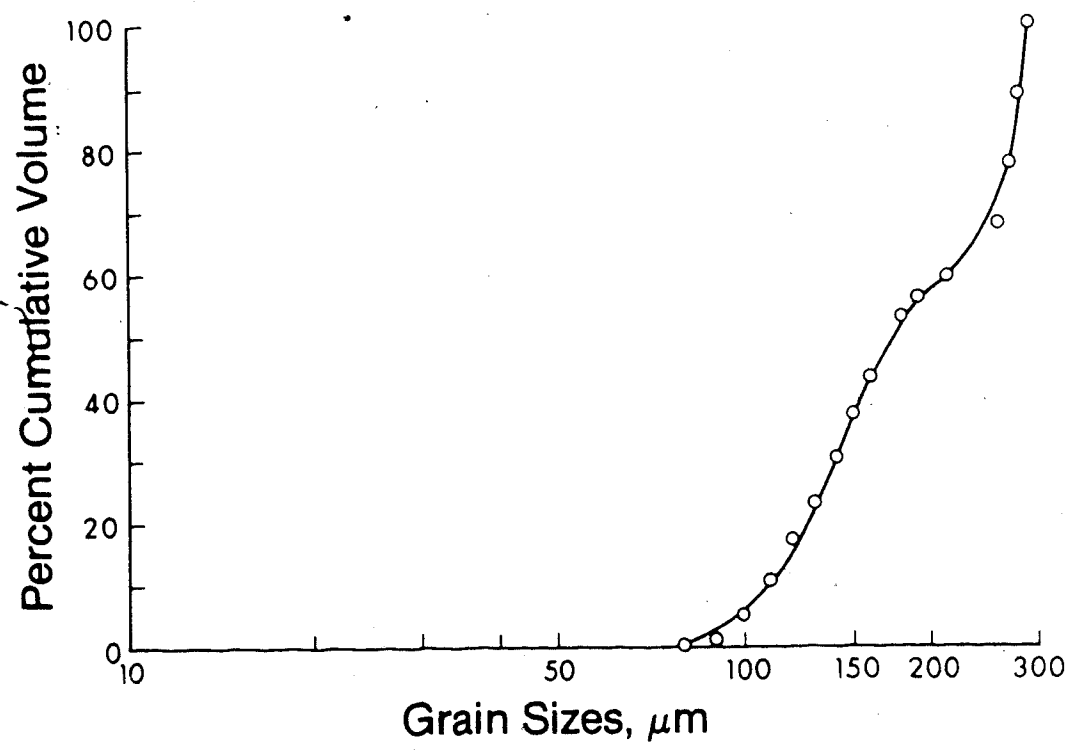


FIGURE 12(b): Size Distribution of Ottawa Sand 70-140 Mesh Produced at 1731.3 kPa

chemical factors played a dominant role. SEM analysis of the glass fines used in the linear experiments showed that the particles ranged from 30  $\mu\text{m}$  to 70  $\mu\text{m}$  in diameter. In this size range, the flow of fines was reported to be influenced by physical variables (Merzig, LeClerc and Le Goff, 1970). The linear flow experiments were designed to identify the various physical factors influencing the flow of fines, and the relative impact of each variable on the flow mechanisms.

The tests were conducted in two core holders of different sizes. The small core flow tests served to develop the experimental technique and obtain qualitative information on the flow of fines, while the large core flow tests were carried out to obtain detailed quantitative data. A summary of the experimental results is provided in Table 5.

#### 5.3.1. Small Core Experiments

Ten runs were carried out using the small core holder. The experimental conditions varied were: the initial mass of fines in the sandpack, the distilled water flow rate, the sandpack grain size, and the packing method.

In Runs 1 and 2, the core holder was packed with glass beads 50 to 100 mesh mixed with 20.0 grams of glass fines, which corresponded to 15.1% of the total pore volume. Distilled water was flowed through the pack at a rate of 8 ml/minute, corresponding to an interstitial velocity of 0.069 cm/s. The concentration of fines in the effluent samples was determined, and the mass of fines in each sample was calculated. The results of the small core linear tests are shown in Tables G1 to C10.

Table 5: Summary of Linear Flow Tests

Run#	Porosity $\phi$ , %	Permeability, $\mu\text{m}^2$	Darcy Vel., cm/s	Inter- stitial Vel., cm/s	Sand Size, $\mu\text{m}$	Sand Shape
S1	42.0		0.029	0.069	147-283	Spherical
S2	42.0		0.029	0.069	147-283	Spherical
S3	27.1*		0.029	0.107	147-283	Spherical
S4	42.0		0.015	0.036	147-283	Spherical
S5	39.7		0.029	0.073	3327-4699	Spherical
S6	39.7		0.029	0.073	3327-4699	Spherical
S7	39.7		0.029	0.073	3327-4699	Spherical
S8	49.5*		0.029	0.059	147-283	Spherical
S9	39.8		0.029	0.073	147-283	Spherical
S10	39.8		0.029	0.073	147-283	Spherical
L1	29.0*	11.570	0.012	0.041	147-283	Angular
L2	20.9*	5.787	0.012	0.057	147-283	Angular
L3	20.9*	5.054	0.012	0.057	147-283	Angular
L4	13.9*	2.308	0.012	0.086	147-283	Angular
L5	11.7*	1.866	0.012	0.103	147-283	Angular
L6	20.9	8.001	0.020	0.096	147-283	Angular
L7	25.1	5.152	0.012	0.048	44-147	Angular
L8	16.2*	3.060	0.012	0.074	44-147	Angular
L9	20.9	19.013	0.012	0.057	187-369	Angular
L10	20.9*	26.619	0.012	0.057	187-369	Angular
L11	12.0*	10.791	0.012	0.100	187-369	Angular
L12	37.2*	1.554	0.012	0.032	44-147	Spherical
L13	30.0	1.57	0.012	0.040	44-147	Spherical
L14	24.2*	9.179	0.012	0.050	147-283	Angular
L15	16.7	1.490	0.012	0.072	147-283	Angular
L16	17.6	6.884	0.012	0.068	187-369	Angular

S: Small Core Holder Experiments  
 L: Large Core Holder Experiments  
 \*: Estimated Values

Table 5: (Continued)

Run#	Type of Fines	Initial Amount of Fines, % Pore Volume	Fines Produced, % of Initial Fines	Table #
S1	Glass beads	15.1	0.125	C1
S2	Glass beads	15.1	0.123	C2
S3	Glass beads	45.3	0.051	C3
S4	Glass beads	15.1	0.049	C4
S5	Glass beads	15.9	0.268	C5
S6	Glass beads	15.9	0.304	C6
S7	Glass beads	15.9	0.371	C7
S8	None added	0.0	*0.022	C8
S9	Glass beads	15.8	0.163	C9
S10	Glass beads	15.8	0.160	C10
L1	None added	0.0	**0.008	C11
L2	Glass beads	29.3	0.241	C12
L3	Glass beads	29.3	0.158	C13
L4	Glass beads	52.2	0.470	C14
L5	Glass beads	59.5	1.330	C15
L6	Glass beads	32.6	0.380	C16
L7	None added	0.0	**0.097	C17
L8	Glass beads	35.4	0.159	C18
L9	None added	0.0	**0.592	C19
L10	None added	0.0	**0.518	C20
L11	Glass beads	42.5	0.781	C21
L12	None added	0.0	**0.576	C22
L13	Glass beads	19.3	0.578	C23
L14	Barite	16.4	0.002	C24
L15	Barite	16.5	0.002	C25
L16	Calcium Carbonate	25.4	0.300	C26

S: Small core Holder Experiments

L: Large Core Holder Experiments

\*: Based on 20 g

\*\* : Based on 100 g

To determine the effect of mass of fines in the pack, Run 3 was carried out by mixing 60.0 grams of fines (45.3% P.V.) in the pack and keeping all other experimental conditions unchanged.

Run 4 was conducted to determine the effect of flow rate. All conditions were similar to those of Run 1, except the flow rate, which was changed to 4 ml/minute (or interstitial velocity of 0.036 cm/s).

To determine the effect of grain size, the core holder in Runs 5, 6 and 7, was packed with glass beads 4 to 6 mesh.

Run 8 differed from Run 1 in that no fines were added to the pack.

While all the experiments discussed above were wet packed, Runs 9 and 10 were conducted using a dry packing procedure in order to evaluate the effect of the packing method.

#### 5.3.2. Small Core Results

The concentration of fines in the effluent samples from Runs 1 and 3 are plotted in Figure 13. Increasing the initial amount of fines in the pack from 15.1% P.V. to 45.3% P.V. resulted in an increase of 22.5% in the concentration of fines, which occurred mostly in the first 80 ml of outlet volume. The concentration of fines in the effluent samples of both runs was found to decrease to zero after the passage of about 140 ml of distilled water through the pack.

The effect of flow rate on the concentration of fines in the effluent is shown in Figure 14. The concentration was reduced by 60.5% when the flow rate was decreased from 8 ml/minute to 4 ml/minute. A decrease in the concentration of fines to a negligible

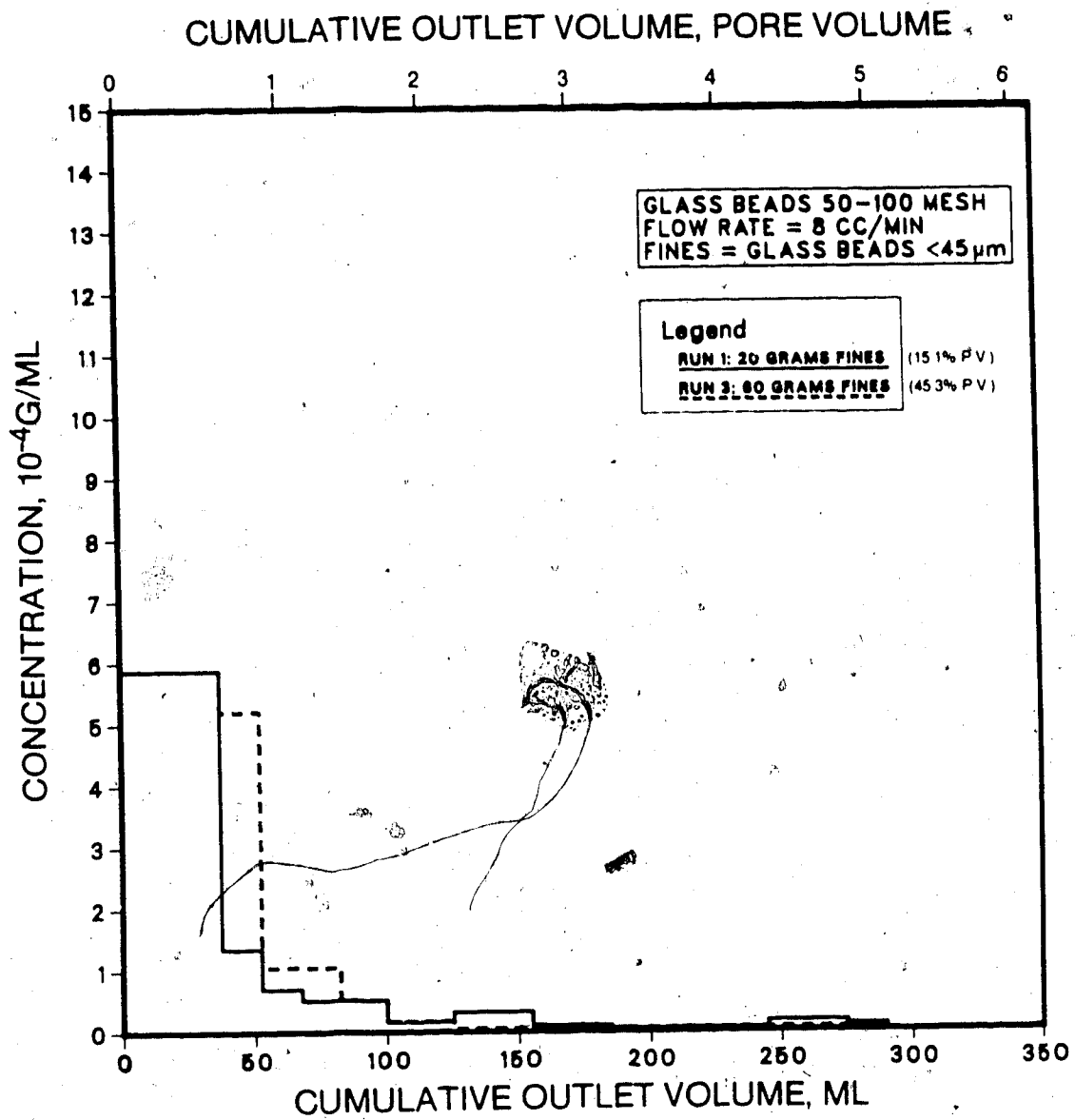


FIGURE 13 : Effect of Mass of Glass Fines

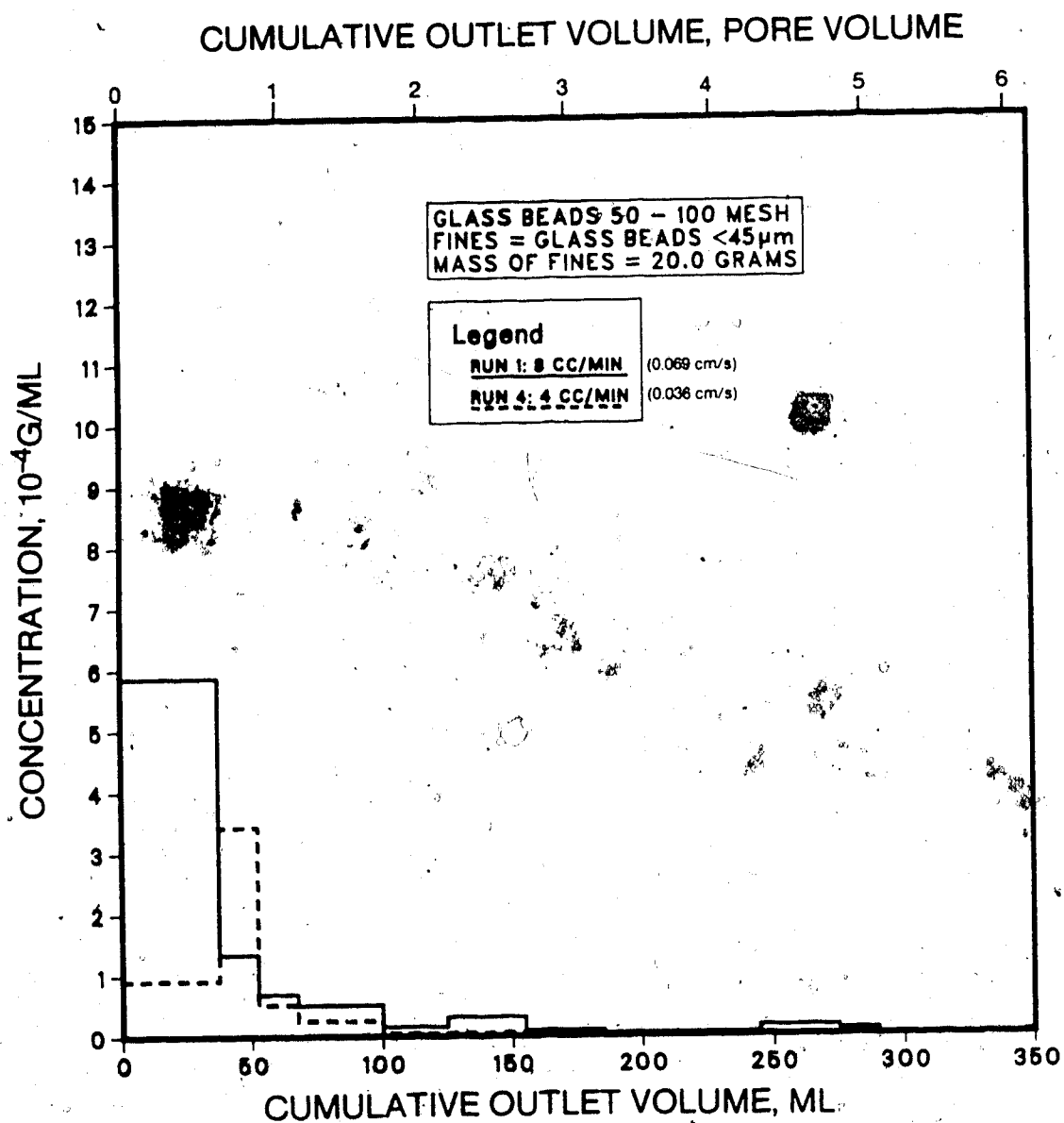


FIGURE 14 : Effect of Flow Rate



value was also noted in Run 4, after flowing about 140 ml of water through the pack.

As shown in Figure 15, the outlet concentration of fines was drastically increased (114.7%) when the core holder was packed with glass beads 4 to 6 mesh in size.

Run 8 was carried out to determine whether the concentration of fines measured at the outlet was exclusively brought about by the amount of fines added to the sandpack. As shown in Figure 16, when no fines were mixed with the pack, a very low concentration was observed, and was probably due to the presence of fines that adhered to larger grains of the glass bead pack, and were not removed by sieving.

The outlet concentrations obtained for dry packing were different from those obtained for wet packing. As shown in Figure 17, dry packing resulted in a high concentration of fines in the first 30 ml of effluent, followed by a sharp decrease in concentration to approximately zero. Wet packing caused a more gradual change in concentration to occur. This difference in the outlet concentrations was probably due to the difference in the interstitial velocities in the packs. As shown in Table 5, the porosity of the wet pack in Run 1 was 42.0%, and that of the dry pack in Run 9 was 39.8%. As a result, the interstitial velocity in Run 9 (0.073 cm/s) was higher than that in Run 1 (0.069 cm/s). This and the fact that dry packing was used in Run 9, caused the total amount of fines released in the dry packing run to be 30.8% higher than the amount released in the wet packing run.

The reproducibility of the experiments was investigated in Runs 2, 6 and 10, which were carried out under the same experimental conditions.

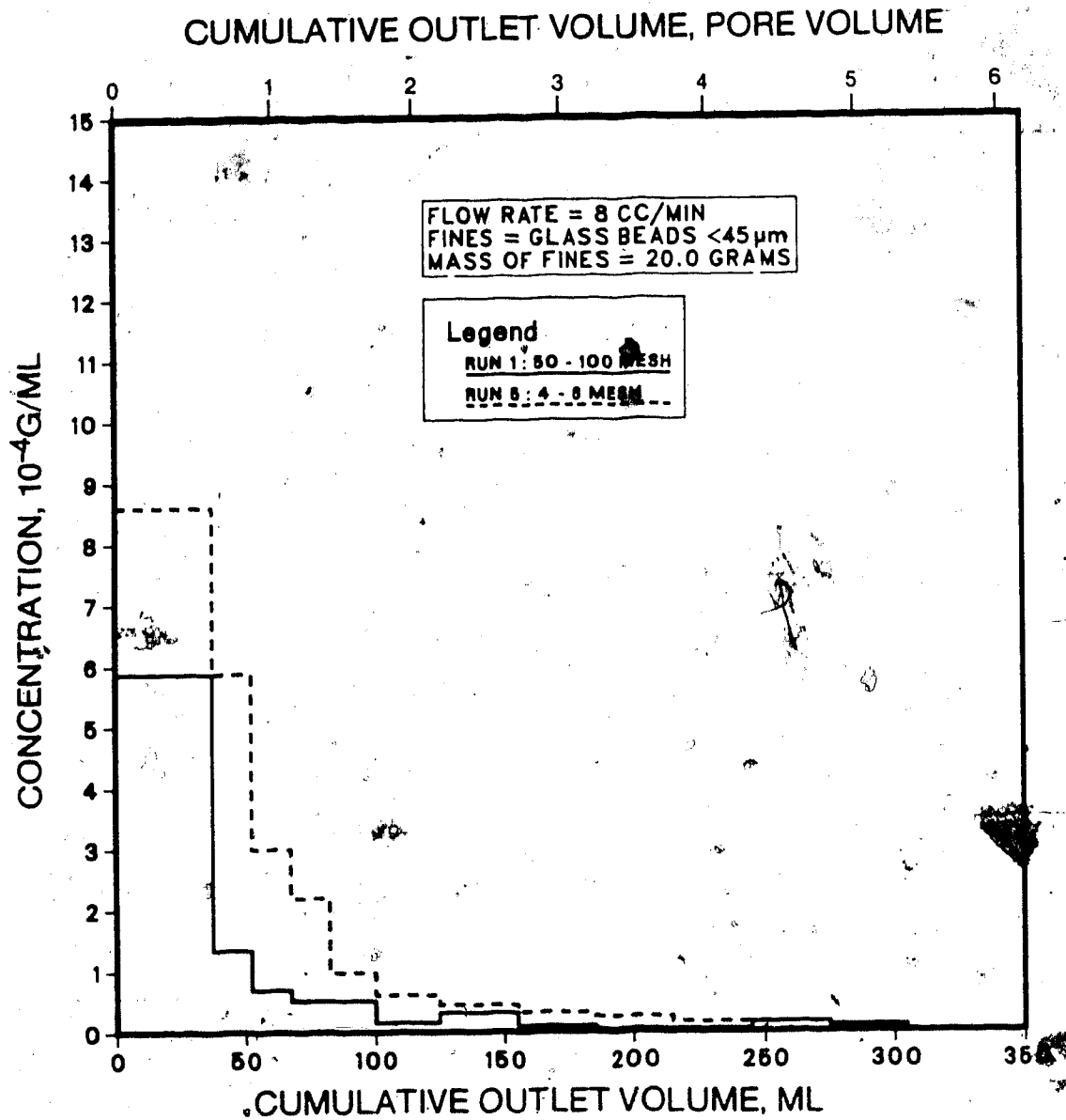


FIGURE 15 : Effect of Grain Size

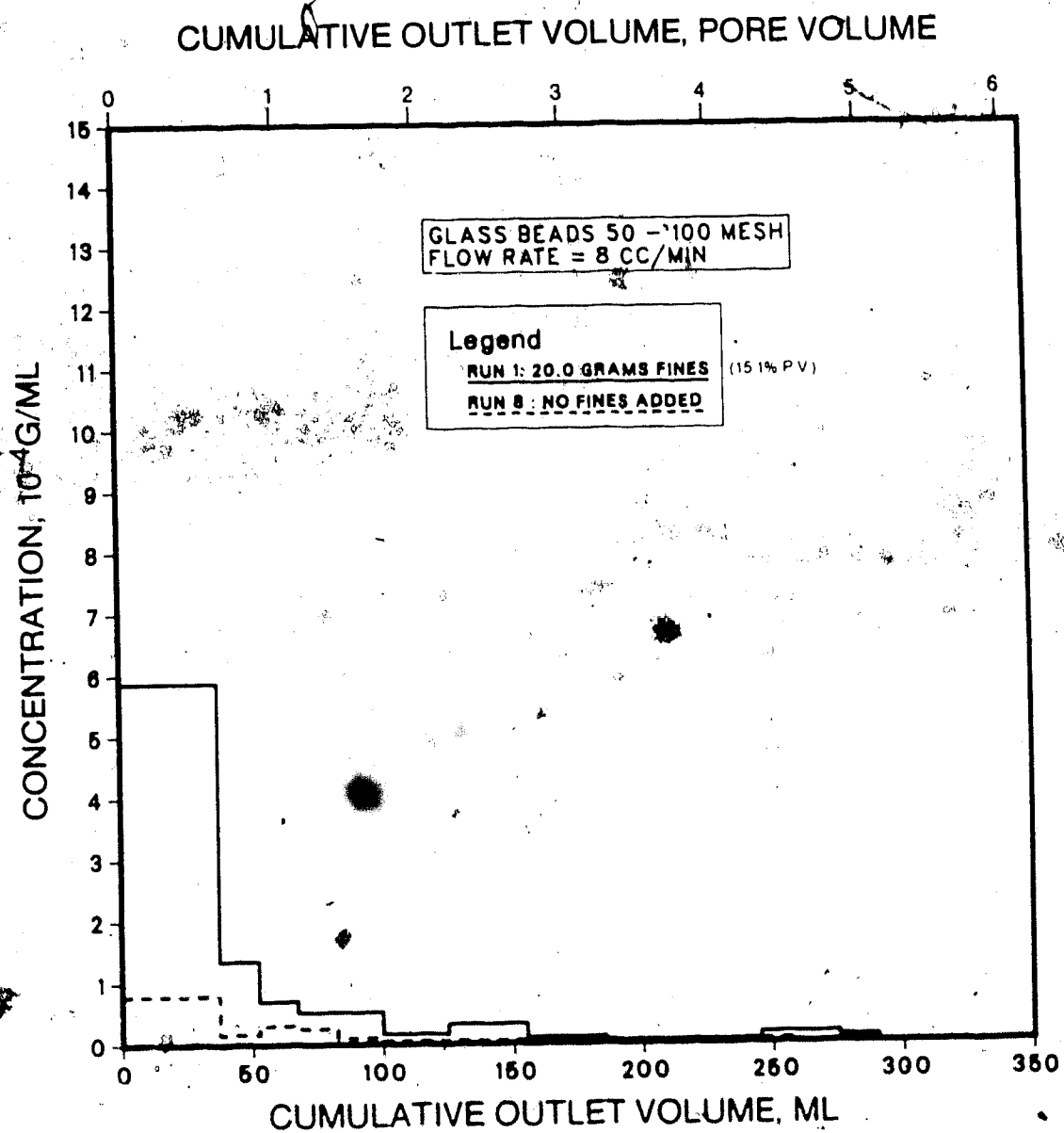


FIGURE 16 : Effect of Absence of Fines

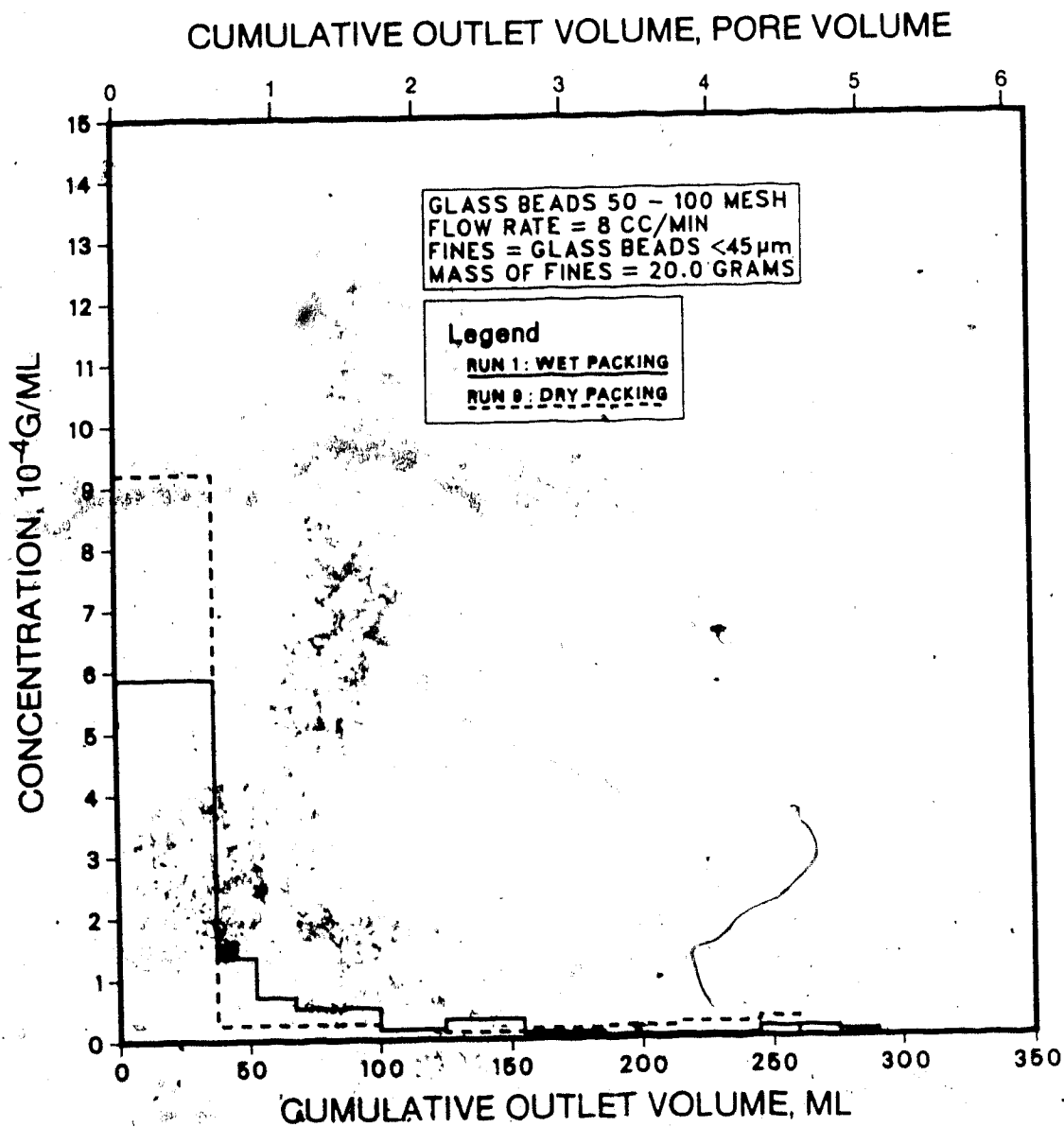


FIGURE 17 : Effect of Packing Method

as those for Runs 1, 5 and 9, respectively. As shown in Figure 18, for the smaller grain size, the concentration of fines in the effluent samples was different for each run, however, the total amount of fines produced in Run 2 was only 1.4% lower than that for Run 1. Figure 19 depicts the reproducibility for the larger grain size. Outlet concentrations also varied for each run, and the amount of fines released in Run 6 was 13.6% higher than that for Run 5. Better reproducibility was obtained when the dry packing method was employed. Figure 20 shows that the concentration of fines in the effluents was approximately the same for Runs 9 and 10, and the total amount of fines released in Run 10 was 1.9% lower than that for Run 9.

### 5.3.3. Large Core Experiments

In addition to the experimental variables investigated in the small core runs, the large core tests were conducted to study the effect of grain shape, fines size and density, and sandpack size. The experimental results of the large core linear tests are listed in Tables C11 to C26.

Runs 2 and 3 consisted of packing the large core holder with 50 to 100 mesh Ottawa sand, mixed with 103 grams of glass fines (29.3% P.V.), and flowing distilled water through the pack at a rate of 8 ml/minute (or interstitial velocity of 0.057 cm/s). The pressure drop across the core was recorded for each effluent sample, and the concentration of fines in the samples was determined.

In Runs 4 and 5, the amount of glass fines mixed with the sand pack was changed to 183 grams (52.2% P.V.) and 209 grams (59.5% P.V.) respectively, while the other variables were kept unchanged.

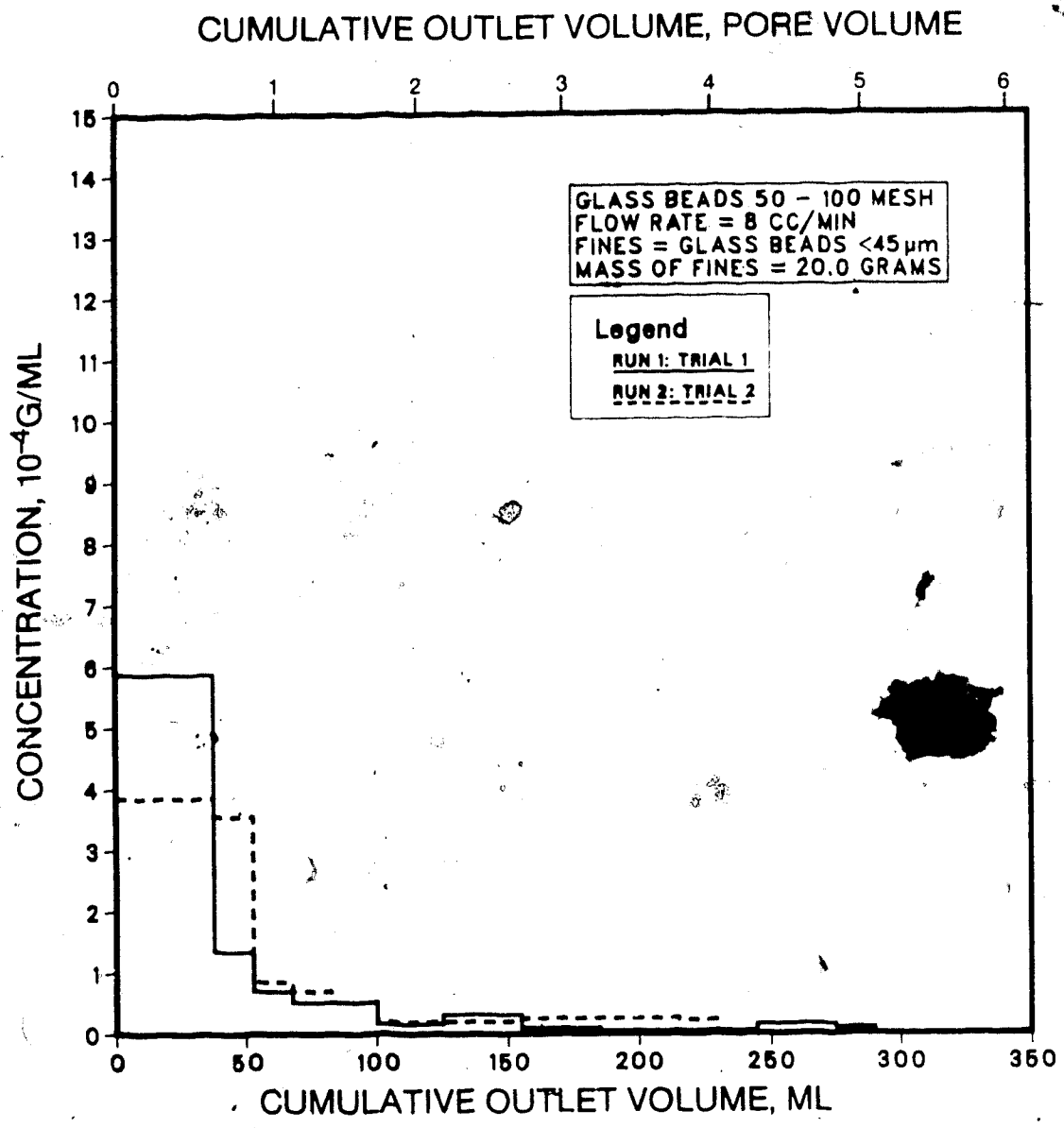


FIGURE 18 : Reproducibility of Small Grain Size

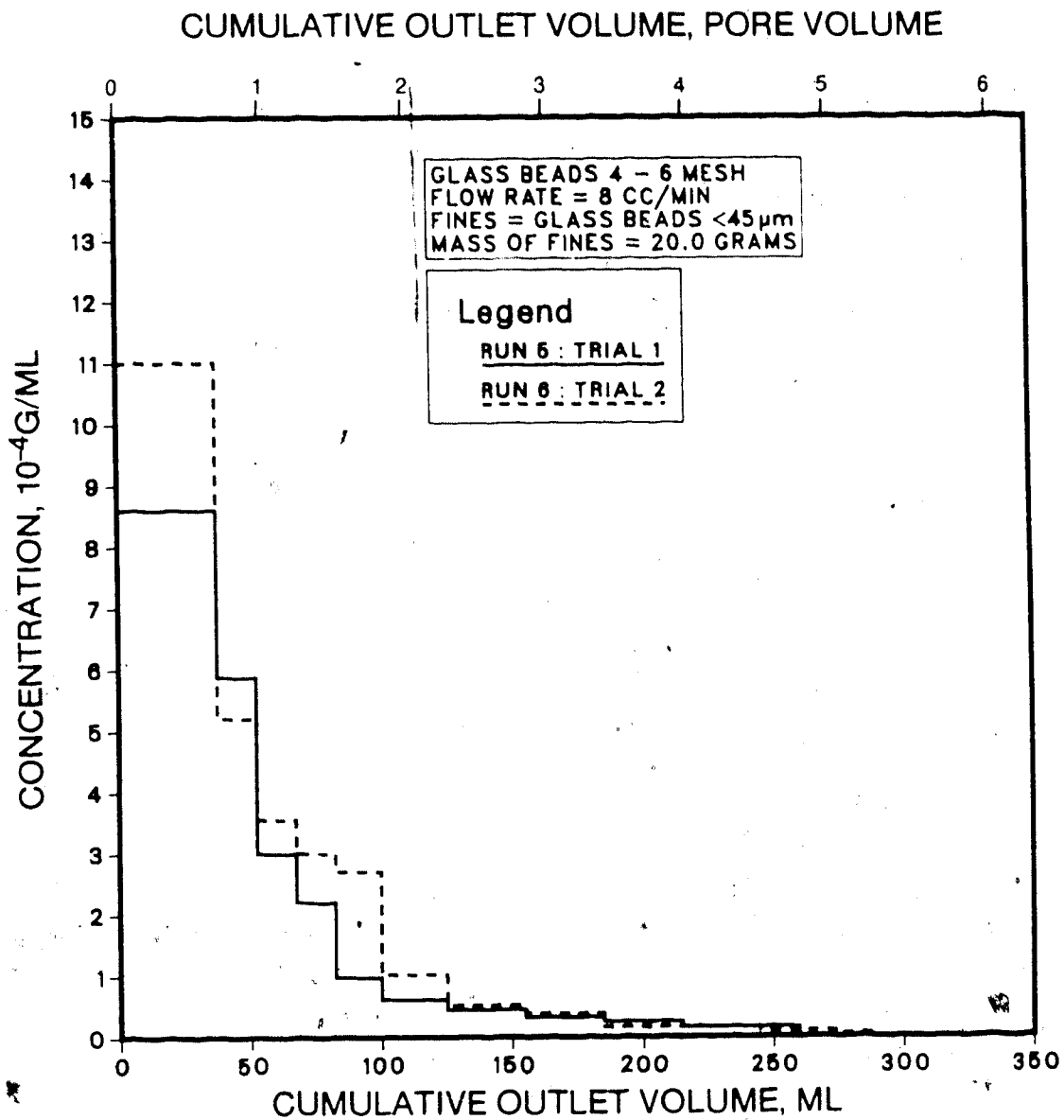


FIGURE 19 : Reproducibility of Large Grain Size

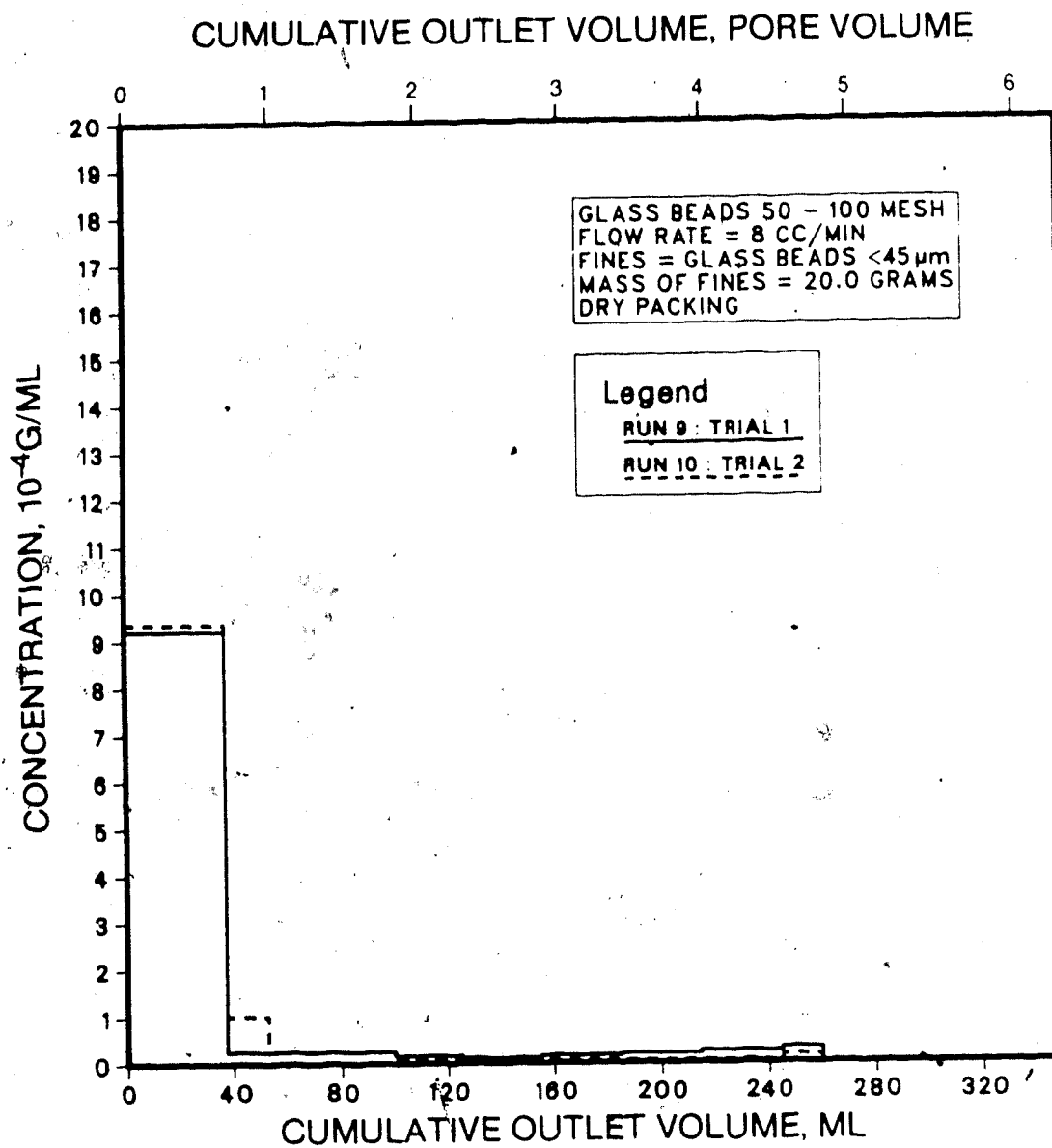


FIGURE 20 : Reproducibility of Dry Packing Method



Run 6 differed from Run 2 in that the flow rate was changed to 13.3 ml/minute (or interstitial velocity of 0.096 cm/s).

The effect of grain size was investigated in Runs 8 and 11. In Run 8, the core holder was packed with 100 to 325 mesh Ottawa sand, and in Run 11, 40 to 70 mesh silica was employed.

Run 13 was carried out to determine the effect of grain shape by packing the core holder with 100 to 325 mesh spherical glass beads.

The effect of size and density of fines was investigated in Runs 14, 15 and 16. Runs 14 and 15 were carried out by mixing 104 grams (16.4% P.V.) and 232 grams (36.5% P.V.) of barite with the sand pack, while in Run 16, 68 grams (25.4% P.V.) of calcium carbonate were mixed with the pack.

Runs 1, 7, 9, 10 and 12 served to determine the outlet concentration of fines when no fines were added to the sand pack, for the various packs used.

#### 5.3.4. Large Core Results

The effect of initial mass of fines in the sand pack is shown in Figure 21. The fines concentration in the effluent increased as the amount of fines in the sand pack mixture was increased. The total amount of fines released in Runs 2, 4 and 5, was 0.241%, 0.470% and 1.330% of initial fines in-place, respectively.

Increasing the flow rate from 8 ml/minute (0.057 cm/s) to 13.3 ml/minute (0.096 cm/s) led to a 69.7% increase in the concentration of fines in the effluent (see Figure 22).

The outlet concentrations of Runs 2, 8 and 11 were compared in order to determine the effect of grain size. As shown in Figure 23,

### CUMULATIVE OUTLET VOLUME, PORE VOLUME

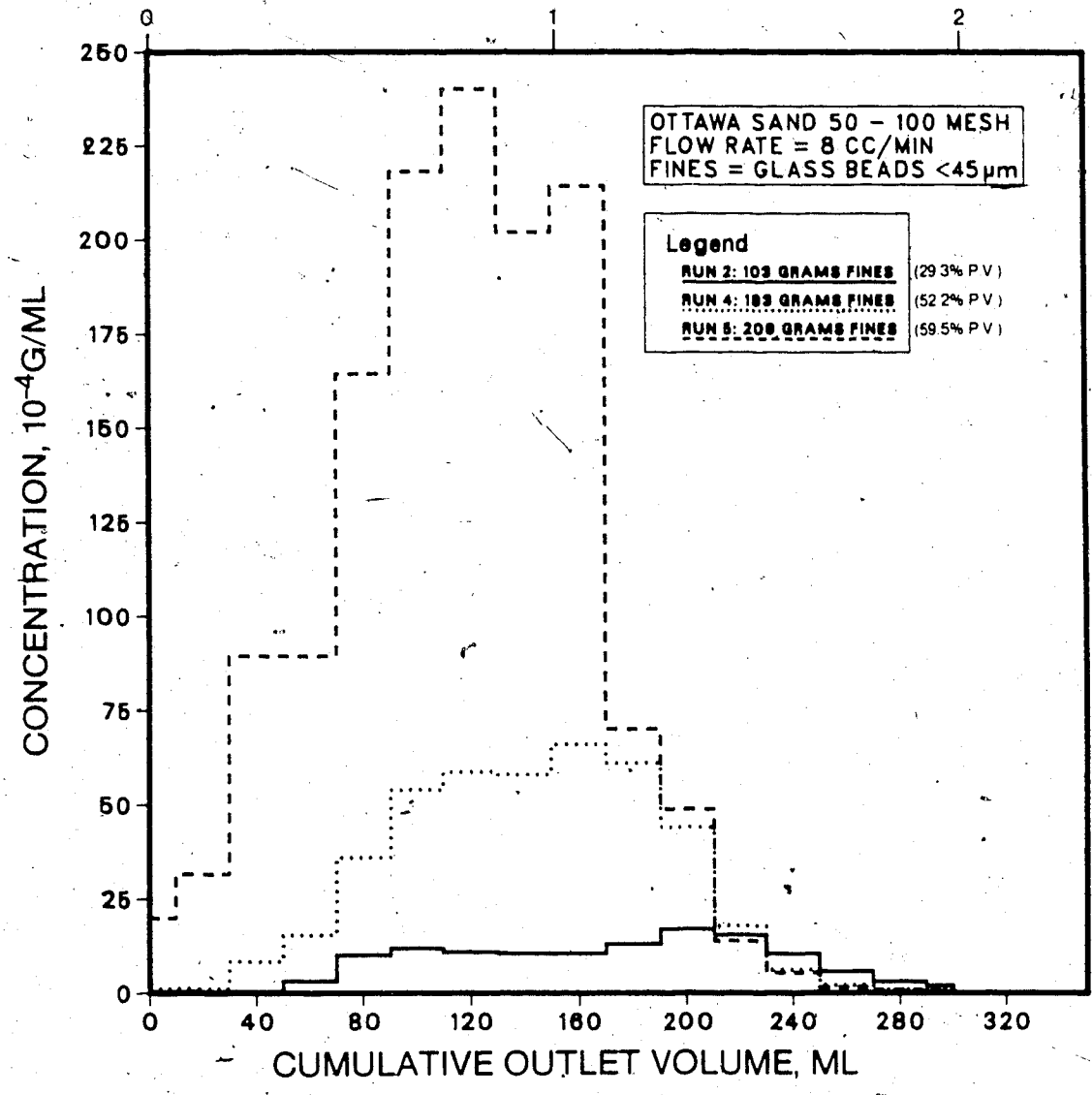


FIGURE 21: Effect of Mass of Glass Fines

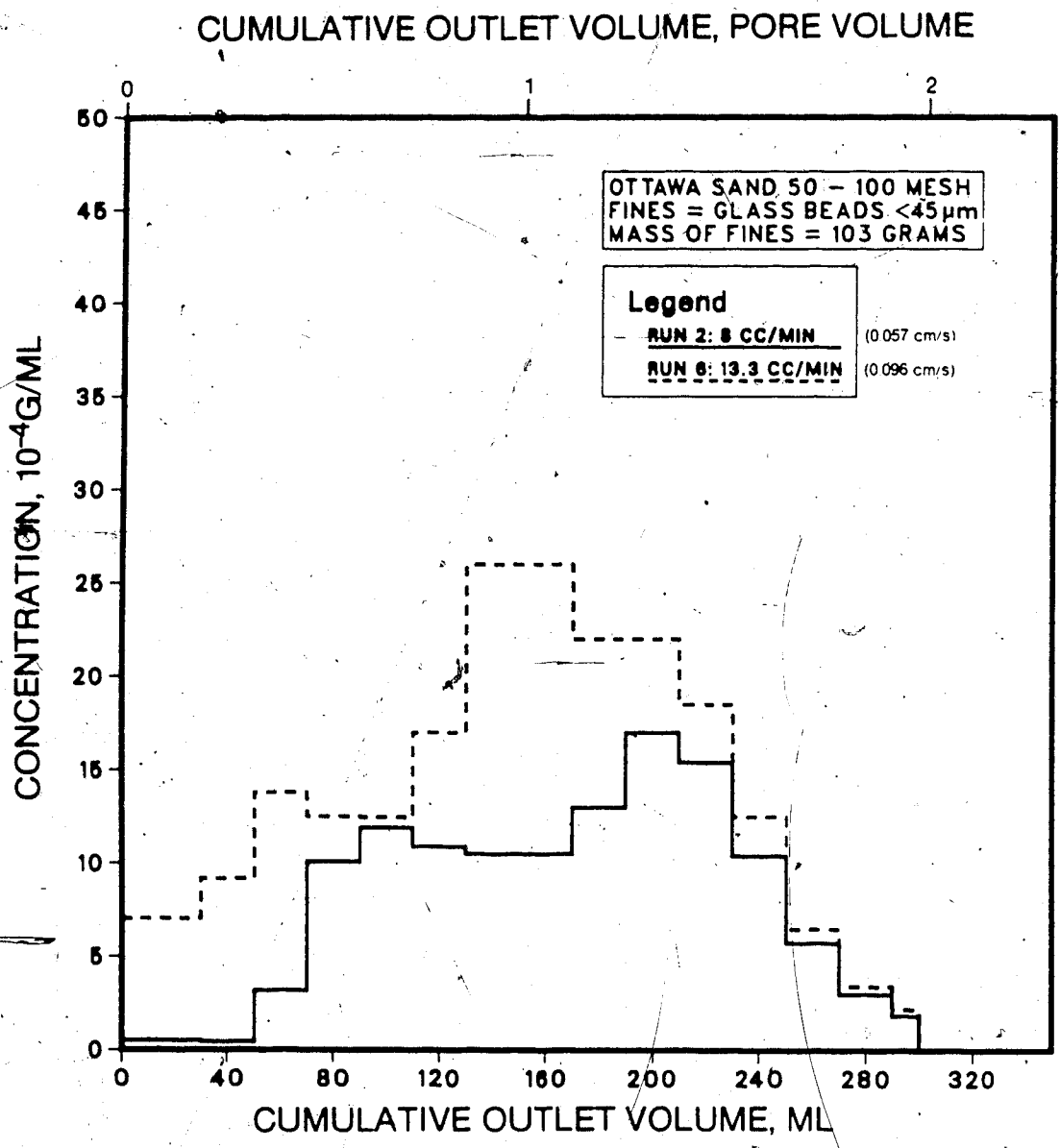


FIGURE 22 : Effect of Flow Rate

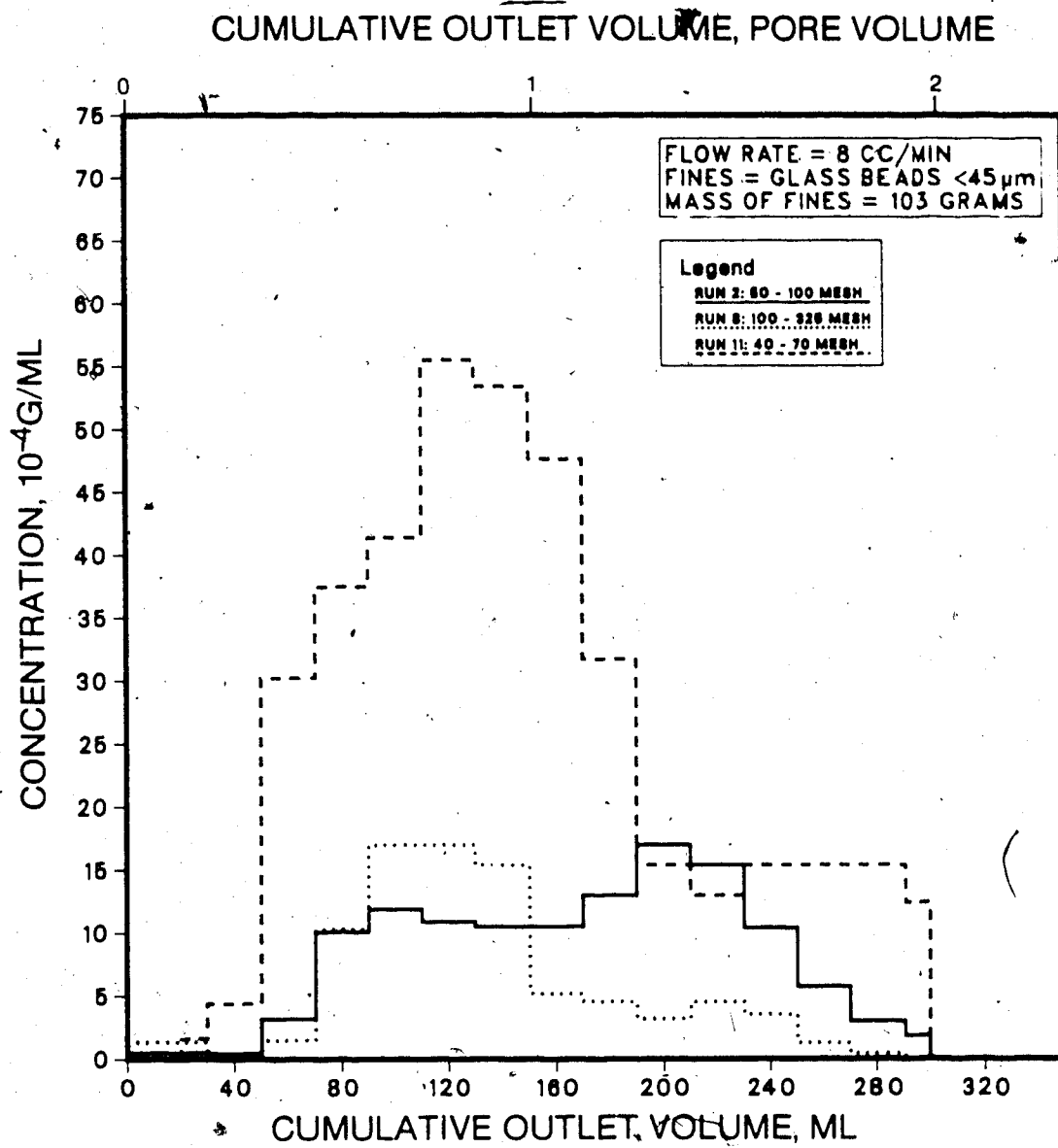


FIGURE 23 : Effect of Grain Size

the concentration of fines slightly increased (31.3%) when a 50 to 100 mesh sand pack was employed instead of a 100 to 325 mesh pack, while a significant increase in concentration (213.7%) occurred when a 40 to 70 mesh sand pack was used.

To determine the effect of grain shape on the movement of fines, Runs 8 and 13 were carried out using spherical glass beads in one case and angular Ottawa sand in the other. The results are shown in Figure 24. The concentration of fines in the effluent was found to be 237.2% higher when the core was packed with spherical sand as opposed to angular sand.

To study the effect of fines density, barite fines having a density of  $4.213 \text{ grams/cm}^3$  were used in Runs 14 and 15. The concentration of fines produced from these runs was compared with that produced in Run 2, which used glass fines with a density of  $2.326 \text{ grams/cm}^3$ . The results are plotted in Figure 25. The concentration of barite fines was very low in the first 20 ml of effluent and decreased to a negligible value thereafter, regardless of the initial amount of barite in the sand pack.

The fines in Run 16 consisted of calcium carbonate, having an average particle size of  $1.4 \text{ }\mu\text{m}$ . The concentration of fines in the effluent was compared with that for Run 11, in which the fines consisted of glass beads 30 to 70  $\mu\text{m}$  in diameter. As shown in Figure 26, the concentration of  $\text{CaCO}_3$  fines was very high in the first 60 ml of effluent, and dropped sharply to zero subsequently. However, the total amount of  $\text{CaCO}_3$  fines released was only 19.5% lower than the amount of glass fines released.

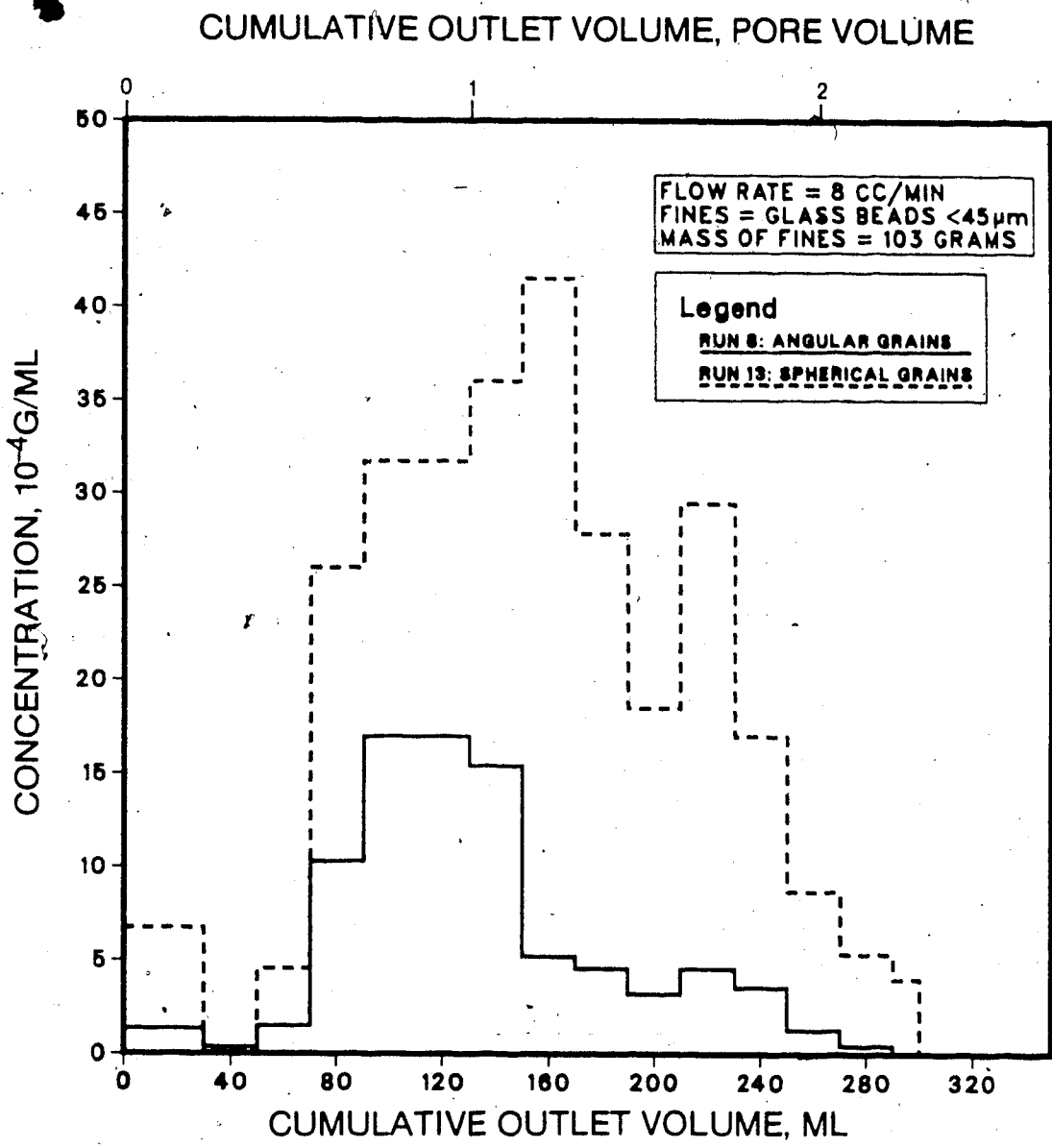
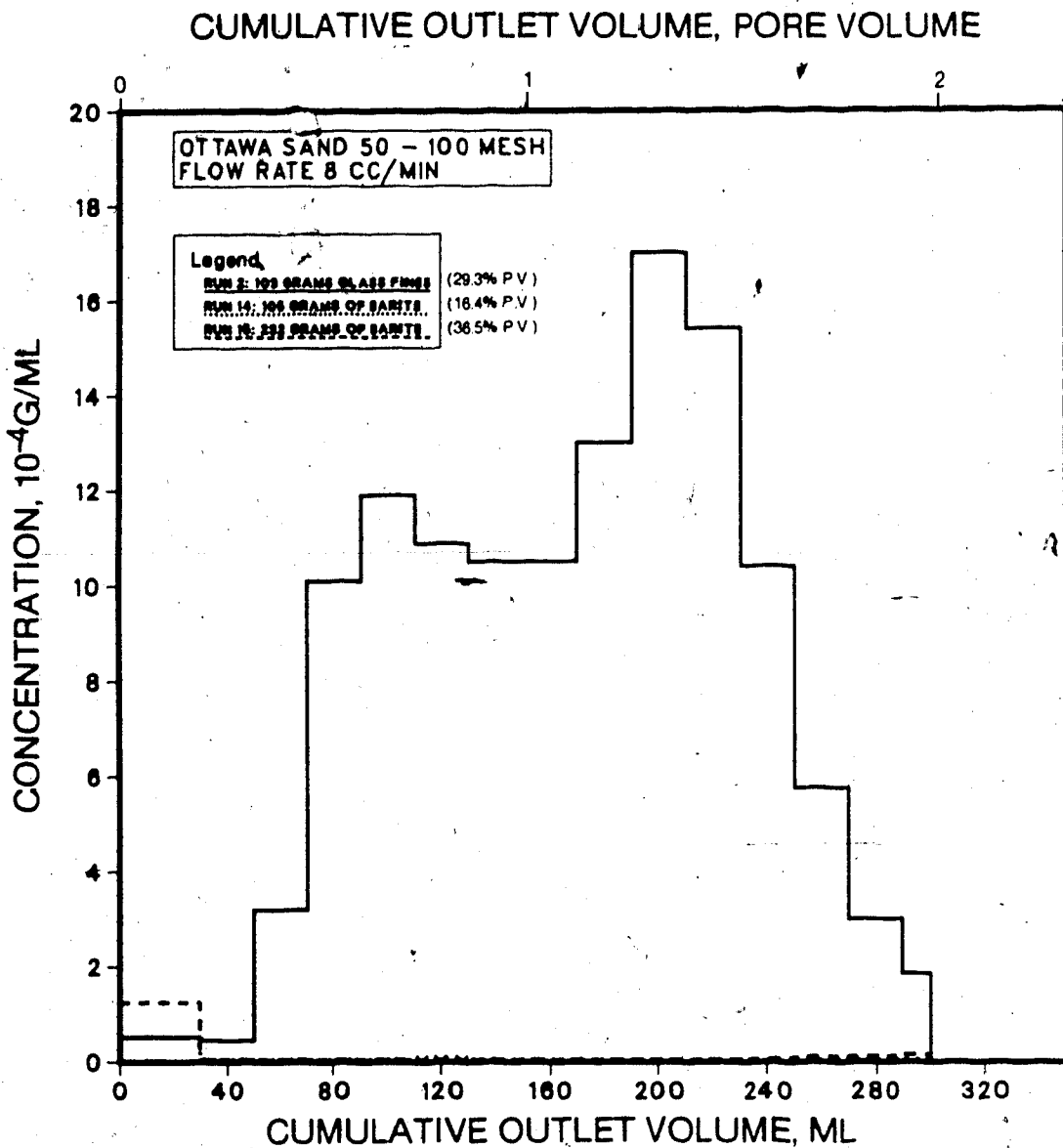


FIGURE 24 : Effect of Grain Shape



**FIGURE 25 : Effect of Fines Density**

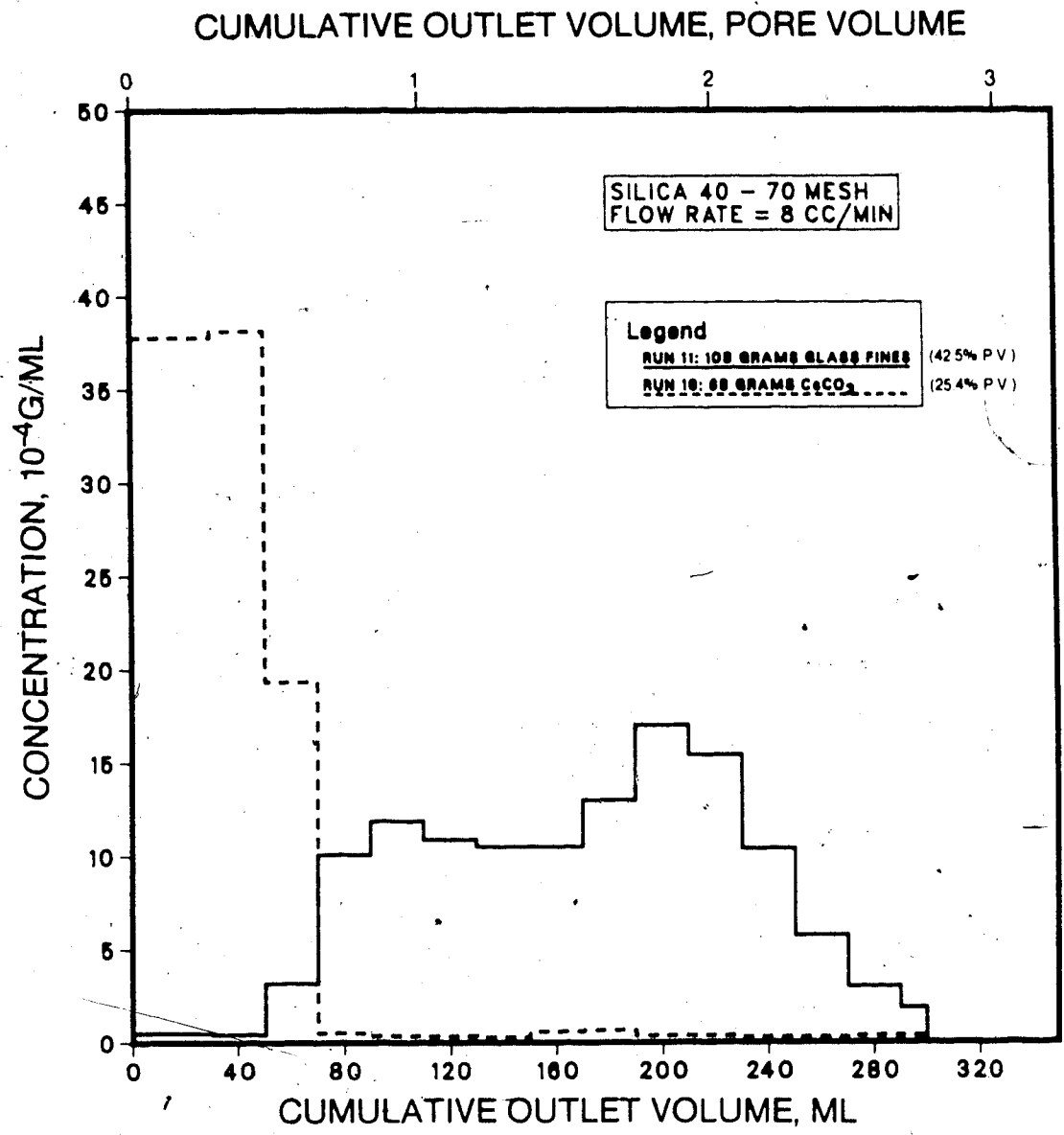


FIGURE 26 : Effect of Fines Size



The concentration of fines in the effluent is shown in Figure 27 for Run 1, in which no fines were initially added to the sand pack. For the Ottawa sand 50 to 100 mesh, a very small amount of fines was detected in the effluent. A significant amount of fines was noted, however, when silica sand, glass beads, or Ottawa sand 100 to 325 mesh was employed (see Figure 29 and Tables C17, C19 and C22). For each sand pack type, the effluent concentrations obtained in the "no-fines" runs were subtracted from those obtained in other runs using a similar sand pack type, and the resulting values were recorded to arrive at a true concentration value.

#### 5.3.5. Reproducibility of Experiments

Runs 3 and 10 were conducted under the same experimental conditions as Runs 2 and 9, respectively, and served to evaluate the reproducibility of the experiments. The results shown in Figures 28 and 29 indicated that the amount of fines released in a run could not be easily reproduced in a different run, carried out under the same conditions. The flow of fines in porous media was found to be a complex process of a random nature. The outlet concentrations obtained in any test indicated only the trend of the transport of fines process, and should not be considered as absolute values.

The results of tests using the large core holder differed from those employing the small core holder mainly in the total amount of fines released and the relative amount of fines in the effluent samples. The concentration of fines in the effluent of the large core holder was consistently higher than that of the small core holder, except when

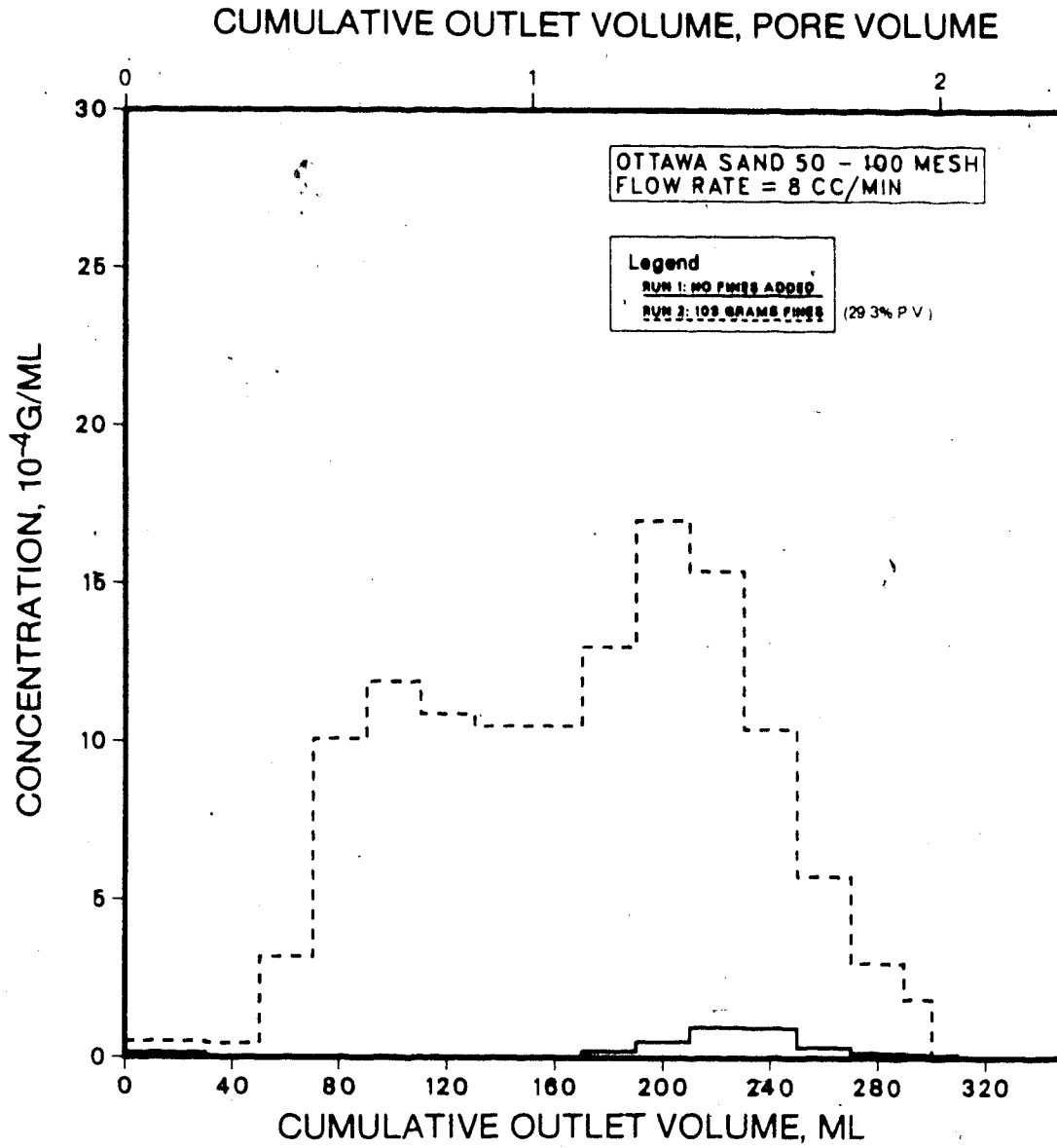


FIGURE 27 : Effect of Absence of Fines

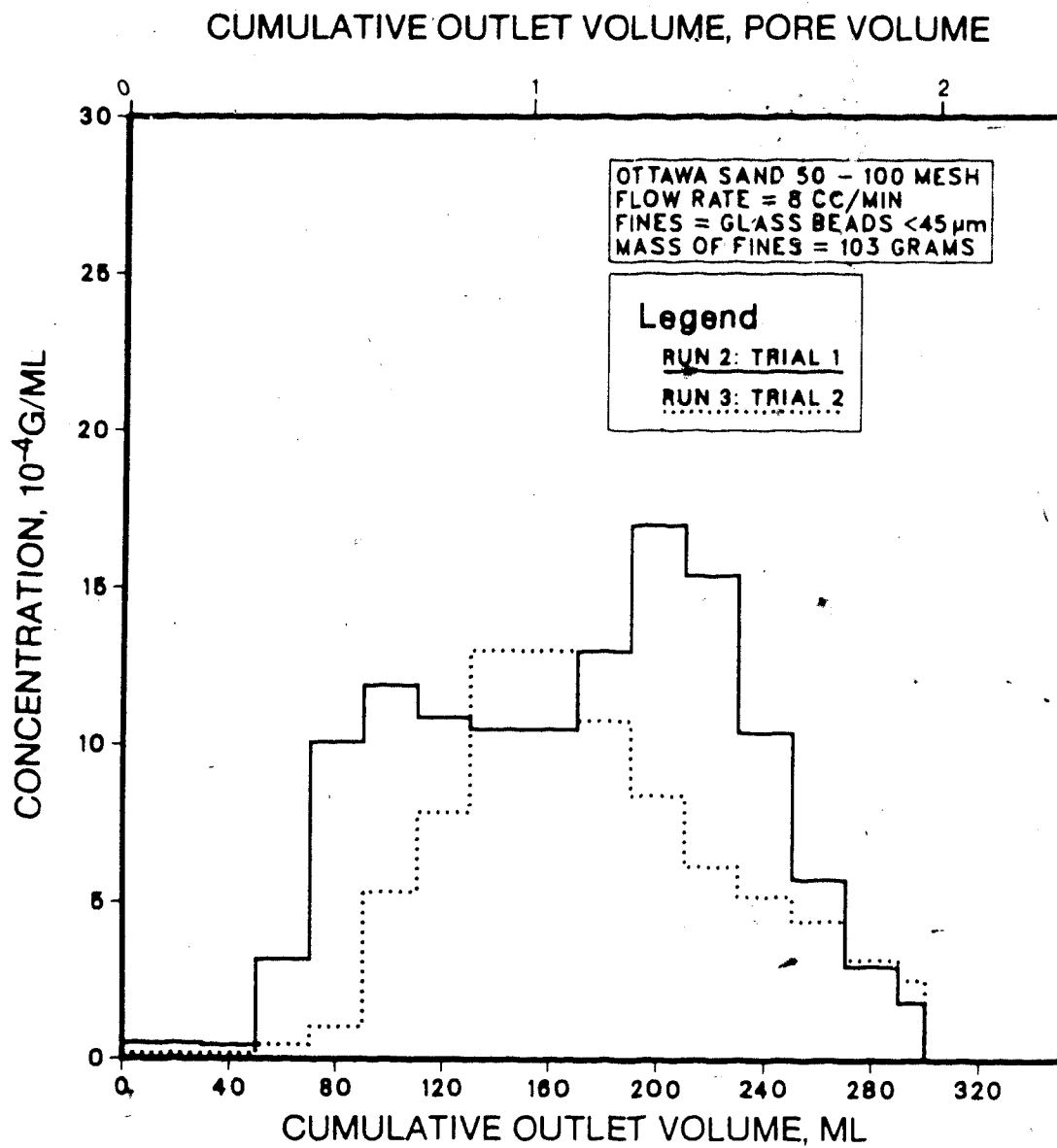


FIGURE 28 : Reproducibility of Ottawa Sand  
50 - 100 Mesh

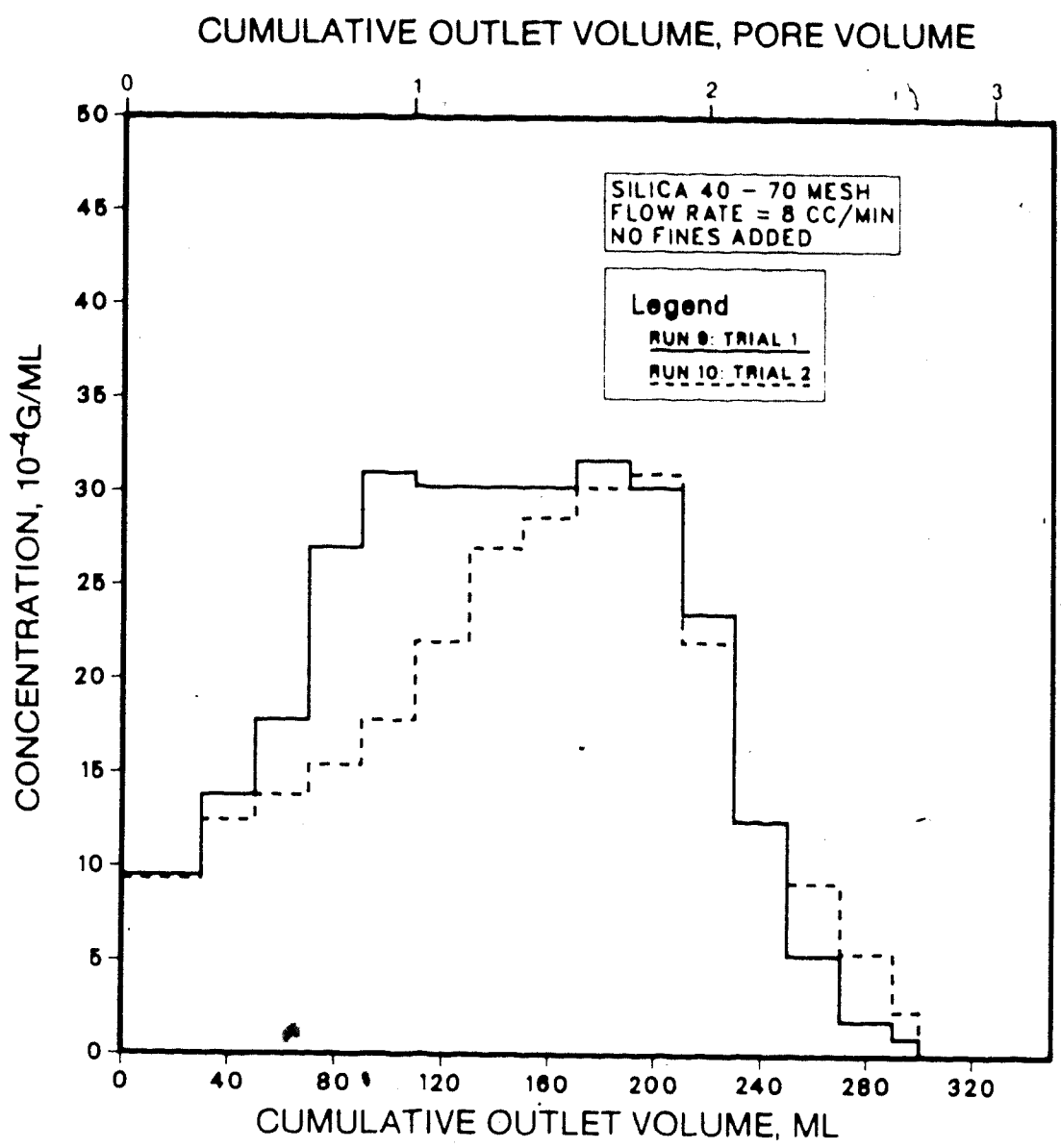


FIGURE 29 : Reproducibility of Silica 40 - 70 Mesh

barite fines were used. The small core outlet concentrations were initially high, but dropped sharply to negligible values after flowing 60 to 80 ml of water through the pack. The large core outlet concentrations generally started at a low value, gradually increased to a maximum value, and decreased thereafter. The various factors studied caused similar changes in the outlet concentrations of both core holders, although not to the same extent. For instance, Figures 13 and 21 both indicate that increasing the initial mass of fines in the sand pack increased the concentration of fines in the outlet. However, the increase in concentration was much more pronounced in the large core tests.

#### 5.3.6. Discussion of Fines Flow Results

From dry-sieve analysis on samples of unconsolidated sandstone formations, Muecke (1979) reported that fine particles constituted 2 to 15 wt% of the formation materials. This range was used in the present investigation to determine the amount of fines that should be added to the sand packs. In most small core tests, the amount of fines added was 20.0 grams, or approximately 12 wt% of the total amount of sand employed. The amount of fines added in most large core tests was 100 grams, corresponding to about 9 wt% of the total amount of sand in the core holder.

Three different types of fine particles were selected. The glass beads were employed because their properties are very similar to those of quartz, which constitutes the major component of naturally occurring fines (Muecke, 1979). Due to its high density, barite was chosen to

investigate the effect of fines density. Calcium carbonate was selected to study the effect of particle size because the  $\text{CaCO}_3$  density is comparable to that of the glass beads ( $2.441 \text{ g/cm}^3$ ), while the particle size is much smaller ( $1.4 \text{ }\mu\text{m}$ ).

#### 5.3.6.1. Effect of Flow Rate

The experimental results demonstrated that the entrainment of fines is influenced by the mass of fines in the porous medium, the fluid flow rate, the size and shape of sand grains, and the size and density of fines. The effect of flow rate can be examined by comparing Experiments L2 and L6 in Table 5. These experiments were carried out under similar operating conditions with the exception of the flow rate, which was changed from 8 ml/minute in Run 2 to 13.3 ml/minute in Run 6. This resulted in a change in interstitial velocity,  $v/\phi$ , from 0.057 cm/s to 0.096 cm/s. The amount of fines produced, FP, expressed as a percent of initial volume of fines in-place, was 0.241% in Run 2 and 0.380% in Run 6. As shown in Table 6, when the amount of fines produced was divided by the interstitial velocity, the value obtained in Run 2 was very close to that obtained in Run 6. A similar calculation was carried out for Experiments S2 and S4 in which the flow rate was changed from 8 ml/minute in Run 1 to 4 ml/minute in Run 4. The resulting values were also found to be in close agreement, suggesting that the amount of fines produced was directly proportional to the interstitial velocity, for the velocity range investigated.

TABLE 6: Effect of Interstitial Velocity

Run #	L2	L6	S2	S4
$v/\phi$ , cm/s	0.057	0.096	0.069	0.036
FP, % of Initial Fines In-Place	0.241	0.380	0.123	0.049
$FP/(\overline{v/\phi})$	4.228	3.958	1.783	1.361

5.3.6.2. Effect of Initial Amount of Fines Present

The effect of initial mass of fines in the porous medium is shown in Table 7. The initial amount of fines in the pack, FI, expressed as a percent of total pore volume, is reported in Table 7 for Experiments L2, L4 and L5. Varying the amount of fines added in these experiments resulted in a change in the porosity of the packs, which in turn altered the interstitial velocities. In order to compensate for the difference in the interstitial velocities, the amount of fines produced in each run was divided by the interstitial velocity in addition to the initial amount of fines in-place. The resulting values were in fair agreement with each other, suggesting that the amount of fines produced was also proportional to the initial amount of fines in-place.

TABLE 7: Effect of Mass of Fines

Run #	L2	L4	L5
$v/\phi$ , cm/s	0.057	0.086	0.103
FI, % Pore Volume	29.3	52.2	59.5
FP, % of Initial Fines In-Place	0.241	0.470	1.330
$FP/(\overline{v/\phi})$	4.228	5.465	12.913
$FP/(\overline{v/\phi}) \cdot FI$	0.144	0.105	0.217

It should be noted that this relationship does not hold for Experiment S3, in which 60.0 grams of fines were added. As shown in Table 5, the amount of fines produced in Experiment S3, as a percentage of initial fines in-place, was smaller than that in Experiment S2, in which 20.0 grams of fines were added. While the amount of fines added in Experiments L4 and L6 corresponded approximately to 15wt% and 17wt% of the total amount of sand employed respectively, the amount of fines added in Experiment S3 corresponded to about 28wt% of the total amount of sand in the pack. It is therefore possible that at this high percentage, the fines were no longer dispersed particles present in the pores of the larger sand grains, but became instead part of the porous medium, yielding smaller-sized pores and restricting particle flow toward the outlet.

#### 5.3.6.3. Effect of Sand Grain Size

The effect of size of sand grains can be determined from Experiments L2, L8 and L11. These experiments differed from each other mainly in the size of sand employed to pack the core holder (see Table 8). For each experiment, the amount of fines produced, FP, was divided by the interstitial velocity and the initial amount of fines in-place, FI. When the resulting value was also divided by the average sand grain size, D, approximately the same number was obtained for all three runs. A similar calculation was carried out for Experiments S2 and S6, which also differed from each other in the size of sand employed. In this case however, the resulting values were not at all in agreement. While the sand size in Experiments L2, L8 and



L11 ranged from 44  $\mu\text{m}$  to 370  $\mu\text{m}$ , the sand grain size in Experiment S6 was as high as 4700  $\mu\text{m}$ . From these results, it was deduced that the amount of fines produced was proportional to the size of sand grains in the pack, for the 44  $\mu\text{m}$  to 370  $\mu\text{m}$  size range.

TABLE 8: Effect of Grain Size

Run #	L2	L8	L11	S2	S6
Sand Size, $\mu\text{m}$	147-283	44-147	187-369	147-283	3327-4699
D, $\mu\text{m}$	215	95.5	287	215	4013
$v/\phi$ , cm/s	0.057	0.074	0.100	0.069	0.073
FI, % Pore Volume	29.3	35.4	42.5	15.1	15.9
FP, % of Initial Fines In-Place	0.241	0.159	0.781	0.123	0.304
FP/( $v/\phi$ ).FI	0.144	0.061	0.184	0.118	0.262
FP/( $v/\phi$ ).FI.D	0.00067	0.00064	0.00066	0.00050	0.00007

#### 5.3.6.4. Flow of Fines Equation

Based on the experimental data collected, the amount of fines produced, FP, may be expressed as:

$$FP = c.(v/\phi).D.FI$$

where  $FP$  is the amount of fines produced in percent of  
initial volume of fines in-place

$v/\phi$  is the interstitial velocity in cm/s

$D$  is the average sand grain diameter in cm

$FI$  is the initial amount of fines in the pack in  
percent of total pore volume

and  $c$  is a constant in  $s/cm^2$ .

Values of the constant  $c$  were calculated for both the small and the large core holder experiments, and are presented in Table 9. It was observed that the values of  $c$  generally fell between 4 and  $10 s/cm^2$ , with the exception of Experiments S3, S6, L13 and L14. As mentioned previously, in Experiment S3 the sand pack contained a very high percentage of fines which may have become part of the porous medium, and thus impeded particle flow. The sand pack in Experiment S6 consisted of very large sand grains in which range the proportionality between grain size and fines produced does not hold. As shown in Table 9, a very high  $c$  value was obtained for Experiment L13 ( $78.4 s/cm^2$ ). The sand pack in this run was prepared using spherical glass beads, which formed pore channels that were less tortuous than those formed by angular sand grains. Because the spherical beads yielded straighter channels and formed less pore constrictions than angular grains, an increased amount of fines was allowed to reach the outlet. In Experiment L14, the fines consisted of barite particles having a high density. Because of their high density, these particles were not carried with the fluid as easily as glass particles, and relatively few particles reached the outlet.

TABLE 9: Experimental Values of the Proportionality Constant

<u>Run #</u>	<u>c, s/cm<sup>2</sup></u>	<u>Run #</u>	<u>c, s/cm<sup>2</sup></u>
L2	6.7	S1	5.6
L4	4.9	S3	0.5
L5	10.1	S4	4.2
L6	5.6	S6	0.7
L8	6.4	S9	6.6
L11	6.6		
L13	78.4		
L14	0.1		
L16	6.2		

#### 5.3.6.5. Fines Concentration Versus Cumulative Volume Curve

It was observed that in most small core experiments, the concentration of fines was at its highest value in the first 30 to 50 ml of effluent (about 1.0 pore volume), and dropped sharply to a low value after flowing 60 to 80 ml of water through the pack. The fines concentration in most large core experiments started at a low value, gradually increased to a high value after flowing 120 to 160 ml of water (1.0 pore volume), then gradually decreased to a negligible value.

It should be noted however that the concentration curve of Experiment S4, characterized by a lower flow rate, was closer in shape to the large core curves than to those of the small core (see Figure 14). Experiment L6 in Figure 22 shows that at a flow rate of 13.3 ml/minute, the concentration curve became closer in shape to the curves obtained in the small core experiments. Although the amount of fines released in Experiments L14 and L15 in which 3 to 15  $\mu\text{m}$  barite fines were

employed, was relatively negligible, the concentration curves of these runs were quite similar to the small core curves (see Figure 25). The curve corresponding to Experiment L16 in which  $1.4 \mu\text{m CaCO}_3$  fines were employed, was also similar to the small core curves (see Figure 26). These observations suggested that the shape of the concentration curves in both small and large core experiments depended on the flow rate and the size of fine particles.

In order to investigate the effect of flow rate and particle size on the shape of the concentration curve, Experiments S1 and L2 in which the concentration curves were characteristic of the small core runs and the large core runs, respectively, were compared to Experiments S4, L6, L14 and L16. For each experiment, the Darcy velocity and the average size of fines reaching the outlet were determined, and the ratio of Darcy velocity over particle size,  $v/D_p$ , was calculated. The resulting values are listed in Table 10.

The highest  $v/D_p$  ratio corresponded to Experiment L16 in which the fines concentration was at a maximum value in the first 80 ml of effluent, and decreased to a negligible value thereafter. The lowest  $v/D_p$  ratio corresponded to Experiment L2 in which the fines concentration started at a low value, then gradually increased to a maximum value. The ratios obtained in the remaining experiments were found to increase as the concentration curves became closer in shape to the curve of Experiment L16.

TABLE 10: Ratio of Darcy Velocity Over Particle Size

Run #	Darcy Velocity v, cm/s	Particle Size Dp, cm	v/Dp, s <sup>-1</sup>	v <sup>2</sup> /Dp, cm/s <sup>2</sup>
L2	0.012	0.0020	6.0	0.072
S4	0.015	0.0020	7.5	0.112
L6	0.020	0.0020	10.0	0.200
L14	0.012	0.0009	13.3	0.160
S1	0.029	0.0020	14.5	0.420
L16	0.012	0.0001	120.0	1.440

Of more important physical significance is the ratio  $v^2/Dp$  shown in Table 10. This ratio, which was found to increase as the shape of the concentration curves became more characteristic of the small core runs, appears in the expression for the inertial force acting on the particle:

$$F_i = mv^2/Dp$$

where  $m$  is the mass of the particle in grams

and  $F_i$  is the inertial force in dynes.

As the ratio  $v^2/Dp$  increases, the inertial force acting on the particle increases, allowing that particle to reach the core holder outlet with little difficulty.

As mentioned in Section 4.7, the particle size was noted to affect the NTU reading of the turbidimeter. At any particle concentration, larger particles yielded a lower NTU reading than

smaller particles. The dependence of the turbidimeter reading on particle size could explain why the curve shape in most large core experiments was characterized by a gradual increase to a maximum value, followed by a gradual decrease to a negligible value: at high  $v^2/D_p$  ratios, both small and large particles were carried towards the outlet due to the high inertial forces present; however, at low  $v^2/D_p$  ratios, particles closest to the outlet were carried out of the core first, followed by the smaller particles (high NTU reading), then the larger particles (low NTU reading).

#### 5.3.7. Discussion of Fines Flow Mechanisms

In all the tests conducted to study the flow of fines, a suspended solid-free fluid was flowed through sand packs that were prepared with an initial content of fines. A review of the literature indicated that previous clarification studies consisted of flowing suspension-laden fluids through sand beds that were initially free of fines, while most studies in porous media were carried out employing sandstone cores that contained naturally occurring fines. It was reported in these studies that the pressure drop across the sand bed increased during fluid injection, indicating that the sand pack permeability decreased due to the movement of fines. In this investigation, although the permeability of sand packs was noted to be strongly dependent on the size of sand grains and the initial amount of fines present, no significant change in permeability was detected during the flow tests. The pressure drop increase in the previous studies was then due not only to the bridging mechanism, but also to the deposition of suspensions injected with the fluid, which increased the mass of fines in the pack.

While the unconsolidated porous media in previous investigations consisted of sand grains between 250 and 2000  $\mu\text{m}$  in diameter, in this study, the grain sizes ranging from 45 to 350  $\mu\text{m}$  were selected to reproduce the sand grain sizes encountered in Lloydminster (see Table 11). The fine particle sizes were arbitrarily defined as particles smaller than 45  $\mu\text{m}$  (325 mesh). Muecke had previously defined fines as particles small enough to pass through 37  $\mu\text{m}$  (400 mesh) openings. As mentioned in Chapter 2, Gruesbeck and Collins stressed the importance of the ratio of pore diameter to particle diameter in determining the flow mechanism. In their investigation, the effective pore size determination was based on geometric consideration of a closest packing of spheres, and was calculated by dividing the average grain size by 6.5. According to this technique, 50 to 100 mesh Ottawa sand would have an effective pore size of 34  $\mu\text{m}$ . The grain size to pore size ratio is approximately 2.0 for a loose packing of spheres, and 4.5 for a medium packing. The ratio for the medium packing would yield an effective pore size of 49  $\mu\text{m}$ . The size of fines should then be at least two or three times smaller than 49  $\mu\text{m}$  in order for the fines to pass through the pores.

TABLE 11: Lloydminster Sand Sieve Analysis

Sieve Opening, $\mu\text{m}$	840	420	177	104	74	<74
% Sand Retained	1.2	1.0	6.3	84.5	5.0	2.0

It was therefore deduced that only a small part of the fines added to the sand packs were able to move through the pore openings. In the unconsolidated formations of Lloydminster, the movable fines would then have a maximum size of about 20  $\mu\text{m}$ , instead of the 45  $\mu\text{m}$  value previously suggested.

It should be noted that although the fines did not all move towards the core outlet in the experiments, the fines detected in the effluent were not produced sporadically, but followed definite trends that depended on the governing variables.

#### 5.4. RADIAL FLOW TESTS

##### 5.4.1. Radial Flow Experiments

Twenty-one experiments were conducted using the radial wellbore model to investigate the variables affecting sand production. In each run, the cell was packed with unconsolidated sand, and an overburden load was applied to the sand pack. Distilled water was flowed through the cell walls into a centre well. The water and sand produced were collected in 50 ml. samples, and the sand volume in each sample was measured. The experimental data for the radial flow tests are provided in Tables C27 to C47, and a summary of the experimental results is provided in Table 12.

The experimental conditions varied were the overburden load, the flow rate, the sandpack grain size and shape, and the perforation size and shape of the centre well. The centre well tubing specifications are listed in Table 13.



Table 12: Summary of Radial Flow Tests

Run#	Flow Rate ml/min	Overburden Press., kPa	Sand Size, μm	Sand Shape
1	8.0	0.0	111-187	Angular
2	8.0	0.0	111-187	Angular
3	8.0	611.0	111-187	Angular
4	8.0	1018.4	111-187	Angular
5	8.0	1731.3	111-187	Angular
6	8.0	1731.3	111-187	Angular
7	8.0	1018.4	119-175	Spherical
8	8.0	0.0	119-175	Spherical
9	8.0	0.0	119-175	Spherical
10	2.0	0.0	111-187	Angular
11	13.3	0.0	111-187	Angular
12	2.0	1731.3	111-187	Angular
13	13.3	1731.3	111-187	Angular
14	8.0	0.0	187-369	Angular
15	8.0	0.0	187-369	Angular
16	8.0	1731.3	187-369	Angular
17	8.0	1018.4	119-175	Spherical
18	8.0	1018.4	44-99	Spherical
19	8.0	1018.4	111-187	Angular
20	8.0	1018.4	111-187	Angular
21	8.0	1018.4	119-175	Spherical

Table 12: (Continued)

Run#	Well #	Flow Area, cm <sup>2</sup>	Orifice Vel., cm/min	Table #
1	1	8.832	0.906	C27
2	1	8.832	0.906	C28
3	1	8.832	0.906	C29
4	1	8.832	0.906	C30
5	1	8.832	0.906	C31
6	1	8.832	0.906	C32
7	1	8.832	0.906	C33
8	1	8.832	0.906	C34
9	1	8.832	0.906	C35
10	1	8.832	0.226	C36
11	1	8.832	1.506	C37
12	1	8.832	0.226	C38
13	1	8.832	1.506	C39
14	1	8.832	0.906	C40
15	1	8.832	0.906	C41
16	1	8.832	0.906	C42
17	3	2.508	3.190	C43
18	3	2.508	3.190	C44
19	3	2.508	3.190	C45
20	2	1.320	6.061	C46
21	2	1.320	6.061	C47

Runs 1 and 2 were carried out using well #1. The cell was packed with 70 to 140 mesh Ottawa sand and no overburden pressure was applied. Distilled water was flowed through the pack at a rate of 8 ml/minute, corresponding to an outlet velocity of 0.906 cm/minute.

In Runs 3, 4, 5 and 6, different overburden pressures were applied, while other experimental conditions were kept similar to those of Runs 1 and 2.

Runs 7, 8 and 9 were conducted using 80 to 120 mesh glass beads, and an overburden load of 1018 kPa in Run 7, and 0 kPa in Runs 8 and 9.

To determine the effect of flow rate, in Runs 10 and 11 the water flow rate was changed to 2 ml/minute (0.226 cm/minute) and 13.3 ml/minute (1.506 cm/minute), respectively, and no load was applied.

In Runs 12 and 13, the overburden load was 1731 kPa, and the fluid flow rate was 2 ml/minute and 13.3 ml/minute, respectively.

Runs 14, 15 and 16 were carried out under different loading pressures using 40 to 70 mesh Silica in order to evaluate the effect of sand grain size on sand production.

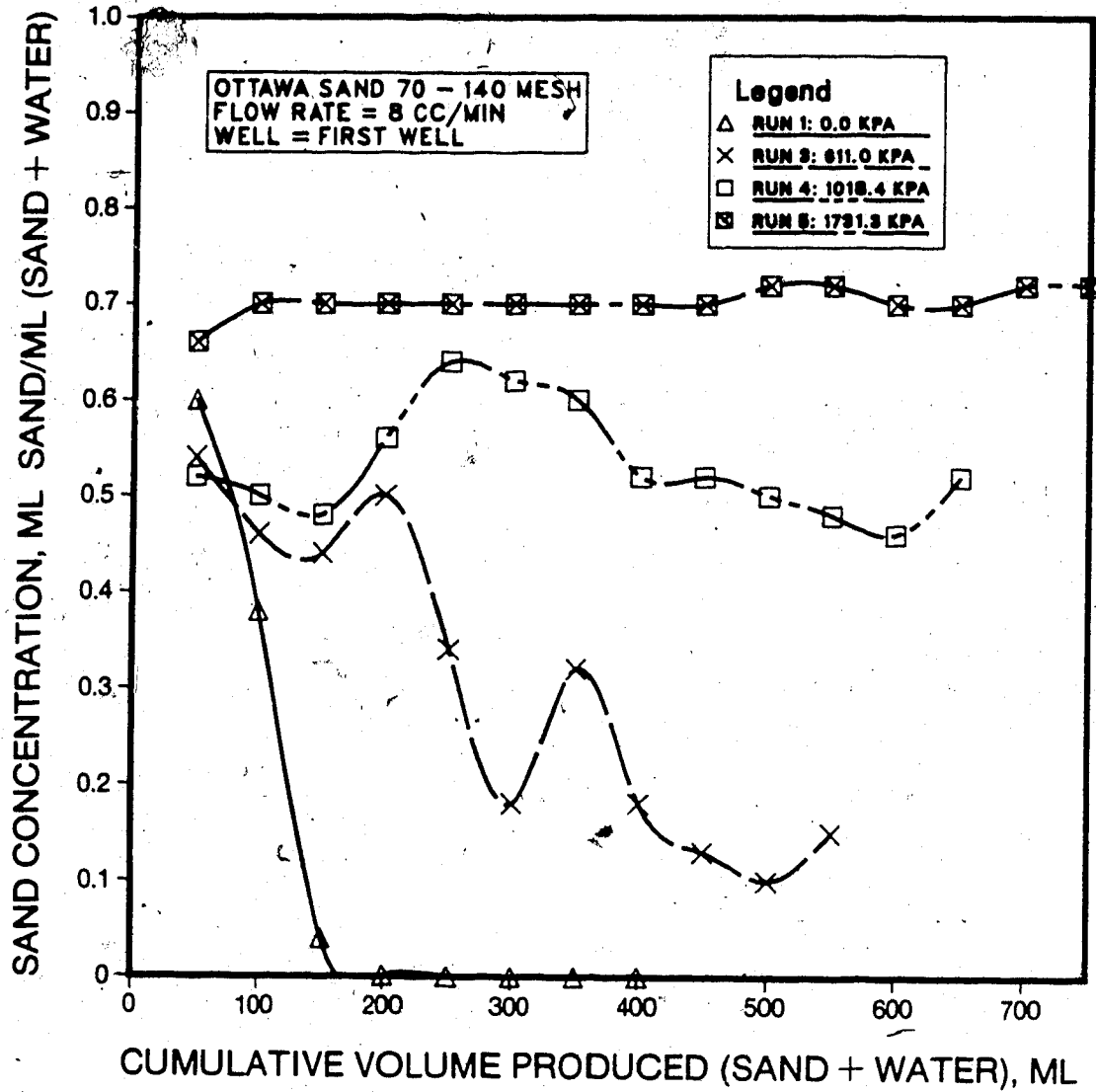
In Run 17, the cell was packed with 80 to 120 mesh glass beads. The test was conducted using well #3, under a load of 1018 kPa. Runs 18 and 19 differed from Run 17 in that the sandpacks consisted of 170 to 325 mesh glass beads and 70 to 140 mesh Ottawa sand, respectively. In Runs 20 and 21, well #2 was employed. In Run 20, the cell was packed with 70 to 140 mesh Ottawa sand, and in Run 21, it was packed with 80 to 120 mesh glass beads.

TABLE 13: Well Tubing Specifications

<u>Well #</u>	
1	Slots 2.3 cm long, 0.16 cm wide, 60° apart, 8.83 cm <sup>2</sup> flow area
2	Round holes 0.08 cm in diameter, 0.32 cm apart, 1.32 cm <sup>2</sup> flow area
3	Round holes 0.11 cm in diameter, 0.32 cm apart, 2.51 cm <sup>2</sup> flow area

#### 5.4.2. Radial Flow Results

For each radial flow test, the volume of wet sand (including the pore volume) in each 50 ml sample of effluent was measured and the sand concentration in the sample was plotted against the cumulative volume of effluent sand and water produced. The effect of overburden pressure on sand production is presented in Figures 30 and 31. Figure 30 shows the results of four runs carried out using 70 to 140 mesh Ottawa sand. The lowest sand production occurred when no overburden pressure was applied (Run 1). The sand concentration in the first sample was 0.60 ml/ml, and the sand production decreased rapidly to zero in subsequent effluent samples. At an overburden load of 1731 kPa, the sand concentration in the first sample was 0.66 ml/ml and increased to 0.70 ml/ml thereafter. As shown in Figure 31, the production of 80 to 120 mesh glass beads under varying loads was also characterized by a higher concentration of beads in the effluent at high overburden pressure. However, the sand production did not decrease to zero in the absence of overburden load. Instead, the concentration of



**FIGURE 30 : Effect of Overburden Pressure (Angular Sand)**

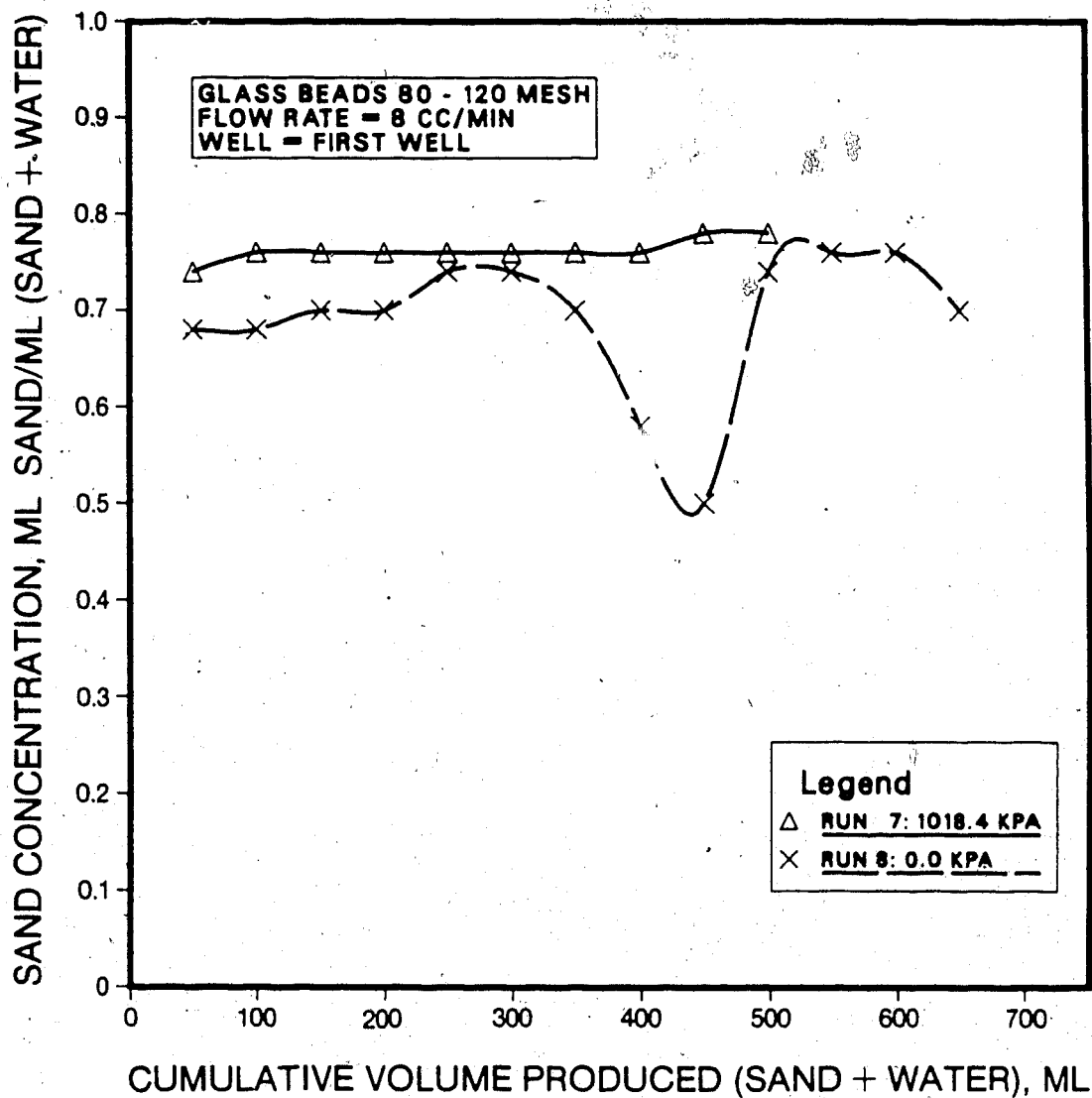


FIGURE 31: Effect of Overburden Pressure (Spherical Sand)

glass beads produced fluctuated with continued fluid injection, decreasing gradually to a low value, and then suddenly increasing to a high value.

Figures 32 and 33 depict the effect of flow rate in the absence of overburden pressure and also at a high overburden pressure. Three flow rates were investigated. Although the sand production was lower when water was injected at a rate of 2 ml/minute than the sand production at 8 ml/minute and 13.3 ml/minute, in the absence of overburden load, the differences in the concentrations of sand produced at these flow rates were not very significant after the first 100 ml of effluent. When a pressure of 1731 kPa was applied, the volume of sand produced at a flow rate of 2 ml/minute was substantially lower than the volume produced at the higher flow rates.

The effect of grain size on sand production is shown in Figures 34, 35 and 36. In Figure 34, the sand concentrations produced at zero overburden load are plotted for 70 to 140 mesh Ottawa sand and 40 to 70 mesh Silica, while in Figure 35, the sand concentrations produced at a pressure of 1731 kPa are presented for these sand grain sizes. It was noted that sand production was more pronounced for the finer grained sand than for the coarser sand, regardless of the value of the overburden load. Similarly, as shown in Figure 36, the 170 to 325 mesh glass beads were produced in greater amounts than the 80 to 120 mesh beads.

The concentration of sand produced in Run 4, in which angular 70 to 140 mesh Ottawa sand was employed, and the concentration of sand

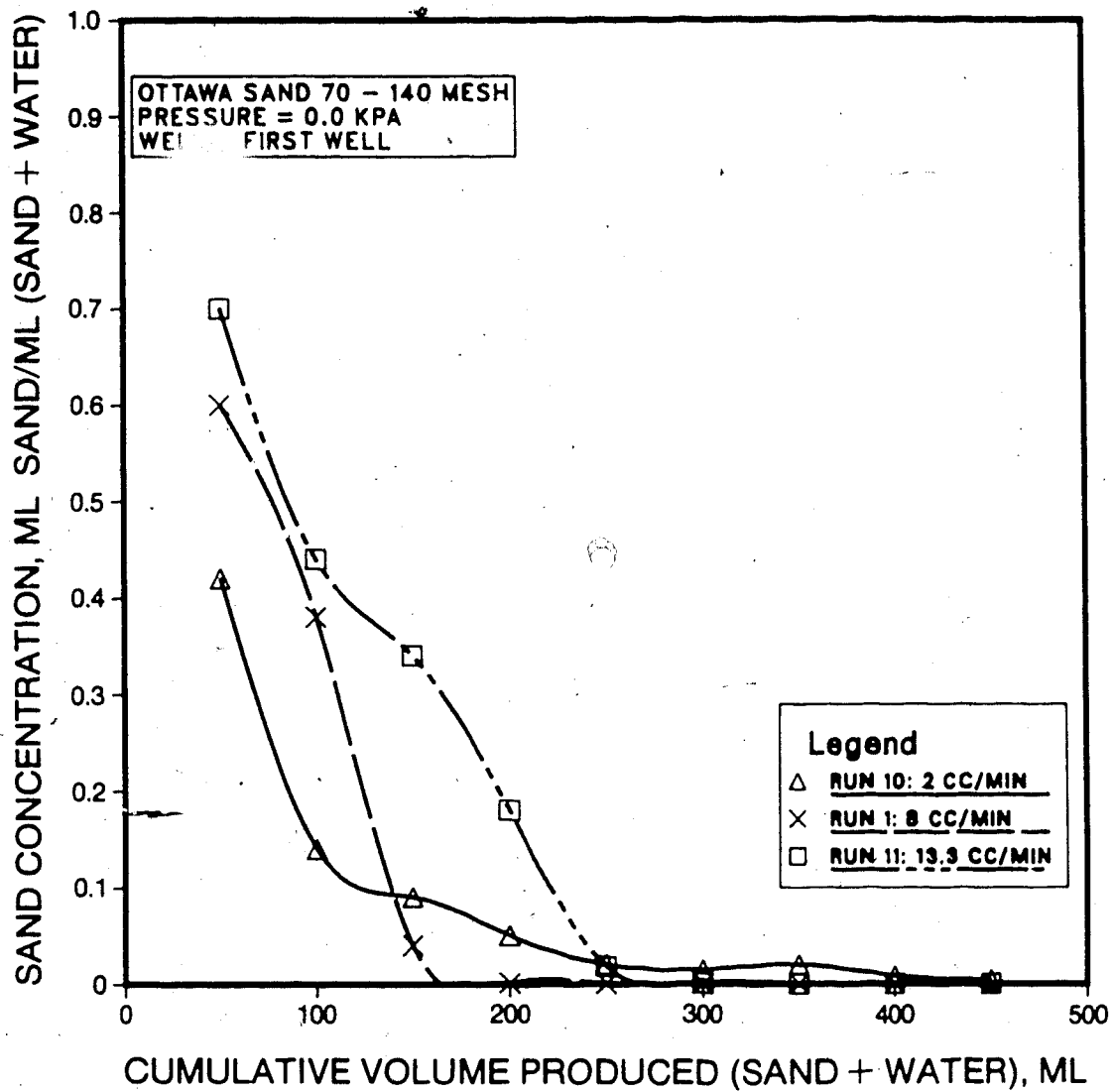
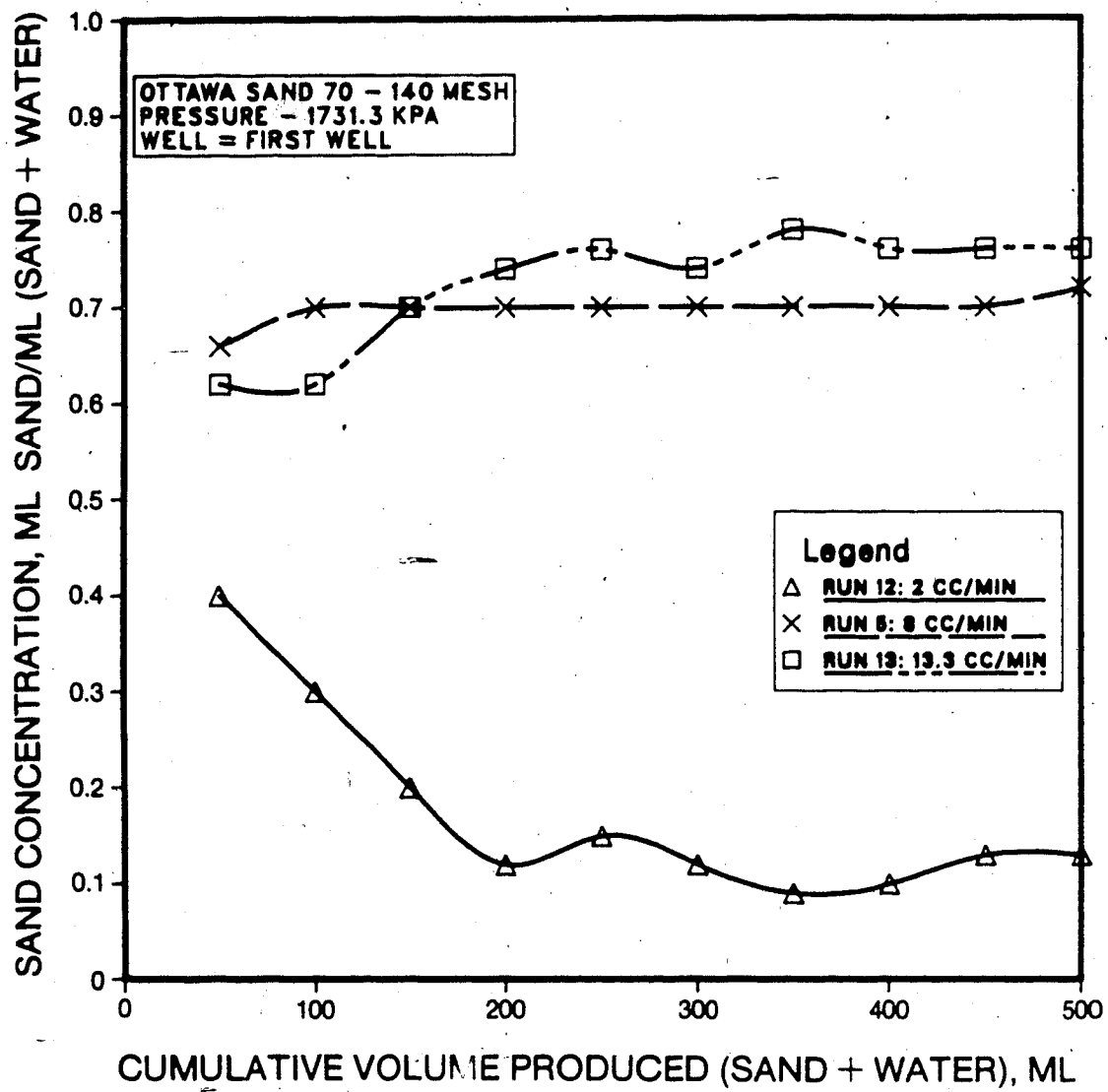
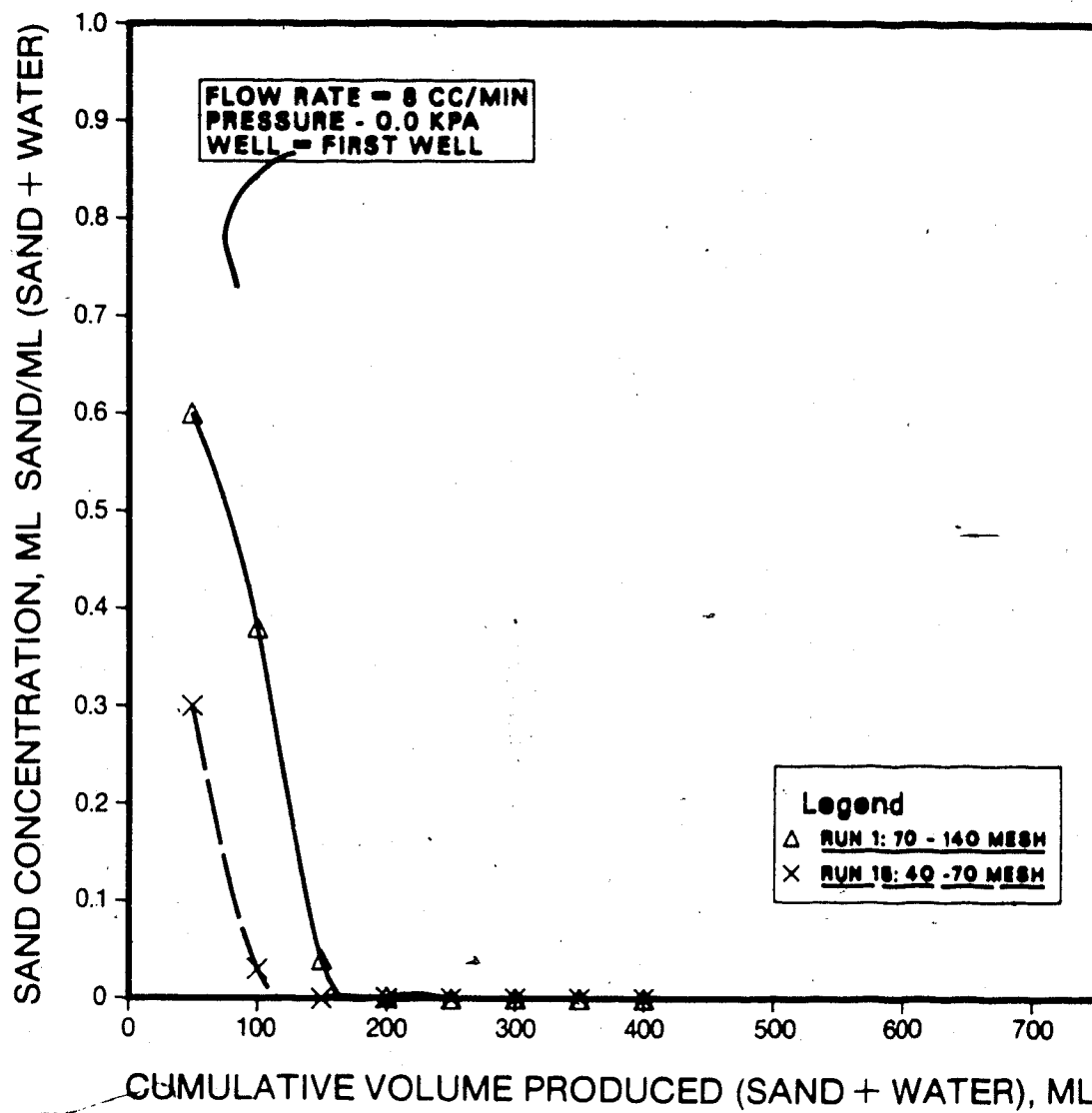


FIGURE 32 : Effect of Flow Rate  
(No Overburden Pressure)





**FIGURE 33 : Effect of Flow Rate  
 (High Overburden Pressure)**



**FIGURE 34 : Effect of Grain Size  
(Angular Sand, No Overburden Pressure)**

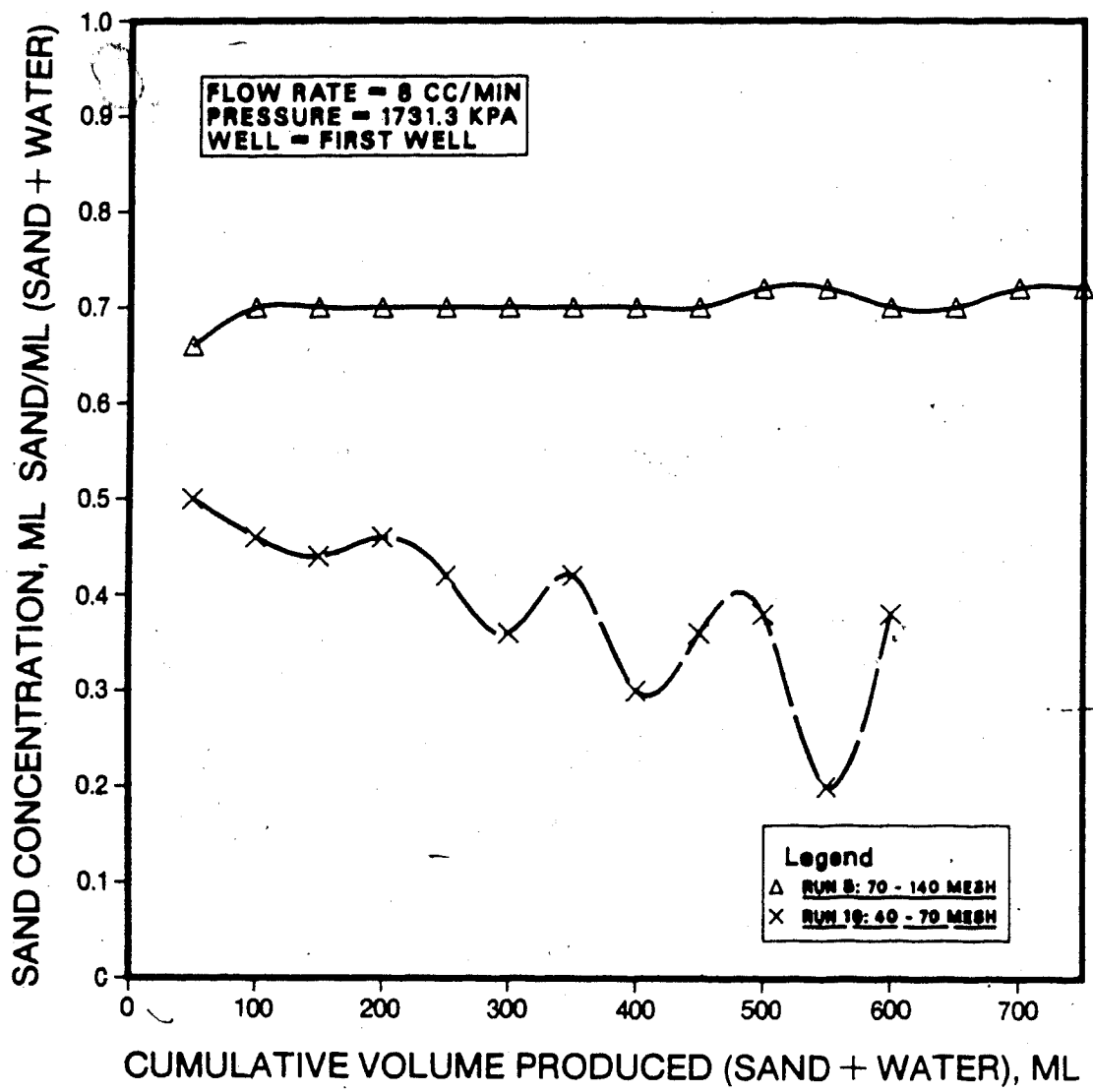


**FIGURE 35 — Effect of Grain Size  
(Angular Sand, High Overburden Pressure)**

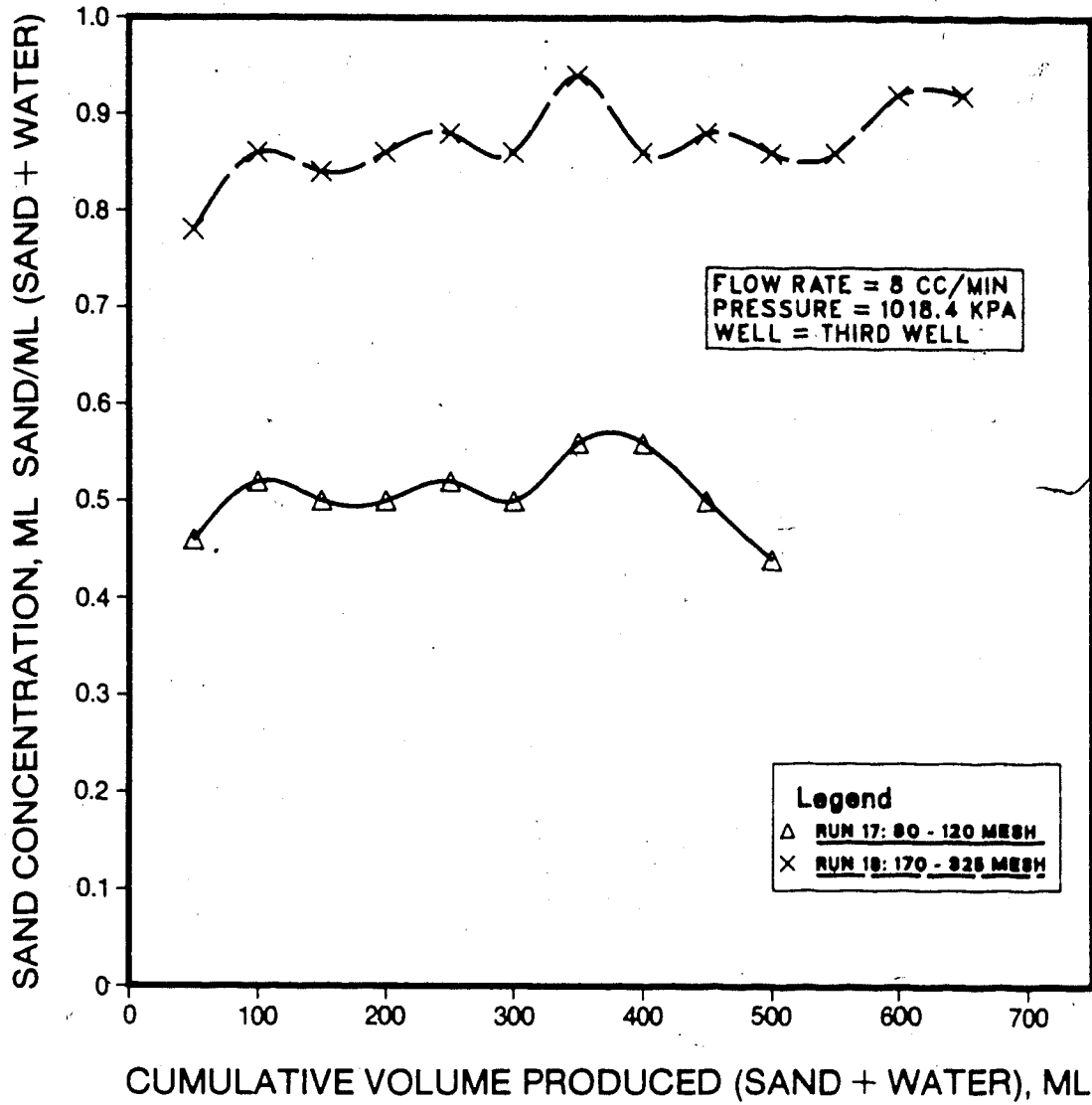


**FIGURE 36 : Effect of Grain Size (Spherical Sand)**

produced in Run 7, which was carried out using spherical glass beads of similar grain size, are plotted in Figure 37. It was observed that the spherical beads were produced in greater amounts than the angular sand. In addition, while the concentration of spherical beads produced remained constant in each effluent sample, the angular sand production was characterized by a gradual decrease to a low value, followed by a production surge to a high value.

The effect of perforation shape and size of the tubing representing the well is shown in Figure 38. All wells led to the production of glass beads in the effluent. However, the greatest concentration of spherical beads produced occurred when using the slotted well (Well #1). Increasing the perforation size from 0.08 cm (Well #2) to 0.11 cm (Well #3) resulted in a slight decrease in the amount of sand produced. Tests were also conducted employing Ottawa sand of grain size similar to that of the spherical sand. No sand was found in the effluent for Runs 19 and 20, which were carried out using Well #3 and Well #2, respectively. Substantial sand production occurred, however, in Run 4, in which Well #1 was employed.

The reproducibility of radial flow tests was investigated for Ottawa sandpacks under overburden pressures of 0 and 1731 kPa. The results are shown in Figures 39 and 40. The reproducibility of the tests was found to be adequate at low overburden loads, while excellent reproducibility was obtained at high loads. In addition, the reproducibilities for glass bead and silica sandpacks not subjected to overburden loads were examined. As indicated by Figures 41 and 42, although the concentration of sand produced in each effluent sample

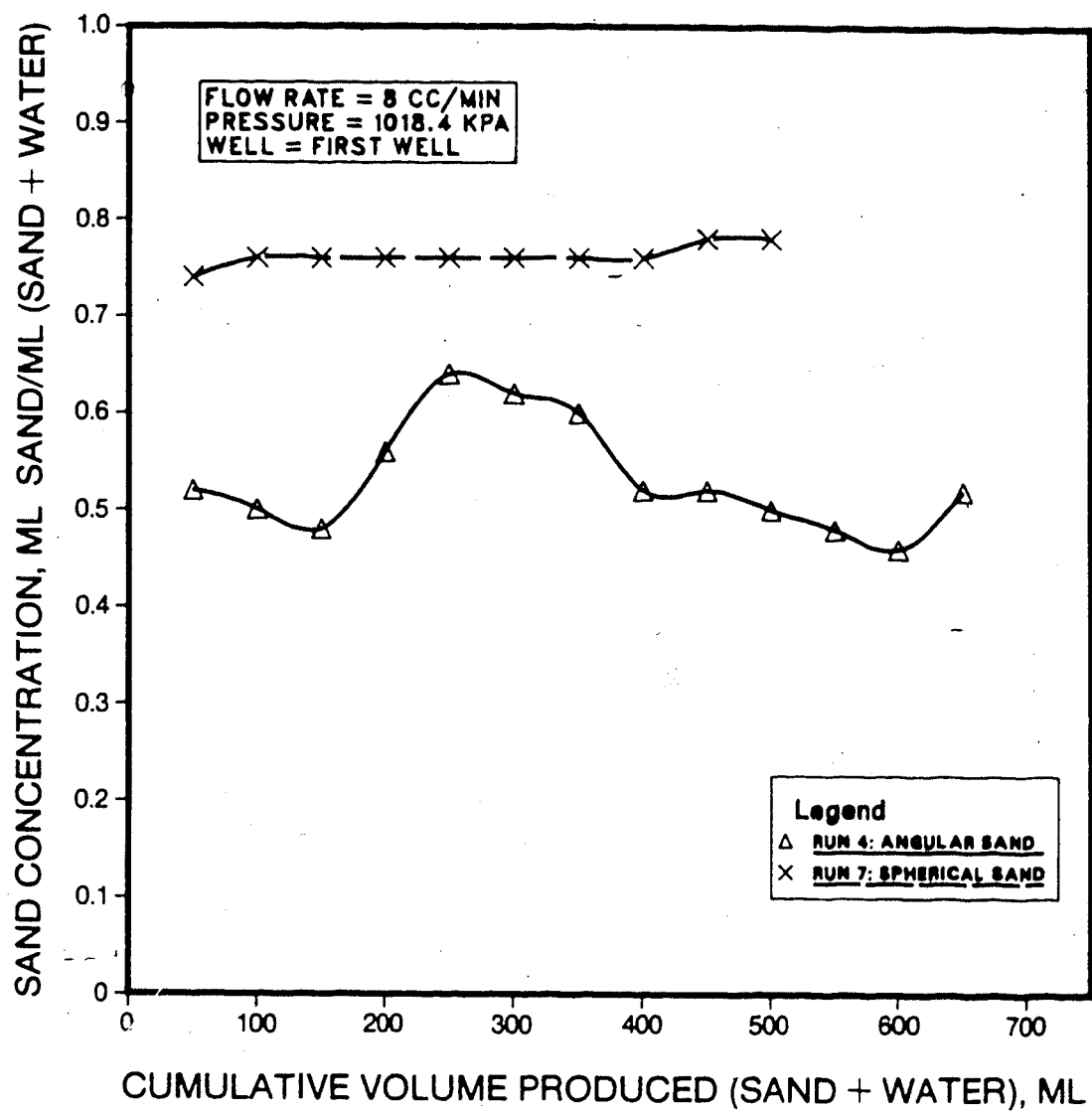


FIGURE 37 : Effect of Sand Shape

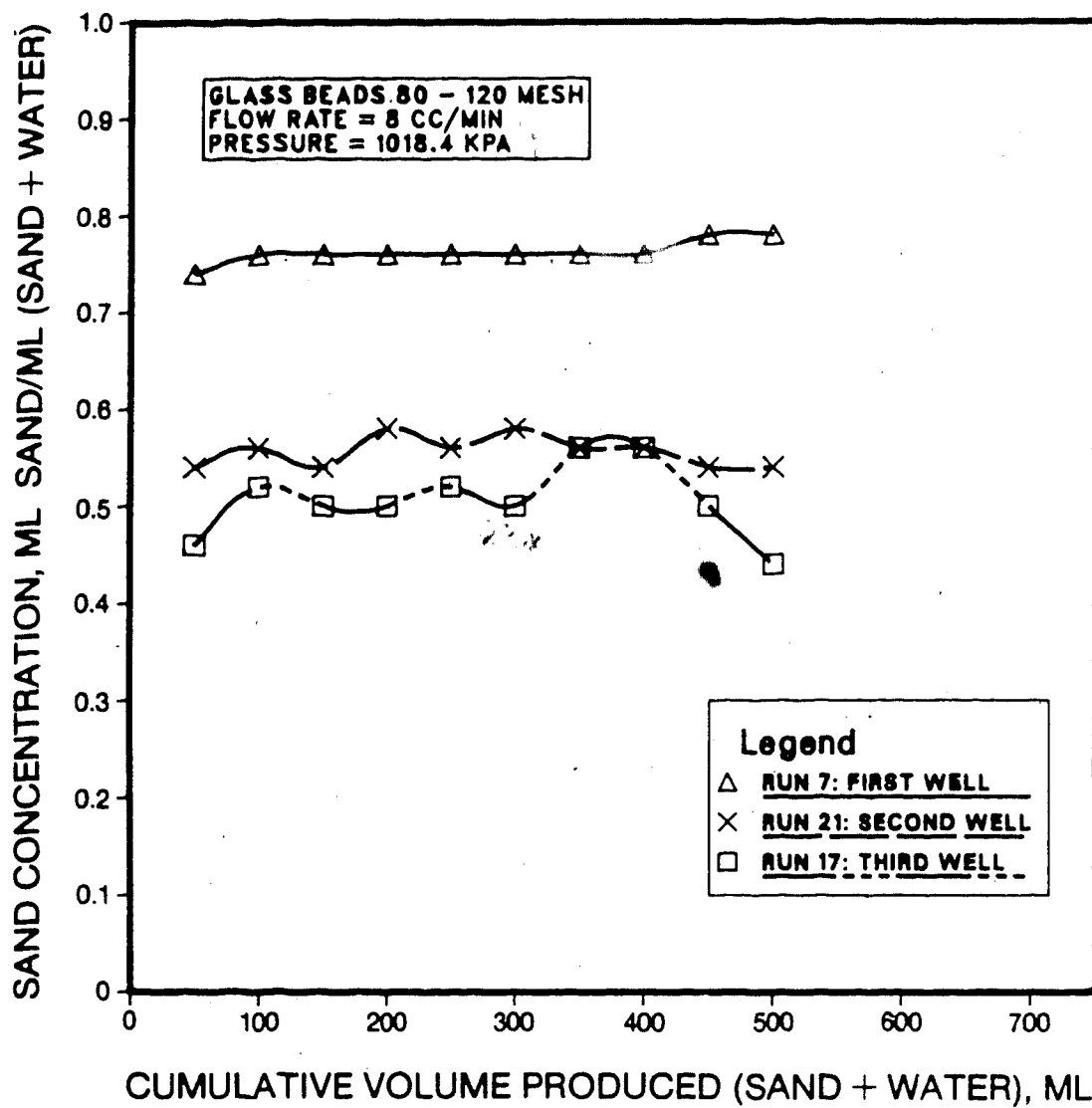


FIGURE 38 : Effect of Tubing Perforations

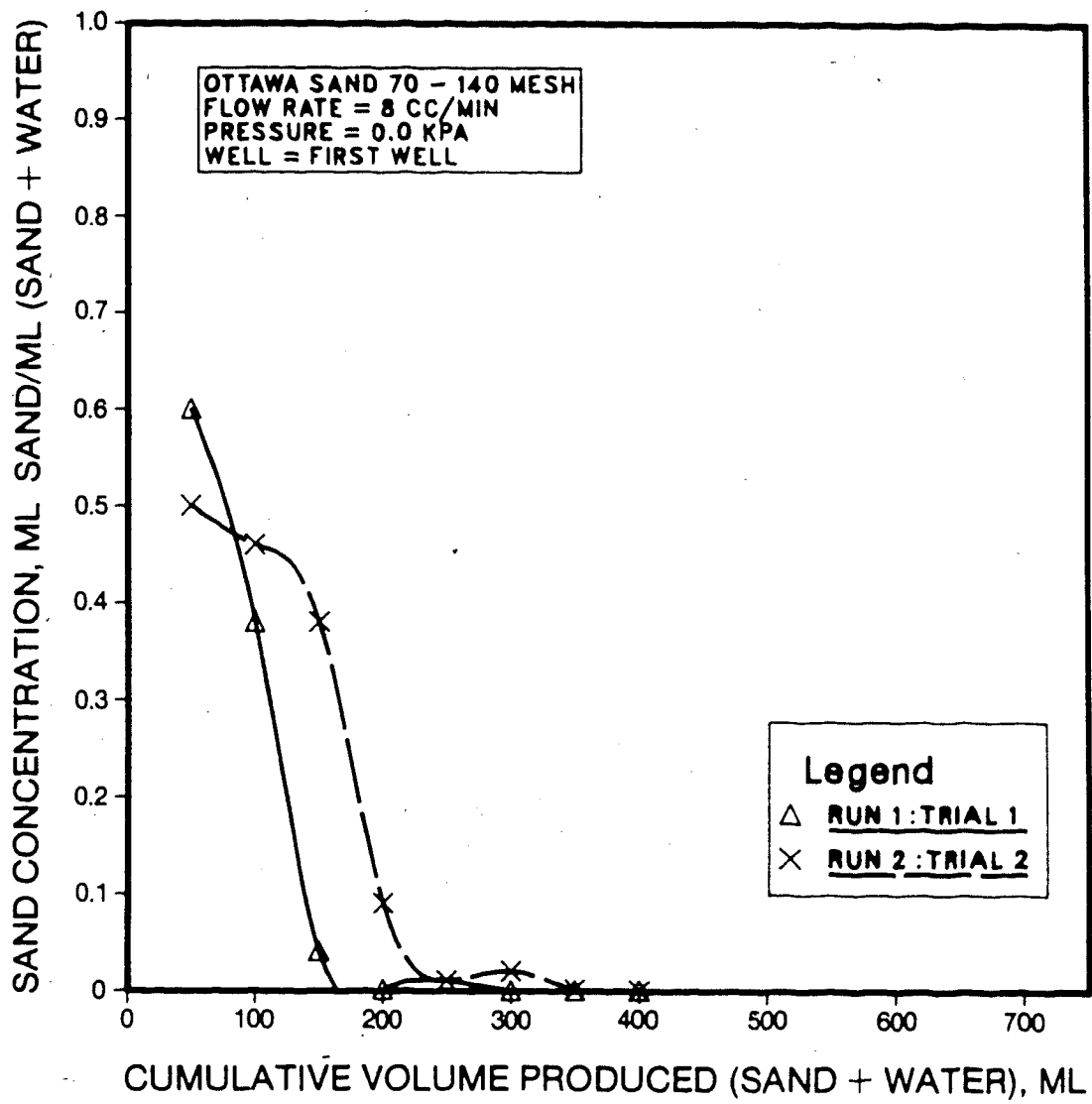


FIGURE 39 : Reproducibility of Ottawa Sand 70 - 140 Mesh  
(No Overburden Pressure)



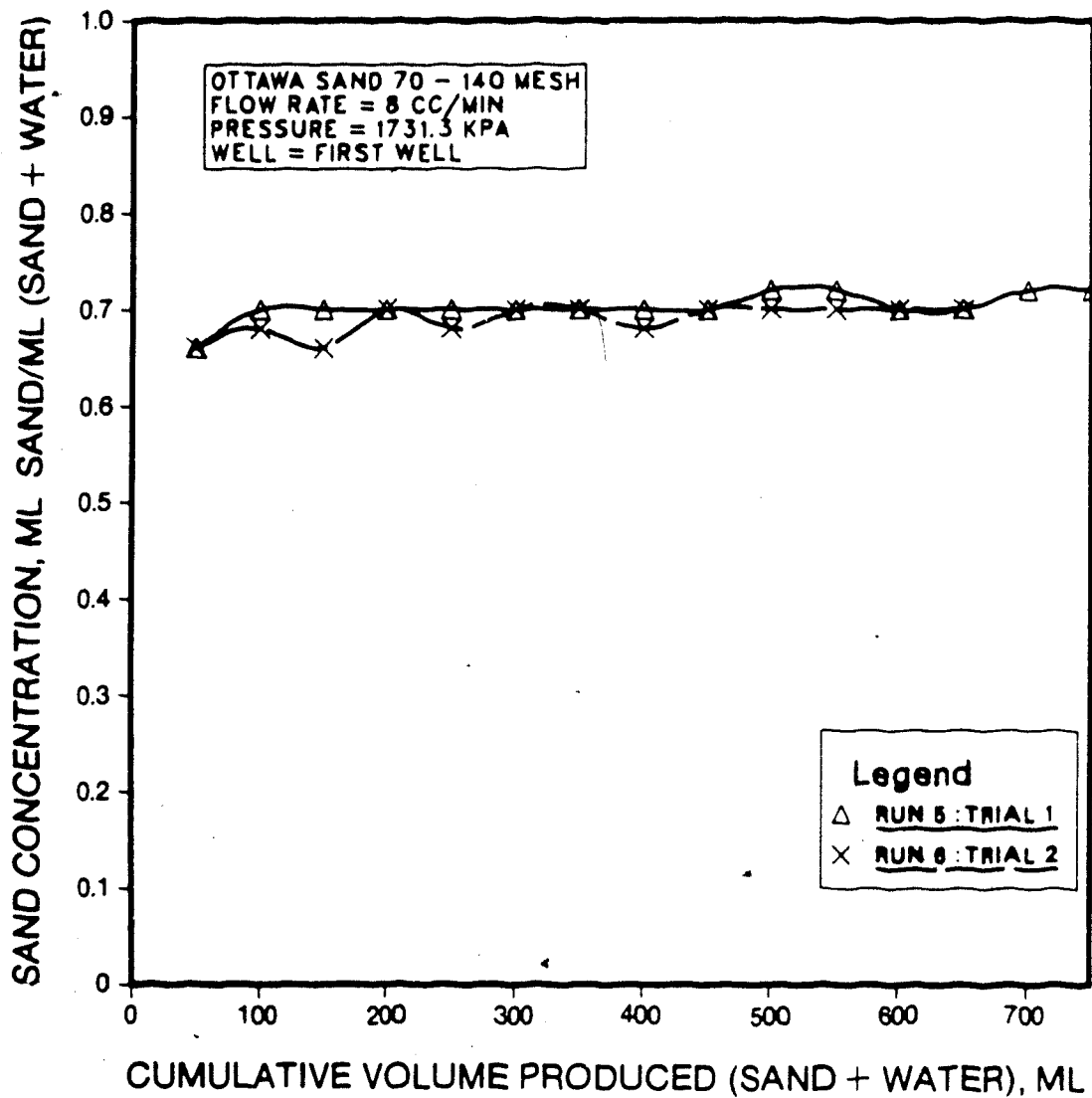


FIGURE 40 : Reproducibility of Ottawa Sand 70 -140 Mesh  
 (High Overburden Pressure)

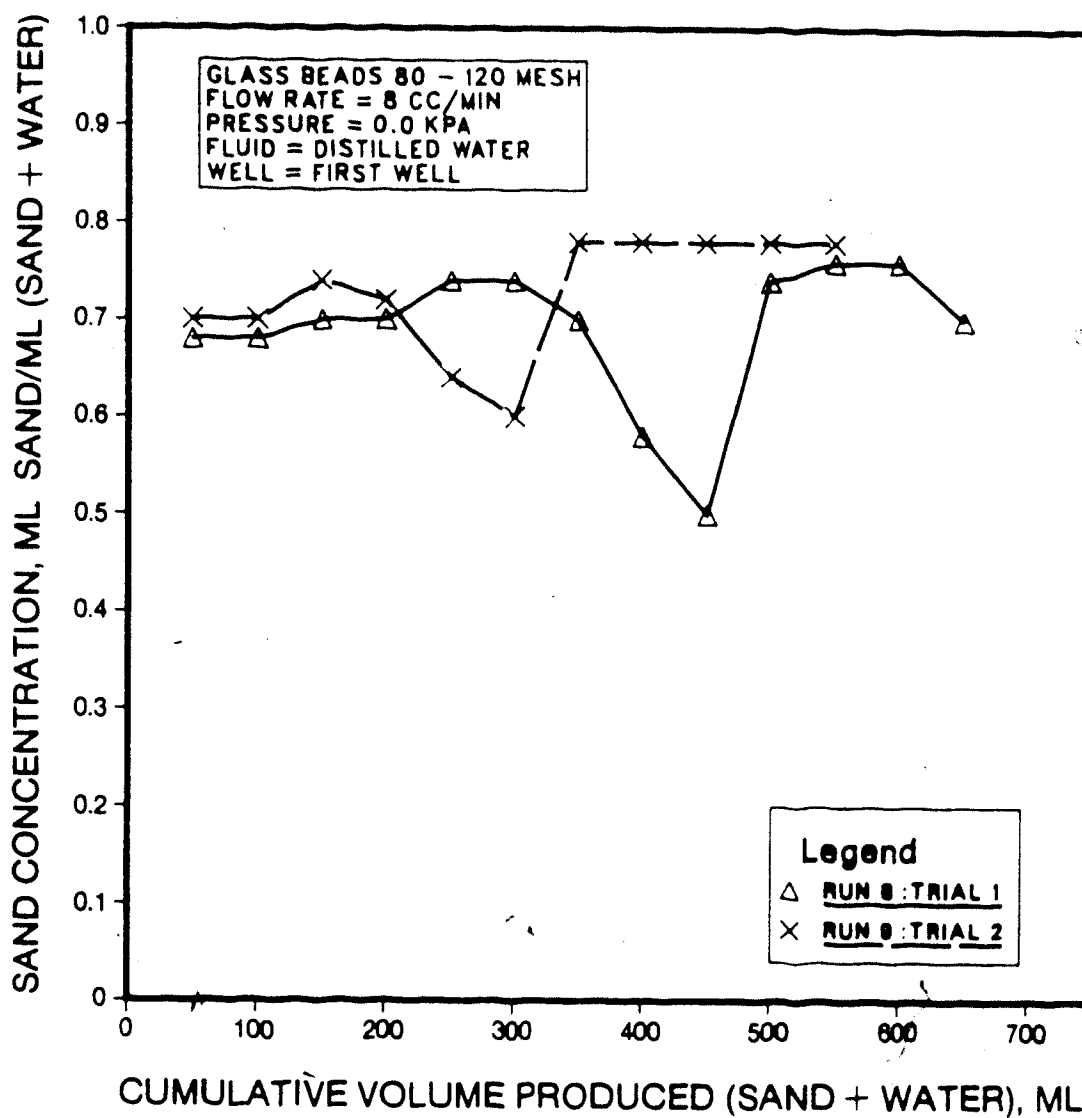


FIGURE 41: Reproducibility of Glass Beads 80 - 120 Mesh

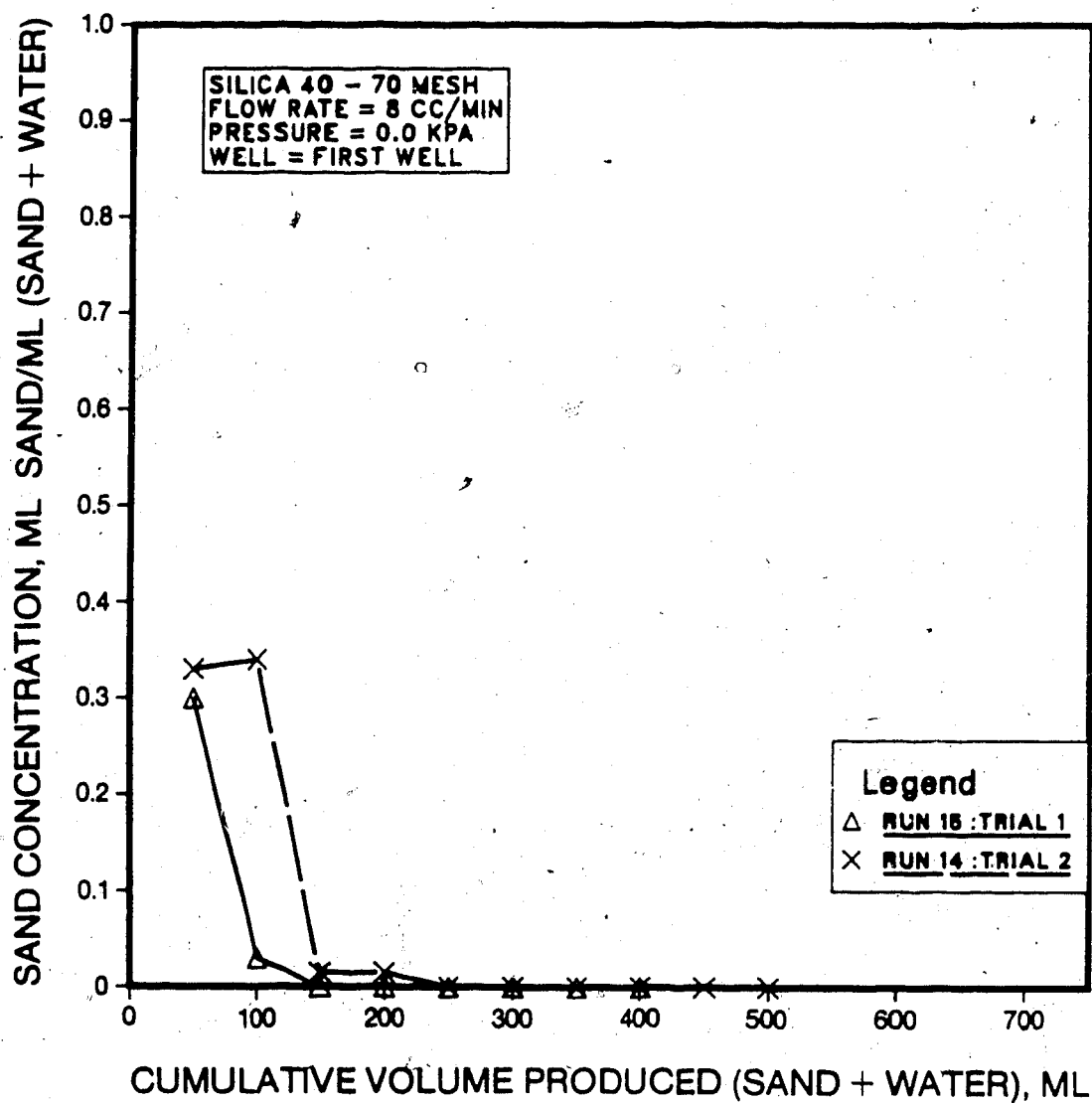


FIGURE 42 : Reproducibility of Silica 40 - 70 Mesh

was not similar for the runs conducted under the same experimental conditions, the concentration of sand in the effluent followed a similar production trend and magnitude range.

#### 5.4.3. Discussion of Sand Production Results

The radial flow experiments revealed that minimal amounts of sand were produced when the following conditions were met: low overburden loads, low flow rates, large sand grain size, and angular grain shape. The variables were found to be interdependent: although each of the stated conditions served to lower sand production, the amount of sand produced depended on the cumulative effect of the governing variables. For instance, the absence of an overburden load led to reducing sand production to zero in Run 1, in which the sand-pack consisted of angular sand. However, the absence of an overburden load reduced only slightly the sand production in Run 8, in which the cell was packed with spherical beads.

The plots presented in Figures 30 to 38 served to compare the amount of sand produced from tests in which one variable was changed while all other experimental conditions were kept constant. However, the radial flow tests were conducted using three well tubings having different flow areas, and were carried out over three different flow rates. In order to compensate for the effect of area and time of flow, the sand flux was determined by calculating the volume of dry sand produced in the effluent assuming a porosity of 40%, and dividing by the total area of flow and the flow time of the effluent. When the resulting values were plotted against time for all radial flow tests,

three types of curves were obtained. In the first type of curve, shown in Figure 43, the sand flux had a high initial value and gradually decreased with time until a sand flux value of zero was obtained. This type of curve was characteristic of experiments where the sand formed stable arches around the perforations, leading to a decrease in sand production until only water was produced. In the second curve type, the sand flux alternately increased and decreased with time (see Figure 44), indicating that unstable sand arches were formed and were subsequently destroyed. As shown in Figure 45, in the third type of curve, no arches were formed and the sand flux gradually increased with time.

The sand flux values obtained were found to range from 0.0 to 2.0 cm/minute for the experiments in which the slotted well tubing (Well #1) was used, and from 0.0 to 10.0 cm/minute for the experiments in which the round hole well tubings (Wells #2 and 3) were employed. The results of the experiments carried out using Well #1 are shown in Figures 46, 47 and 48, while the results of the experiments conducted using Wells #2 and 3 are shown in Figure 49.

The sand flux curves are presented in Figure 46 for Runs 1, 3, and 5, in which the overburden pressure was changed, while other operating conditions were kept constant. It was noted that in the absence of an overburden load (Run 1), the sand around the perforations bridged readily, and sand production decreased to zero 14 minutes after the start of the experiment. At an overburden load of 611.0 kPa (Run 3), the amount of sand produced decreased gradually and became negligible 64 minutes after the start of the experiment.

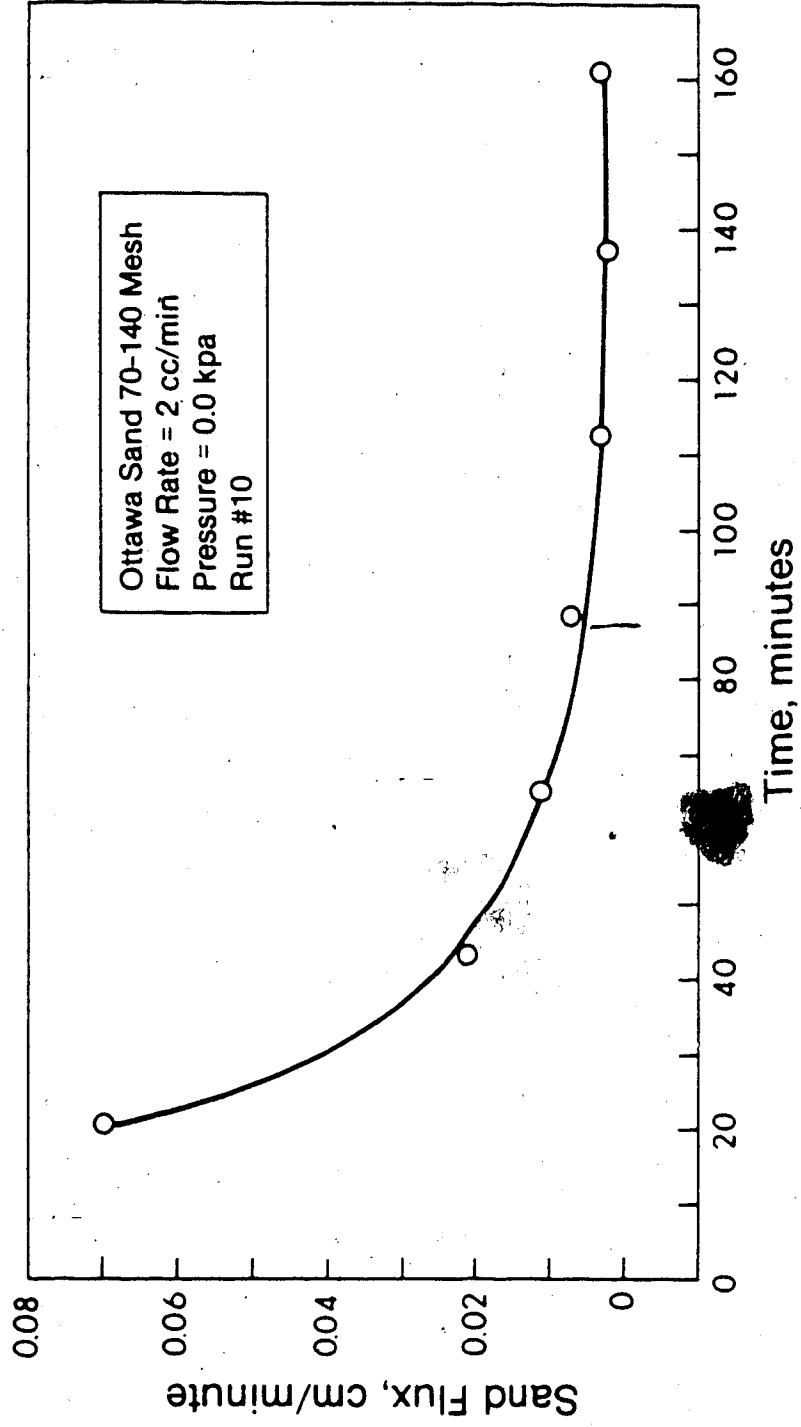


FIGURE 43: Sand Flux Versus Time Curve For Stable Sand Arches

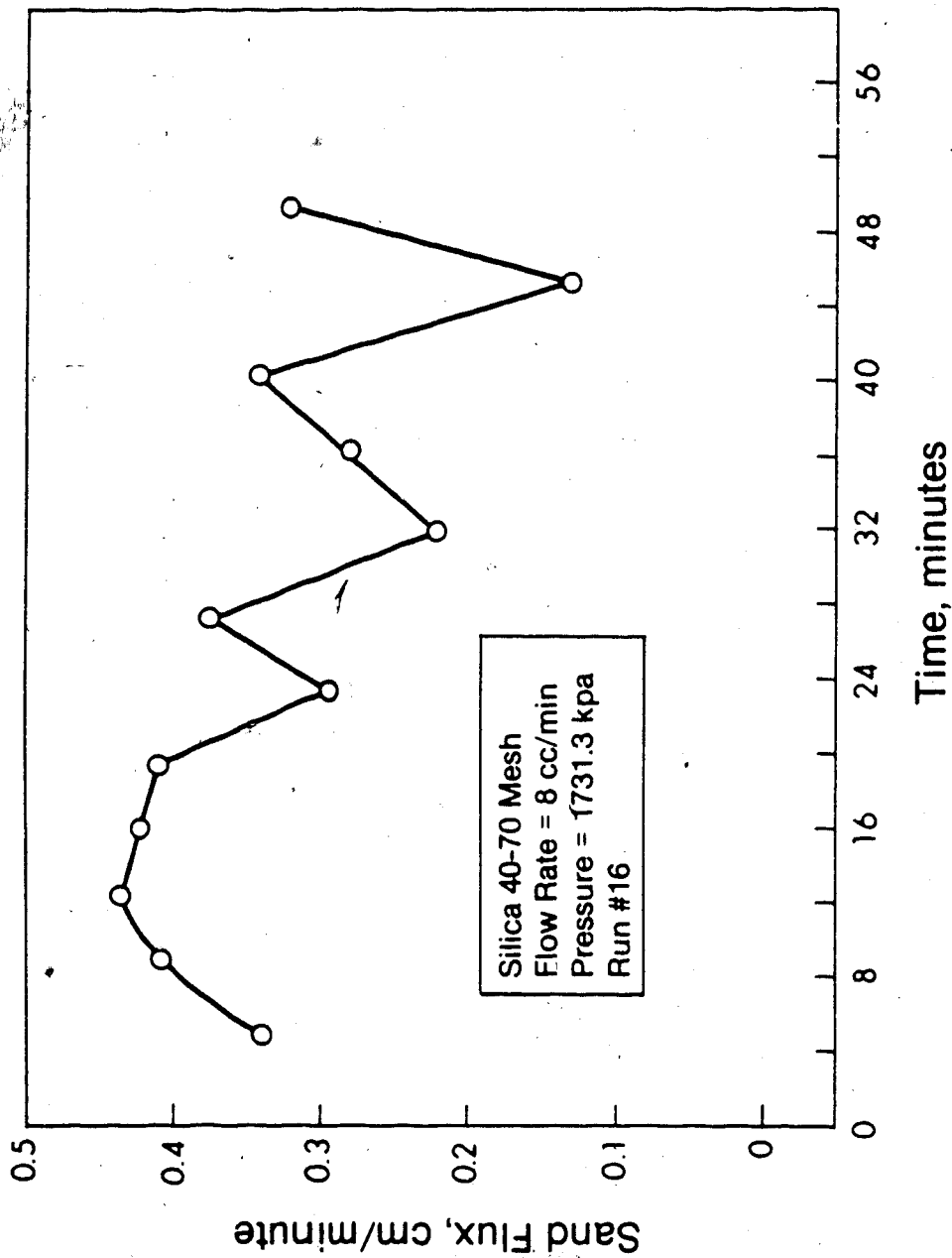


FIGURE 44: Sand Flux Versus Time Curve For Unstable Sand Arches

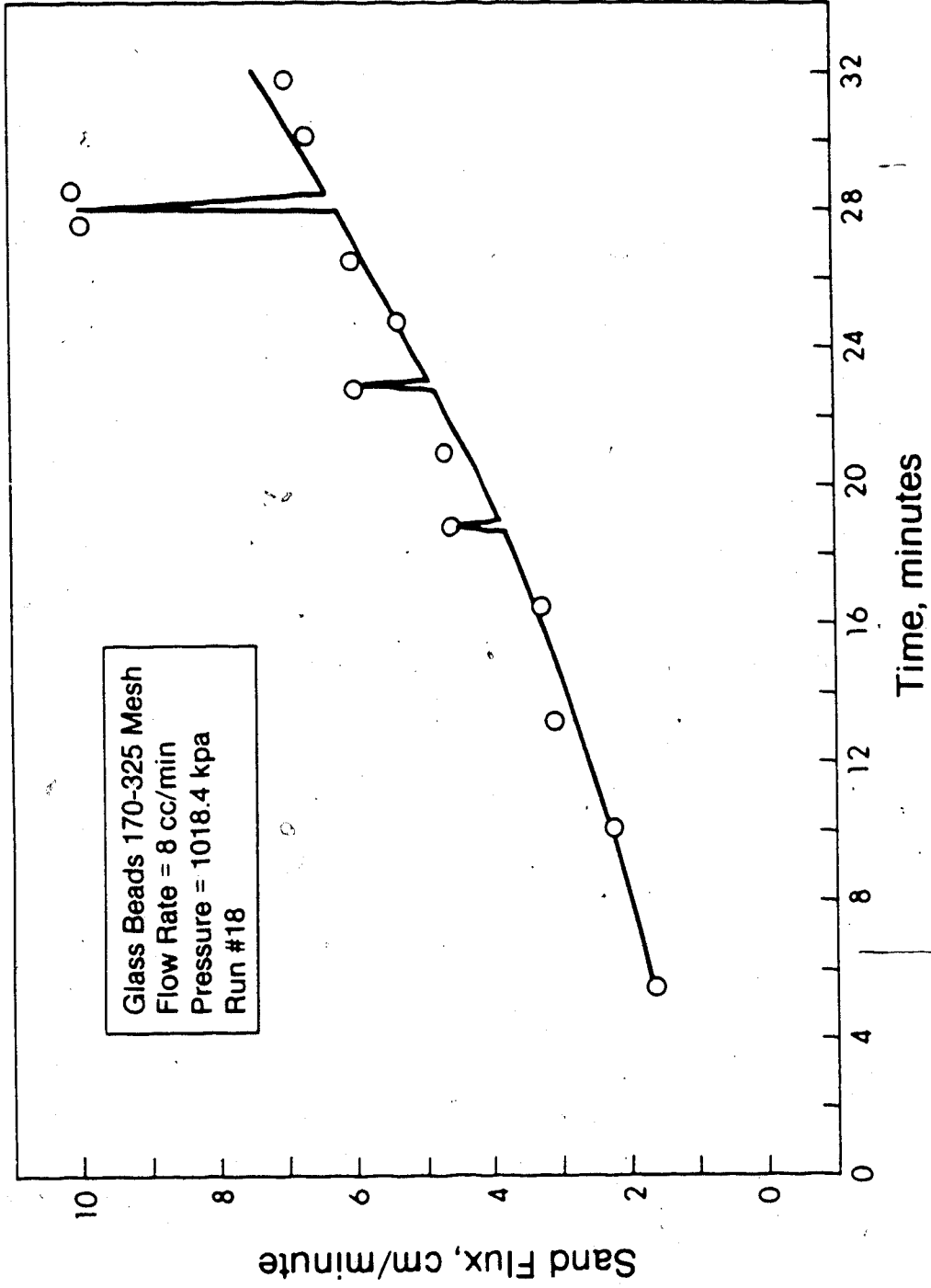


FIGURE 45: Sand Flux Versus Time Curve For Absence of Sand Arches



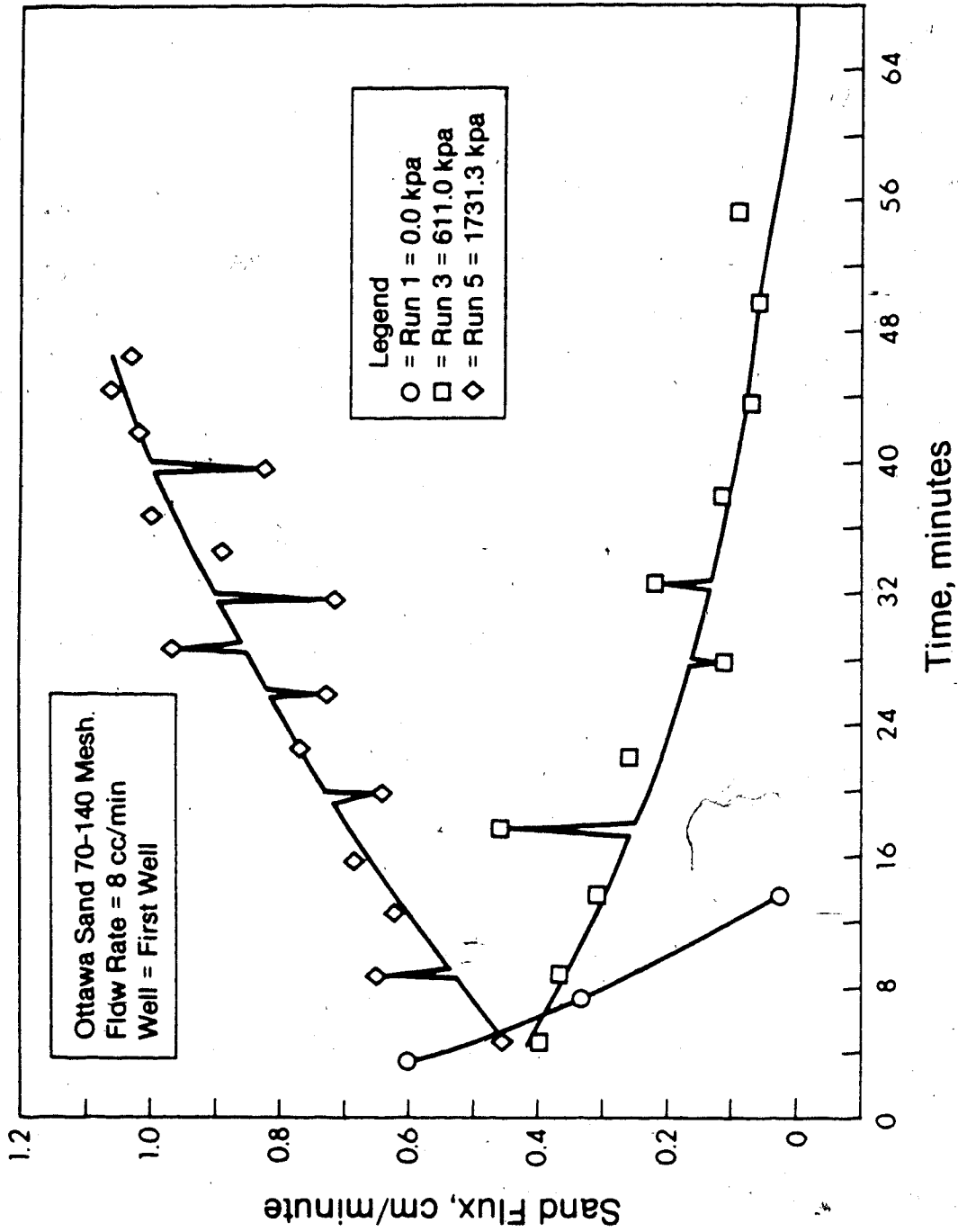


FIGURE 46: Effect of Overburden Pressure (Slotted Tubing Perforations)

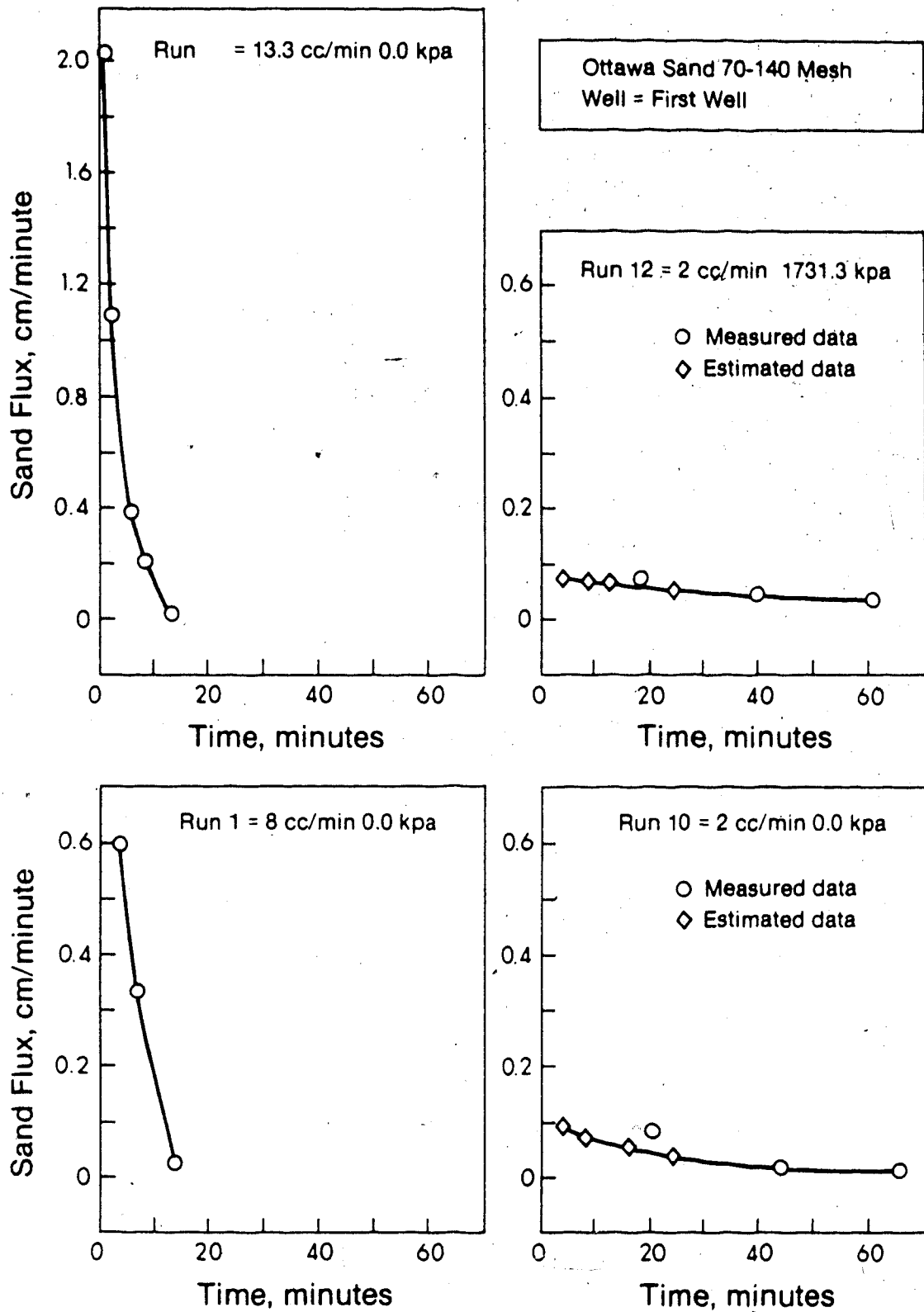


FIGURE 47: Effect of Flow Rate (Slotted Tubing Perforations)

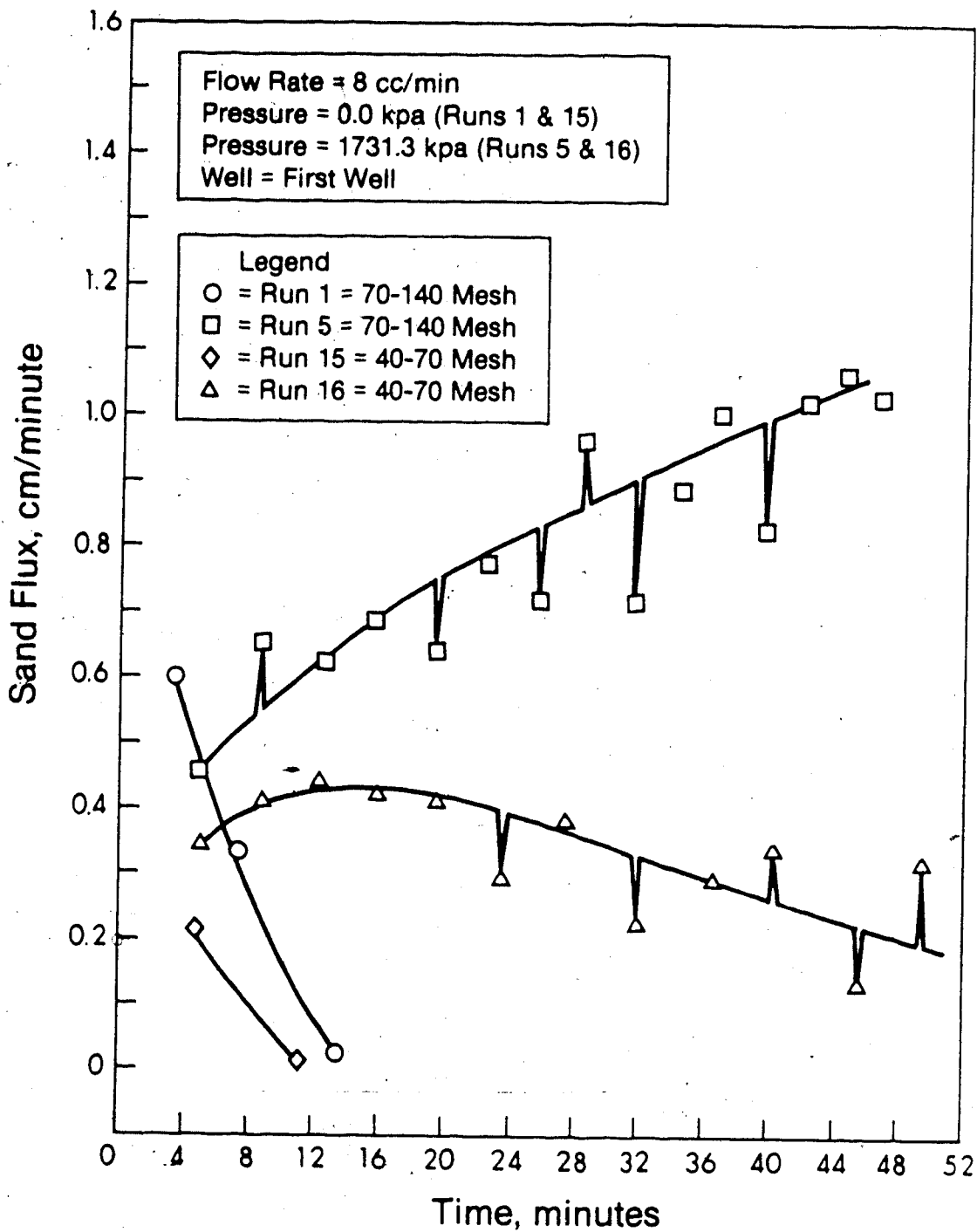


FIGURE 48: Effect of Grain Size (Slotted Tubing Perforations)

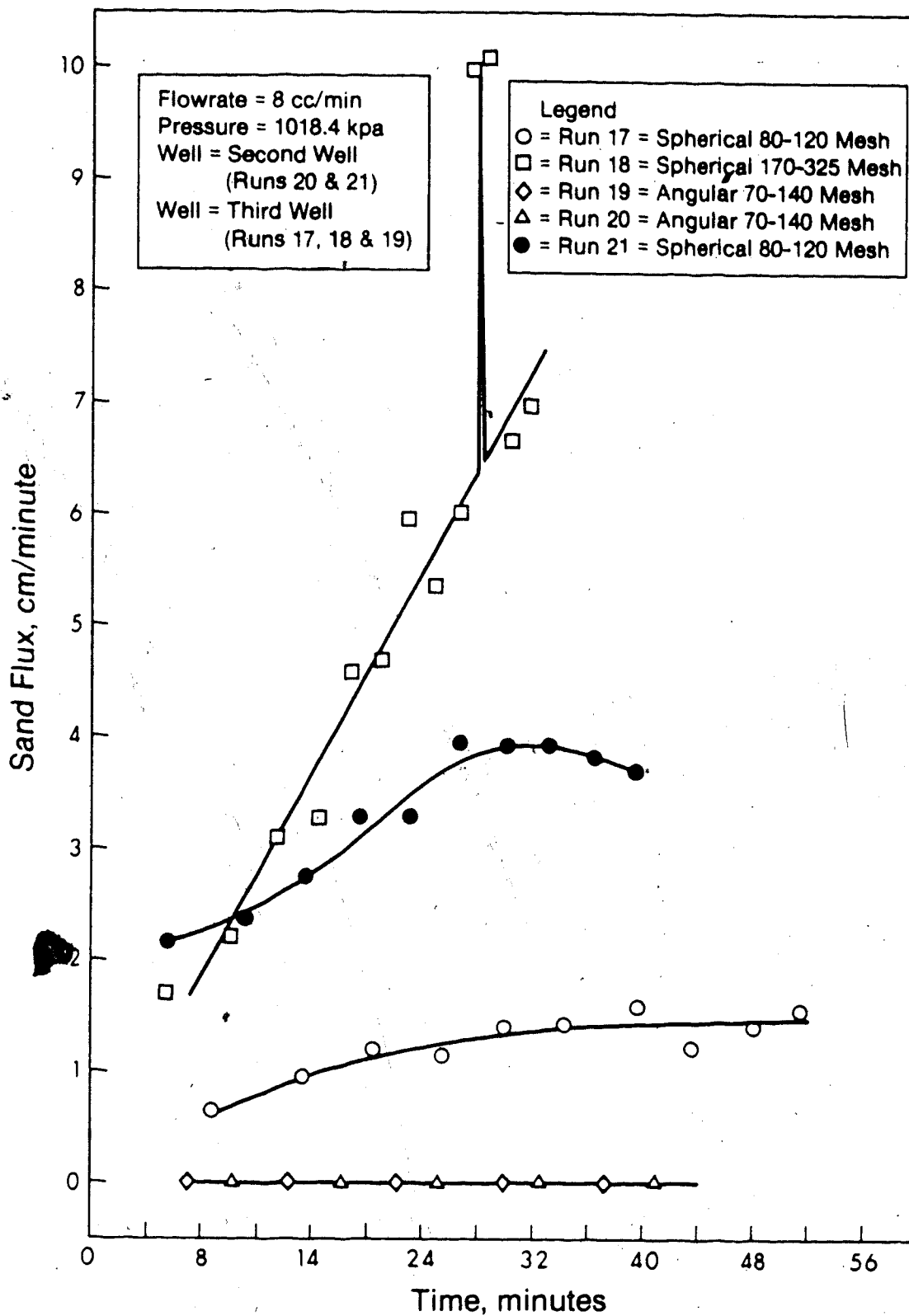


FIGURE 49: Effect of Grain Size and Shape (Round Tubing Perforations)

The overburden pressure in Run 5 was 1731.3 kPa, and led to a gradual increase in the sand production, indicating that the sand did not arch at this high load. The sudden fluctuations in the sand flux values shown in the curves of Runs 3 and 5 reflected the manner in which the sand flowed from the tubing outlet. Increasing sand flux pulses corresponded to sand flow in gushes, while decreasing pulses indicated sand flow in trickles.

The results of Runs 1, 10, 11 and 12 are shown in Figure 47. Runs 1, 10 and 11, in which a flow rate of 8, 2 and 13.3 ml/minute was employed respectively, were conducted in the absence of an overburden load. Run 12 was conducted under a pressure of 1731.3 kPa at a flow rate of 2 ml/minute. Because of the low flow rate employed in Experiments 10 and 12, the time required to collect the initial samples of effluent was about 20 minutes, thus rendering the comparison of results at low times difficult. In order to extend the curves of Runs 10 and 12 to low times, additional data points were determined by assuming that the rate of sand produced was related to time by a function of the form:

$$\dot{Q} = a_0 + a_1 t + a_2 t^2$$

where  $\dot{Q}$  is the rate of dry sand produced in ml/minute  
 $t$  is the time from the start of the experiment in minutes  
 and  $a_0$ ,  $a_1$  and  $a_2$  are constants.

A sample calculation is provided in Appendix B.

The curves of Runs 1, 10 and 11 in Figure 47 show that arching of the sand occurred in the absence of an overburden pressure, regardless of the flow rates used to conduct the experiments. It was noted, however, that the time required for sand production to cease increased as the flow rate decreased, while the initial sand flux values increased as the flow rate increased. Although the sand still formed arches at a flow rate of 2 ml/minute when the overburden load was 1731.3 kPa (Run 12), the sand flux values were found to be generally higher than those obtained when the load was 0.0 kPa (Run 10). No sand arches were formed at high overburden pressures when the flow rate was 8 ml/minute or higher (see Run 5 in Figure 46).

The curves in Figure 48 show the effect of sand grain size at low overburden pressures (Runs 1 and 15) and high overburden pressures (Runs 5 and 16). Sand arching occurred in both experiments 1 and 15 when no overburden load was applied. However, the sand flux values of Run 1, in which the cell was packed with 70 to 140 mesh Ottawa Sand, were higher than those of Run 15, in which the sand pack consisted of 40 to 70 mesh silica. At high overburden pressures, no arching was noted in Run 5, prepared using smaller sand grains, while unstable arches were formed in Run 16, prepared using larger sand grains.

The effect of grain size on sand production is also shown in Figure 49, Runs 17 and 18. Because both experiments were prepared using spherical glass beads, no arches were formed in either experiment, and the sand flux curves gradually increased with time. The sand flux values of Run 18, in which the pack consisted of smaller

grains, were much higher than those of Run 17.

Runs 17 and 19 differed from each other in the shape of sand used to pack the cell. The pack in Run 17 consisted of spherical glass beads and that of Run 19 consisted of angular sand. It was observed that no sand was produced in Run 19, which indicated that sand arches were almost spontaneously formed around the perforations. As mentioned previously, the sand flux curve in Run 17 increased with time, and no arches were formed.

The effect of tubing perforation size on sand production is shown in Runs 17 and 21 of Figure 49. Although Run 17 was conducted using a tubing with larger perforations (0.11 cm in diameter) than the tubing used in Run 21 (0.08 cm in diameter), the sand flux values of Run 21 were much higher than those of Run 17. As shown in Table 12, the flow velocity out of the well was 3.19 cm/minute in Run 17, and 6.06 cm/minute in Run 21. The increase in outlet velocity resulted from the decrease in the total flow area of the perforations, and caused the sand to be produced at higher rates.

#### 5.4.4. Discussion of Sand Production Mechanisms

In their experimental study of the failure mechanisms of unconsolidated sands, Hall and Harrisberger (1970) observed that sand production was caused by failure of the sand to form stable arches. The stability of an arch was found to depend on the degree of dilatancy and cohesiveness of the sand. Angular sand was noted to form stable arches, while round-grain sand failed to arch due to lack of surface restraint. Their observation was confirmed in the present

tests. Hall and Harrisberger reported that at high loads, the arches formed by angular sand failed due to grain crushing and breaking. In the present study, the SEM photomicrographs did not indicate any difference in the grain size of angular sand produced at high loads and that produced in the absence of overburden loads. The failure of sand arches at high overburden pressures must then have been due to other factors. Based on calculations made assuming elastic material behaviour, Durrett et al. (1977) predicted that overburden pressures would cause formation failure around a wellbore during production. It is believed that the continuous sand production observed at high loads is due to the replacement of the sand produced by the overlying material, thus leading to the destruction of arches (Vaziri, private communication).

The effect of flow rate on sand production was investigated by Tippie and Kohlhaas (1973). They reported that the smaller arches formed at low flow rates were more stable than the larger arches associated with large flow rates. These observations would explain why less sand is produced when the fluid is injected through the pack at a low flow rate. The authors also observed two types of arch failure: continuing failure that led to a continuous production of small amounts of sand, and massive failure in which large amounts of sand were produced in a short period of time. Both types of arch failure were noted in the radial flow tests conducted. At high loads, sand flowed in gushes, while at low loads, the sand tended to flow with the water at a steady rate.



The conditions which led to the formation of sand arches, or to increased sand production from the radial model are summarized in Table 14. As shown in Table 14, when a low overburden pressure was applied, arching of the sand occurred in all tests except those packed using spherical sand. In the tests carried under high overburden pressures, stable sand arches were formed when a low flow rate was employed, while no arching occurred at higher flow rates. However, unstable arches were formed at higher flow rates when the pack consisted of large sand grains. None of the experiments conducted using spherical glass beads showed any tendency to form arches around the perforations.

As indicated in Table 14, in the tests which exhibited arching behaviour, the time required for the sand production to cease varied with the operating conditions. While sand arches were formed very slowly at low flow rates in the tests using the slotted tubing, arching occurred rapidly at higher flow rates when no overburden pressure was applied. It was noted, however, that sand arches were formed instantaneously when round hole tubings were used, even though the tests were conducted under moderate overburden loads.

#### 5.5. TWO-PHASE FLOW TESTS

The linear flow tests conducted in unconsolidated porous packs showed that the permeability of the packs was not altered due to the flow of fines. An experiment consisting of four steps was therefore conducted in a consolidated core to investigate the effect of fines.

**Table 14: Factors Affecting Sand Production**

Run#	Pressure	Flow Rate	Grain Size	Grain Shape
1	Low	Medium	Medium	Angular
3	Medium	Medium	Medium	Angular
5	High	Medium	Medium	Angular
7	Medium	Medium	Medium	Spherical
8	Low	Medium	Medium	Spherical
10	Low	Low	Medium	Angular
11	Low	High	Medium	Angular
12	High	Low	Medium	Angular
13	High	High	Medium	Angular
15	Low	Medium	Large	Angular
16	High	Medium	Large	Angular
17	Medium	Medium	Medium	Spherical
18	Medium	Medium	Small	Spherical
19	Medium	Medium	Medium	Angular
20	Medium	Medium	Medium	Angular
21	Medium	Medium	Medium	Spherical

Table 14: (Continued)

Run#	Perforation Size and Shape	Comments
1	Slotted, large flow area	Sand flux decreased; Arched rapidly
3	Slotted, large flow area	Sand flux decreased; Arched slowly
5	Slotted, large flow area	Sand flux increased; No arching
7	Slotted, large flow area	Sand flux increased; No arching
8	Slotted, large flow area	Sand flux increased; No arching
10	Slotted, large flow area	Sand flux decreased; Arched slowly
11	Slotted, large flow area	Sand flux decreased; Arched rapidly
12	Slotted, large flow area	Sand flux decreased; Arched slowly
13	Slotted, large flow area	Sand flux increased; No arching
15	Slotted, large flow area	Sand flux decreased; Arched rapidly
16	Slotted, large flow area	Sand flux fluctuated; Unstable arches
17	Round holes, medium flow area	Sand flux increased; No arching
18	Round holes, medium flow area	Sand flux increased; No arching
19	Round holes, medium flow area	No sand produced; Spontaneous arching
20	Round holes, small flow area	No sand produced; Spontaneous arching
21	Round holes, small flow area	Sand flux increased; No arching.

migration on relative permeability. The first part of the experiment involved oil flooding a Berea sandstone core with Hamilton Lake crude, followed by waterflooding with 2% (w) NaCl. In the second part of the experiment, the core was again oil flooded with Hamilton Lake crude, then waterflooded with 30% (w) brine to examine the effect of salt concentration on relative permeability. In Parts 3 and 4, the first and second experimental steps were repeated in order to allow the movement of fines to be detected. The relative permeabilities to the brine and the crude were calculated for each step, and the absolute permeability of the Berea core was determined before and after testing. The experimental results are given in Tables C48 to C51.

Plots of relative permeabilities to the crude and the brine versus water saturation are presented in Figure 50 for the four experimental steps. The highest relative permeability values were obtained in Step 1, in which the Berea core was waterflooded with 2% brine. When the core was waterflooded with 30% brine in Step 2, the relative permeability to Hamilton Lake crude decreased significantly (66.7% decrease at connate water saturation), and the relative permeability to brine decreased moderately. In Step 3, when the core was waterflooded once again with 2% brine, the relative permeability to the crude was found to be higher than its value in Step 2, but lower than the initial relative permeability calculated in Step 1 (19.6% lower at connate water saturation). In the final step, waterflooding the core with 30% brine led to a substantial decrease in the relative permeabilities to oil and brine. The relative

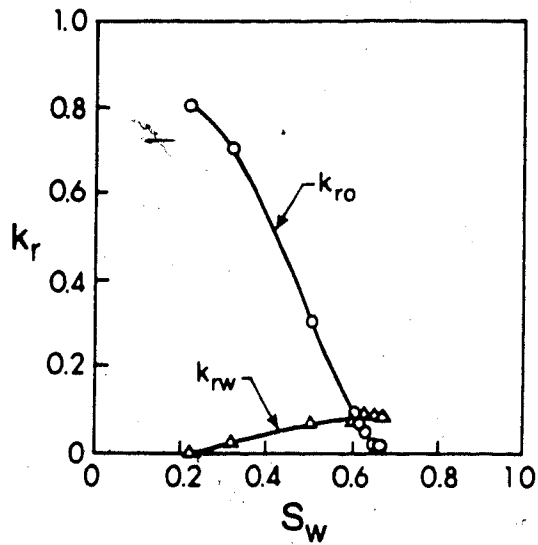


FIGURE 50(a) : Relative Permeability of Hamilton Lake Crude and 2% NaCl Brine - Step 1

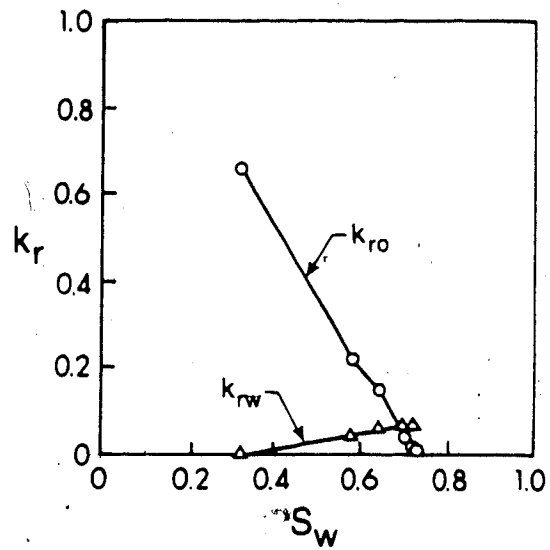


FIGURE 50(c) : Relative Permeability of Hamilton Lake Crude and 2% NaCl Brine - Step 3

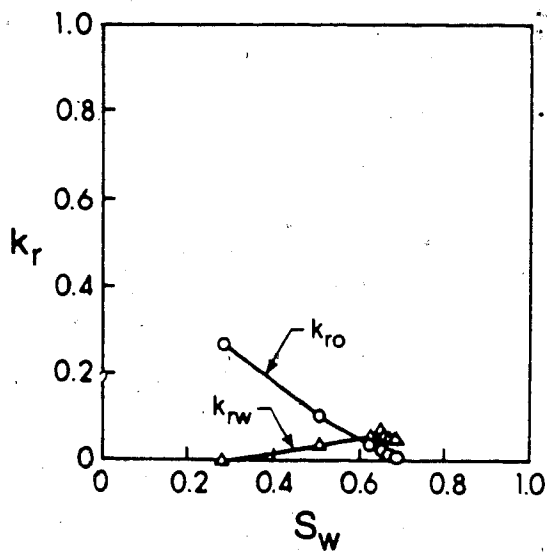


FIGURE 50(b) : Relative Permeability of Hamilton Lake Crude and 30% NaCl Brine - Step 2

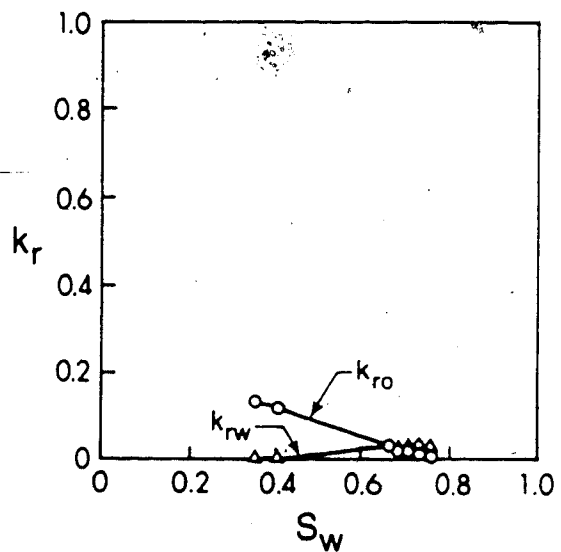


FIGURE 50(d) : Relative Permeability of Hamilton Lake Crude and 30% NaCl Brine - Step 4

permeability to the crude was noted to decrease by 83.7% at connate water saturation over its initial value, and by 50.9% over its value in Step 2.

In a study of the effect of salt concentration on core permeability, Khilar (1981) reported that a critical salt concentration existed, above which no reduction to core permeability due to migration of fines occurred. The reduction in core permeability was attributed to the release of clay particles from the pore walls when the salt concentration fell below the critical salt concentration, and their plugging of pore constrictions as they travelled with the fluid. It was suggested that particle release was mainly due to the double layer forces of repulsion, which are large at low salt concentrations. In the present test, by comparing Steps 1 and 2, and Steps 3 and 4, of Figure 43, it was observed that increasing the salt concentration from 2% NaCl to 30% NaCl led to a decrease in the relative permeabilities. The highest salt concentration investigated in the work of Khilar was 3% (w) NaCl. It is possible that the effect of salt concentration on permeability would be different or even reversed at the high concentrations used in this test.

Comparing Steps 1 and 3, which were carried out using 2% NaCl, it was noted that the values of relative permeability in Step 3 were smaller than those in Step 1, although the concentration of salt in the brine was similar. The relative permeability values were also found to be lower in Step 4 than in Step 2, although both steps were conducted using 30% NaCl. The decrease in relative permeability may have been due to further plugging of the core pores by fines migration. The

absolute permeability of the Berea core decreased from an initial value of  $0.661 \mu\text{m}^2$  to a value of  $0.247 \mu\text{m}^2$  at the end of the experiment. This drastic reduction in absolute permeability also suggested that more pores became plugged with continued fluid flow through the core.

The presence of an oil phase in addition to the water phase may also have contributed to the reduction in core permeability. As discussed by Muecke (1979), particle wettability and surface/interfacial forces tend to play a dominant role in the flow of fines when multfluid phases are present in the porous medium. Muecke observed that in two-phase flow experiments, the oil/water interface displaced the fines ahead of it, causing some fines to bridge at pore restrictions. No movement of fines was discerned when the wetting phase became immobile.

This experiment constituted a preliminary study of the effect of fines migration on relative permeability. Although several observations were drawn from the experimental results, additional research is needed to better identify the various factors affecting the migration of fines associated with multiphase flow.

## 6. CONCLUSIONS

This investigation was designed to examine how various operating conditions affect the flow of fines in porous media and sand production in a radial flow model simulating a wellbore. Based on the experimental work conducted, the following conclusions can be drawn:

1. The concentration of fines in the effluent increases as the fluid flow rate and the initial amount of fines in the pack are increased. Sand packs consisting of large, spherical sand grains yield a higher concentration of fines in the effluent than packs with small, angular grains. Very little movement of fines is detected when the density of fines is increased.
2. Within certain ranges of experimental conditions, the amount of fines produced is directly proportional to the interstitial velocity, the initial amount of fines in-place, and the sand grain size. This relationship does not hold when the sand pack consists of large spherical glass beads, or when high-density fines are employed.
3. For the sand grain sizes employed, which reproduce the grain sizes encountered in Lloydminster, only a small part (less than 1%) of the fines initially present in the pack are able to move through the pores. It is therefore concluded that the size of movable fines in the unconsolidated formations of Lloydminster does not exceed 20  $\mu\text{m}$ .



4. Sand production increases as the overburden pressure and the fluid flow rate are increased. More sand is produced from spherical, small-grained sandpacks than from angular, large-grained packs.

5. Arching of the sand occurs when low overburden pressures are applied, unless the pack consists of spherical glass beads. When high overburden loads are applied, sand arches are formed when the fluid is flowed at a low rate.

6. In two-phase flow in a Berea sandstone core, the relative permeabilities to oil and brine decreased when the salt concentration in the brine was increased from 2% NaCl to 30% NaCl. The absolute permeability of the core decreased after continued fluid flow due to plugging of pore restrictions caused by the migration of fines.

## 7. RECOMMENDATIONS

1. The effect of the suspension - carrying fluid on the flow of fines should be determined by conducting experiments using fluids of different viscosities and densities.

2. Flow of fines studies should be undertaken at different ratios of pore diameter to particle diameter in order to determine how the flow mechanism of fines is influenced by the ratio of pore diameter to particle diameter.

3. Linear flow tests should be conducted by placing the core holder in a vertical position and flowing the fluid in both the upward and downward directions, to investigate the effect of gravity on the flow of fines.

4. Experiments should be carried out to examine how the operating variables affect sand production in multiphase flow.

5. Investigations of fines migration in multiphase flow should be conducted to determine to what extent relative permeabilities to oil and brine are altered when the salt concentration in the brine and the displacement sequences are varied.

## REFERENCES

- Adams, D.M.: "Experiences With Waterflooding Lloydminster Heavy Oil Reservoirs", Paper SPE 10196 presented at the 56th Annual Fall Technical Conference and Exhibition, San Antonio, Texas (October 5-7, 1981).
- Bratli, R.K. and Risnes, R.: "Stability and Failure of Sand Arches", Society of Petroleum Engineers Journal (April, 1981), p. 236-248.
- Byrne, P.M. and Vaziri, H.H.: "Stress, Deformation and Flow Analysis in Oil Sand Masses", Paper presented at the XI International Conference on Soil Mechanics and Foundation Engineering, San Francisco, California (August, 1985).
- Cleary, M.P., Melvan, J.J. and Kohlhaas, C.A.: "The Effect of Confining Stress and Fluid Properties on Arch Stability in Unconsolidated Sands", Paper SPE 8426 presented at the 54th Annual Fall Technical Conference and Exhibition, Las Vegas, Nevada (September 23-26, 1979).
- Donaldson, E.C., Baker, B.A. and Carroll, H.B.: "Particle Transport in Sandstones", Paper SPE 6905 presented at the 52nd Annual Fall Technical Conference and Exhibition, Denver, Colorado (October 9-12, 1977).
- Durrett, J.L., Golbin, W.T., Murray, J.W. and Tighe, R.E.: "Seeking a Solution to Sand Control", Journal of Petroleum Technology (December, 1977), p. 1664-1672.
- Eliassen, R.: "Clogging of Rapid Sand Filters", Journal of American Water Works Association, Vol. 33 (1941), p. 926-942.
- Gabriel, G.A. and Inamdar, G.R.: "An Experimental Investigation of Fines Migration in Porous Media", Paper SPE 12168 presented at the 58th Annual Technical Conference and Exhibition held in San Francisco, California (October 5-8, 1983).
- Gruesbeck, C. and Collins, R.E.: "Entrainment and Deposition of Fine Particles in Porous Media", Society of Petroleum Engineers Journal (December, 1982), p. 847-856.
- Gurel, D.O.: "How Husky Makes a Profit in Heavy Oil Production", World Oil (September, 1979), p. 63-67.
- Hall, C.D. and Harrisberger, W.H.: "Stability of Sand Arches: A Key to Sand Control", Journal of Petroleum Technology (July, 1970), p. 821-829.

- Herzig, J.P., LeClerc, D.M. and Le Goff, P.: "Flow of Suspensions Through Porous Media - Application to Deep Filtration", Industrial and Engineering Chemistry, Vol. 62 (1970), p. 8-35.
- Ives, K.J.: "A Theory of the Functioning of Deep Filters", Symposium on Interactions Between Fluids and Particles, Institution of Chemical Engineers (London, 1962), p. 260-268.
- Iwasaki, T.: "Some Notes on Sand Filtration", Journal of American Water Works Association, Vol. 29 (1937), p. 1591-1602.
- Jones, S.C. and Roszelle, W.O.: "Graphical Techniques for Determining Relative Permeability From Displacement Experiments", Journal of Petroleum Technology (May, 1978), p. 807-817.
- Khilar, K.C.: "The Water Sensitivity of Berea Sandstone", Ph.D. Thesis, University of Michigan (1981).
- Likwartz, D.J.: "A History of Sand Control in the Teak Field", Journal of Petroleum Technology (September, 1976), p. 9-18.
- Mantooth, M.A. and Williams, R.H.: "Sand Control by Application of Special Fluids and Techniques in a Shallow Sand, Offshore, Louisiana: A Case History", Paper SPE 8800 presented at the Fourth Symposium on Formation Damage Control, Bakersfield, California (January 28-29, 1980).
- Maroudas, A. and Eisenklam, P.: "Clarification of Suspensions: A Study of Particle Deposition in Granular Media", Chemical Engineering Science, Vol. 20 (1965), p. 867-888.
- Methven, N.E. and Kemick, J.G.: "Drilling and Gravel Packing with an Oil Base Fluid System", Journal of Petroleum Technology (June, 1969), p. 671-679.
- Muecke, T.W.: "Formation Fines and Factors Controlling Their Movement in Porous Media", Journal of Petroleum Technology (February, 1979), p. 144-150.
- O'Melia, C.R. and Crapps, D.K.: "Some Chemical Aspects of Rapid Sand Filtration", Journal of American Water Works Association, Vol. 56 (1964), p. 1326-1344.
- O'Melia, C.R. and Stumm, W.: "Theory of Water Filtration", Journal of American Water Works Association, Vol. 59 (1967), p. 1393-1412.
- Ornatskii, N.V., Sergeev, E.M. and Shekhtman, Y.M.: "Investigations of the Process of Clogging of Sands, University of Moscow (1955).
- Potter, J.M. and Dibble, W.E.: "Chemical Aspects of Iron Colloid Plugging in Quartz Sands and Implications for Formation Damage", Journal of Petroleum Technology (September, 1985), p. 1682-1688.

- Reeves, M.: "Mechanical Behaviour of Unconsolidated Heavy-Oil Sands During Production/Injection Cycles", CIM preprint No. 9 presented at the First Annual Technical Meeting of the South Saskatchewan Section, Regina, Saskatchewan (September 15-17, 1985).
- Rike, J.L.: "Shortcomings of Present Sand - Control Methods Suggest New Fail - Safe Concept", Oil and Gas Journal (February, 1975), p. 97-102.
- Risnes, R., Bratli, R.K. and Horsrud, P.: "Sand Stresses Around a Wellbore", Society of Petroleum Engineers Journal (December, 1982), p. 883-898.
- Rogers, E.B.: "Sand Control in Oil and Gas Wells", Oil and Gas Journal (November, 1971), p. 54-60.
- Sawolo, N., Krueger, R.F. and Maly, G.P.: "Case History of Yakin Field: Its Development and Sand Control", Journal of Petroleum Technology (January, 1983), p. 23-30.
- Schwartz, D.H.: "Successful Sand Control Design for High Rate Oil and Water Wells", Journal of Petroleum Technology (September, 1969), p. 1193-1198.
- Sinclair, A.R. and Graham, J.W.: "Resin-Coated Gravel is Used to Help Control Sand", Oil and Gas Journal (April, 1977), p. 58-60.
- Stein, N., Kelly, J., Baldwin, W.F. and McNeely, W.E.: "Sand Production Determined from Noise Measurements", Journal of Petroleum Technology (July, 1972), p. 803-806.
- Stein, N. and Hilchie, D.W.: "Estimating the Maximum Production Rate Possible from Friable Sandstones Without Using Sand Control", Journal of Petroleum Technology (September, 1972), p. 1157-1160.
- Stein, N., Odeh, A.S. and Jones, L.G.: "Estimating Maximum Sand-Free Production Rates from Friable Sands for Different Well Completion Geometries", Journal of Petroleum Technology (October, 1974), p. 1156-1158.
- Stein, N.: "Mechanical Properties of Friable Sands from Conventional Log Data", Journal of Petroleum Technology (July, 1976), p. 757-763.
- Stein, P.C.: "A Study of the Theory of Rapid Sand Filtration", D. Sc. Thesis, Massachusetts Institute of Technology (1940).
- Suman, G.O.: "Sand Control Handbook", Gulf Publishing Company, Houston, Texas (1975).

- Terwilliger, P.L., Smith, F.M. and Goodwin, R.J.: "Warm-Air Coking - A New Completion Method for Unconsolidated Sands", Journal of Petroleum Technology (April, 1964), p. 367-371.
- Tippie, D.B. and Kohlhaas, C.A.: "Effect of Flow Rate on Stability of Unconsolidated Producing Sands", SPE preprint No. 4533 presented at the 48th Annual Fall Meeting, Las Vegas, Nevada (September 30-October 3, 1973).
- Tixier, M.P., Loveless, G.W. and Anderson, R.A.: "Estimation of Formation Strength from the Mechanical - Properties Log", Journal of Petroleum Technology (March, 1975), p. 283-293.
- Toma, P., Livesey, D.B., and Heidrick, T.R.: "A New Sand Control Filter for Thermal Recovery Wells, SPE preprint No. 15057 presented at the 56th California Regional Meeting, Oakland, California (April 2-4, 1986).
- Treadway, B.R., Brandt, H. and Parker, P.H.: "Studies of a New Process to Consolidate Oil Sands with Plastics", Journal of Petroleum Technology (December, 1966), p. 1537-1543.
- Vaziri, H.H.: "Mechanics of Fluid and Sand Production from Oil Sand Reservoirs", CIM preprint No. 86-37-75 presented at the 37th Annual Technical Meeting, Calgary, Alberta (June 8-11, 1986).
- Vaziri, H.H.: "Finite Element Analysis of Oil Sands Subjected to Thermal Effects", CIM preprint No. 86-37-74 presented at the 37th Annual Technical Meeting, Calgary, Alberta (June 8-11, 1986).
- Vonde, T.R.: "Specialized Pumping Techniques Applied to a Very Low Gravity, Sand Laden Crude: Cat Canyon Field, California", Paper SPE 8900 presented at the 50th Annual California Regional Meeting, Los Angeles, California (April 9-11, 1980).

APPENDIX A: EXPERIMENTAL EQUIPMENT SPECIFICATIONS

<u>Item</u>	<u>Supplier</u>
Ruska Volumetric Displacement Pump .40 to 480 cm <sup>3</sup> /hr 230 Volts Max. Pressure 4000 psi	Ruska Instrument Corporation 6121 Hillcroft Avenue Houston, TX 77036 U.S.A.
Stainless Steel Cylinder Volume 1000 cm <sup>3</sup> Max. Pressure 8000 psi	Robinson D.B. & Associates Ltd. 9419 - 20 Avenue Edmonton, Alberta Canada
Millipore Block Filter Filter Type SC	Millipore Corporation Bedford, Massachusetts U.S.A. 01730
Pressure Transducer Model DP 215 Plates Model 9 - 40	Validyne Engineering Corporation Northridge, CA 91324 U.S.A.
Fluke Digital Multimeter Model 8010 A	R.A.E. Industrial Electronics Ltd. 11680 - 170 Street Edmonton, Alberta Canada
Sampler 10 RPM 115 Volts Timer 10 A 125 Volts	Technical Services Rm 132 Chem/Min Bldg. University of Alberta Edmonton, Alberta Canada

<u>Item</u>	<u>Supplier</u>
Turbidimeter DRT - 200 Series 0 to 1 and 4 to 20 mA	H.F. Instruments Division Shaban Manufacturing 3052 Metro Parkway S.E. Ft. Myers, FL. 33901 - 7539 U.S.A.
Enerpac Hydraulic Press 0 to 10,000 lb f	Acklands Limited 12410 - 142 Street Edmonton, Alberta Canada
Graduated Centrifuge Tubes 50 ml Pyrex #8080	Fisher Scientific Co. Ltd. 10720 - 178 Street Edmonton, Alberta Canada
Rotair Industrial Glass Beads 80 - 120 mesh 120 - 200 mesh 170 - 325 mesh	Dyer S.J. Specialties Ltd. 10505 - 114 Street Edmonton, Alberta Canada
Brass Tyler Sieves	Fisher Scientific Co. Ltd. 10720 - 178 Street Edmonton, Alberta Canada
Mettler Balance Model AE 166 0 to 162 grams	Mettler Instrument Corporation P.O. Box 71 Hightstown, N.J. 08520 U.S.A.



<u>Item</u>	<u>Supplier</u>
Vibrator	Leader Equipment Ltd. 17630 - 102 Avenue Edmonton, Alberta Canada
Abbe Refractometer Model A300A 110 Volts 0.5A	Fisher Scientific Co. Ltd. 10720 - 178 Street Edmonton, Alberta Canada

## APPENDIX B: SAMPLE CALCULATIONS

### DETERMINATION OF POROSITY IN THE RADIAL MODEL

Ottawa Sand                      70 - 140 Mesh

Overburden Pressure = 0 kPa

Radius of cell = 9.975 cm

Area of cell =  $312.59 \text{ cm}^2$

Radius of central tubing = 0.635 cm

Area of central tubing =  $1.267 \text{ cm}^2$

Effective sand pack area =  $311.323 \text{ cm}^2$

Height of sand in the cell = 13.4 cm

Volume of sand in the cell =  $4171.73 \text{ cm}^3$

Pore volume from refraction analysis =  $800.0 \text{ cm}^3$

Porosity =  $800/4171.73 = 0.1918$  or 19.18%

### DETERMINATION OF POROSITY IN THE LINEAR MODEL

Large Core Linear Flow Run # 15

Mass of barite in core holder and column = 280.0 g

Mass of sand in core holder and column = 1204.568 g

Mass of sand and barite in core holder and column = 1484.568 g

Mass of sand and barite in column = 254.764 g

Mass of barite in column =  $(280.0)(254.764)/1484.568$

= 48.050 g

Mass of barite in core holder = 231.949 g

Mass of sand in column =  $254.764 - 48.050 = 206.714$  g

Mass of sand in core holder = 997.854 g

Volume of sand in core holder =  $997.854/2.634 = 378.836$  cm<sup>3</sup>

Volume of barite in core holder =  $231.949/4.213 = 55.056$  cm<sup>3</sup>

Total solids volume = 433.892 cm<sup>3</sup>

Volume of core holder = 521.20 cm<sup>3</sup>

Porosity =  $(521.20 - 433.892)/521.20 = 0.1675$  or 16.75%

#### DETERMINATION OF PARTICLE SIZE DISTRIBUTION

Barite Fines

Particles Measured From Figure 7(b)

Photograph Magnification = 2400×

The equivalent particle radius was determined from the equation

$$R = \sqrt{\frac{W \cdot L}{\pi}}$$

where R is the equivalent particle radius in mm

W is the measured particle width in mm

and L is the measured particle length in mm

Dimensions of the particles measured from the microphotograph are listed in Table B1.

The volume of each particle was determined using the equation:

$$V = \frac{4}{3} \pi r^3$$

where V is the sphere volume in  $\mu\text{m}^3$

and r is the sphere radius in  $\mu\text{m}$ .

Table B1: Dimensions of Barite Particles

Length, mm	Width, mm	Equivalent Radius, mm	Unmagnified Radius, $\mu\text{m}$
10	8	5.046	2.103
15	6	5.352	2.230
9	8	4.787	1.997
6	3	2.394	0.997
4	2	1.596	0.665
6	2	1.954	0.814
4	3	1.954	0.814
34	27	17.094	7.122
4	4	2.257	0.940
20	20	11.284	4.702
23	7	7.159	2.983
2	2	1.128	0.470
3	3	1.693	0.705
18	17	9.869	4.112
5	4	2.523	1.051
24	20	12.361	5.150
38	26	17.734	7.389
5	4	2.523	1.051
3	3	1.693	0.705
43	32	20.928	8.720

The total volume was obtained by adding the volume of all particles.

$$\text{Total particle volume} = 7536.1 \mu\text{m}^3$$

For  $r \leq 1 \mu\text{m}$ , particle volume =  $16.8 \mu\text{m}^3$  or 0.223% of total volume.

For  $1 < r \leq 2 \mu\text{m}$ , particle volume =  $42.9 \mu\text{m}^3$  or 0.570% of total volume.

For  $2 < r \leq 3 \mu\text{m}$ , particle volume =  $196.6 \mu\text{m}^3$  or 2.608% of total volume.

For  $3 < r \leq 4 \mu\text{m}$ , particle volume =  $0 \mu\text{m}^3$ .

For  $4 < r \leq 5 \mu\text{m}$ , particle volume =  $726.6 \mu\text{m}^3$  or 9.642% of total volume.

For  $5 < r \leq 6 \mu\text{m}$ , particle volume =  $572.3 \mu\text{m}^3$  or 7.593% of total volume.

For  $6 < r \leq 7 \mu\text{m}$ , particle volume =  $0 \mu\text{m}^3$ .

For  $7 < r \leq 8 \mu\text{m}$ , particle volume =  $3203.4 \mu\text{m}^3$  or 42.508% of total volume.

For  $8 < r \leq 9 \mu\text{m}$ , particle volume =  $2777.5 \mu\text{m}^3$  or 36.856% of total volume.

#### DETERMINATION OF RELATIVE PERMEABILITIES

The Berea sandstone core was saturated with 2% NaCl, having a viscosity of 1.07 cp, and the pore volume and absolute permeability of the core were determined.

$$\text{Pore volume} = 253 \text{ cm}^3$$

$$\text{Absolute Permeability} = 0.6611 \mu\text{m}^2$$

The core was then oilflooded with Hamilton Lake crude, and the initial water saturation was obtained.

$$\text{Initial water saturation} = 0.2213$$

The core was then waterflooded with 2% NaCl, injected at  $200 \text{ cm}^3/\text{hr}$ . Effluent samples were collected, and the amounts of oil and water in each sample were measured. The data is provided in Table B2.

Table B2: Waterflooding Data

#	Tot. Vol.,ml	Water Vol.,ml	Oil Vol.,ml	Pres.,kPa
1	20	0.00	20.00	350
2	20	0.00	20.00	353
3	20	0.00	20.00	355
4	20	0.00	20.00	358
5	20	0.00	20.00	360
6	10	2.50	7.50	354
7	10	7.00	3.00	348
8	10	9.00	1.00	346
9	10	9.25	0.75	345
10	10	9.50	0.50	343
11	10	9.50	0.50	342
12	20	19.00	1.00	341
13	25	19.50	0.50	340
14	50	49.00	1.00	340

The relative permeabilities were obtained using the following calculation steps:

Step 1: The average water saturation was calculated from the equation:

$$\bar{S}_w = S_{wi} + N_p/V_p$$

where  $\bar{S}_w$  is the average water saturation

$S_{wi}$  is the initial water saturation

$N_p$  is the volume of oil produced in  $\text{cm}^3$

and  $V_p$  is the core pore volume in  $\text{cm}^3$ .

Step 2: Values of  $\bar{S}_w$  were plotted against the cumulative pore volume of water injected,  $Q_i$ , and the slopes  $d\bar{S}_w/dQ_i$  were obtained.

Step 3: The water saturation at the outlet was calculated using the equation:

$$S_{w_2} = \bar{S}_w - Q_i d\bar{S}_w/dQ_i$$

where  $S_{w_2}$  is the water saturation at the outlet.

Step 4: The fractional flow of oil and the fractional flow of water were determined from:

$$f_{o_2} = (\bar{S}_w - S_{w_2})/Q_i$$

$$f_{w_2} = 1 - f_{o_2}$$

where  $f_{o_2}$  is the fractional flow of oil at the outlet.

and  $f_{w_2}$  is the fractional flow of water at the outlet.

The calculated results of Steps 1, 2, 3 and 4 are shown in Table B3.

Step 5: The average effective viscosity of fluids in the core was calculated from the equation:

$$\overline{\lambda^{-1}} = \mu_b(\Delta p/q)/(\Delta p_b/q_b)$$

where  $\mu_b$  is the viscosity of the brine in mPa.s

$\Delta p$  is the pressure drop across the core during the waterflood in kPa

$\Delta p_b$  is the pressure drop during the single-phase flow in kPa

$q$  is the volumetric injection rate during the waterflood in  $\text{cm}^3/\text{hr}$

$q_b$  is the volumetric injection rate during the single-phase flow in  $\text{cm}^3/\text{hr}$ .

and  $\overline{\lambda^{-1}}$  is the average effective viscosity in mPa.s.

Step 6: Values of  $\overline{\lambda^{-1}}$  were plotted against  $Q_i$  and the slopes  $d\overline{\lambda^{-1}}/dQ_i$  were obtained.

Step 7: Point values of effective viscosity were determined using the equation:

$$\lambda_2^{-1} = \overline{\lambda^{-1}} - Q_i \frac{d\overline{\lambda^{-1}}}{dQ_i}$$

where  $\lambda_2^{-1}$  is the point effective viscosity in mPa.s.



**Table B3: Intermediate Steps Results**

Sample#	$\bar{S}_w$	$Q_i$	$d\bar{S}_w/dQ_i$	$S_{w2}$	$f_{O2}$	$f_{w2}$
1	0.3004	0.079	1.000	0.2214	1.0000	0.0000
2	0.3794	0.158	1.000	0.2241	1.0000	0.0000
3	0.4585	0.237	1.000	0.2215	1.0000	0.0000
4	0.5375	0.316	1.000	0.2215	1.0000	0.0000
5	0.6166	0.395	0.750	0.3206	0.7494	0.2506
6	0.6462	0.435	0.308	0.5122	0.3080	0.6920
7	0.6581	0.474	0.100	0.6107	0.1000	0.9000
8	0.6620	0.514	0.077	0.6224	0.0770	0.9230
9	0.6650	0.553	0.050	0.6373	0.0501	0.9499
10	0.6670	0.593	0.051	0.6368	0.0501	0.9499
11	0.6689	0.632	0.051	0.6367	0.0509	0.9491
12	0.6729	0.711	0.020	0.6587	0.0200	0.9800
13	0.6749	0.810	0.020	0.6587	0.0200	0.9800
14	0.6788	1.010	0.020	0.6586	0.0200	0.9800

Step 8: The oil and water relative permeabilities were calculated using the equations:

$$k_{rw} = \mu_w \cdot f_{w2} / \lambda_2^{-1}$$

$$k_{ro} = \mu_o \cdot f_{o2} / \lambda_2^{-1}$$

where  $\mu_w$  is the brine viscosity in mPa.s

$\mu_o$  is the oil viscosity in mPa.s

$k_{rw}$  is the brine relative permeability

and  $k_{ro}$  is the oil relative permeability.

The calculations resulting from Steps 5, 6, 7 and 8 are presented in Table B4.

#### DETERMINATION OF ADDITIONAL DATA POINTS FOR RUN 10

The rate of sand produced was assumed to be related to time by a function of the form:

$$\dot{Q} = a_0 + a_1 t + a_2 t^2$$

where  $\dot{Q}$  is the rate of dry sand produced in ml/minute

$t$  is the time from the start of the experiment in minutes

and  $a_0$ ,  $a_1$  and  $a_2$  are constants.

The volume of sand produced is then given by the equation:

Table B4: Final Steps Results

Sample#	$\lambda^{-1}$ , mPa.s	$d\lambda^{-1}/dQ_i$	$\lambda_2^{-1}$ , mPa.s	krw	kro
1	13.249	1.443	13.135	0.000	0.815
2	13.363	0.949	13.213	0.000	0.810
3	13.438	1.443	13.096	0.000	0.817
4	13.552	0.962	13.248	0.000	0.808
5	13.628	5.676	13.386	0.024	0.704
6	13.401	5.846	10.858	0.068	0.304
7	13.173	1.875	12.284	0.078	0.087
8	13.098	0.974	12.597	0.078	0.065
9	13.060	1.900	12.009	0.085	0.045
10	12.984	0.974	12.406	0.082	0.043
11	12.946	0.468	12.650	0.083	0.043
12	12.909	0.384	12.636	0.083	0.017
13	12.871	0.000	12.871	0.081	0.017
14	12.871	0.000	12.871	0.082	0.017

$$V_s = a_0 t + \frac{1}{2} a_1 t^2 + \frac{1}{3} a_2 t^3$$

If the porosity of sand in the sample is assumed to be 40%, from Table C36, the volumes of dry sand produced are:

$$V_s = (21.0)(0.60) = 12.6 \text{ ml for } t \text{ ranging from 0 to 20.5 min.}$$

$$V_s = (7.0)(0.60) = 4.2 \text{ ml for } t \text{ ranging from 20.5 to 43.3 min.}$$

$$V_s = (4.5)(0.60) = 2.7 \text{ ml for } t \text{ ranging from 43.3 to 64.8 min.}$$

The  $V_s$  values were substituted into the expression for volume of sand produced using the corresponding time ranges. Three equations were obtained:

$$20.5a_0 + 210.1a_1 + 2,871.7a_2 = 12.6$$

$$22.8a_0 + 727.3a_1 + 27,189.2a_2 = 4.2$$

$$21.7a_0 + 1,175.1a_1 + 64,480.8a_2 = 2.7$$

These equations were solved for  $a_0$ ,  $a_1$  and  $a_2$ , and the resulting values were substituted into the equation for rate of sand produced to yield the following expressions:

$$\dot{Q} = 0.9228 - 0.0349t + 0.0004t^2$$

The rate of sand produced  $t = 4$  minutes is:

$$\dot{Q} = 0.7889 \text{ ml/minute.}$$

The sand flux at  $t = 4$  minutes is:

$$\dot{Q}/A = 0.7889/8.832 = 0.089 \text{ cm/minute.}$$

APPENDIX C: EXPERIMENTAL DATA

Table C1: Small Core linear Flow Run #1

## Legend:

Glass Beads 50-100 mesh  
Flow Rate = 8cc/min  
Fines = Glass Beads < 45 $\mu$ m  
Mass of Fines = 20.0 grams

Sample#	Volume, ml	Conc., NTU	Conc., G/ML	Mass, G
1	30	40.0	0.0005870	0.017610
2	15	10.0	0.0001350	0.002030
3	15	5.0	0.0000700	0.001050
4	15	4.0	0.0000520	0.000780
5	15	4.0	0.0000520	0.000780
6	20	1.5	0.0000165	0.000330
7	30	2.5	0.0000325	0.000975
8	30	1.2	0.0000100	0.000300
9	30	1.0	0.0000050	0.000150
10	30	0.8	0.0000050	0.000150
11	30	1.5	0.0000165	0.000495
12	30	1.2	0.0000100	0.000300

Table C2: Small Core Linear Flow Run #2

## Legend:

Glass Beads 50-100 mesh  
 Flow Rate = 8cc/min  
 Fines = Glass Beads < 45 $\mu$ m  
 Mass of Fines = 20.0 grams

Sample#	Volume, ml	Conc., NTU	Conc., G/ML	Mass, G
1	30	25.0	0.0003850	0.011550
2	15	23.0	0.0003550	0.005325
3	15	6.0	0.0000860	0.001290
4	15	5.0	0.0000700	0.001050
5	15	4.0	0.0000520	0.000780
6	20	1.8	0.0000220	0.000440
7	30	1.6	0.0000200	0.000600
8	30	1.6	0.0000200	0.000600
9	30	2.0	0.0000255	0.000765
10	30	2.0	0.0000255	0.000765
11	30	2.0	0.0000255	0.000765
12	30	1.8	0.0000220	0.000660

Table C3: Small Core Linear Flow Run #3**Legend:**

Glass Beads 50-100 mesh  
 Flow Rate = 8cc/min  
 Fines = Glass Beads < 45 $\mu$ m  
 Mass of Fines = 60.0 grams

Sample#	Volume, ml	Conc., NTU	Conc., G/ML	Mass, G
1	30	40.0	0.0005870	0.017610
2	15	35.0	0.0005200	0.007800
3	15	8.0	0.0001050	0.001575
4	15	8.0	0.0001050	0.001575
5	15	4.0	0.0000520	0.000780
6	20	0.5	0.0000165	0.000330
7	30	0.5	0.0000050	0.000150
8	30	0.6	0.0000050	0.000150
9	30	0.6	0.0000050	0.000150
10	30	0.8	0.0000050	0.000150
11	30	0.8	0.0000050	0.000150
12	30	0.8	0.0000050	0.000150



Table C4: Small Core Linear Flow Run #4

## Legend:

Glass Beads 50-100 mesh  
 Flow Rate = 4cc/min  
 Fines = Glass Beads < 45 $\mu$ m  
 Mass of Fines = 20.0 grams

Sample#	Volume, ml	Conc., NTU	Conc., G/ML	Mass, G
1	30	6.5	0.000220	0.0027600
2	15	22.0	0.0003430	0.0051450
3	15	4.0	0.0000520	0.0007800
4	15	2.0	0.0000255	0.0003825
5	15	2.0	0.0000255	0.0003825
6	20	1.0	0.0000050	0.0001000
7	30	0.6	0.0000050	0.0001500
8	30	0.3	0.0000000	0.0000000
9	30	0.3	0.0000000	0.0000000
10	30	0.3	0.0000000	0.0000000
11	30	0.3	0.0000000	0.0000000
12	30	0.4	0.0000050	0.0001500

Table C5: Small Core Linear Flow Run #5

## Legend:

Glass Beads 4-6 mesh  
 Flow Rate = 8cc/min  
 Fines = Glass Beads < 45 $\mu$ m  
 Mass of Fines = 20.0 grams

Sample#	Volume, ml	Conc., NTU	Conc., G/ML	Mass
1	30	60.0	0.0008600	0.002580
2	15	40.0	0.0005870	0.0008805
3	15	20.0	0.0003000	0.0004500
4	15	15.0	0.0002200	0.0003300
5	15	15.0	0.0002200	0.0003300
6	20	7.0	0.0000980	0.001960
7	30	4.5	0.0000615	0.001845
8	30	3.5	0.0000450	0.001350
9	30	2.5	0.0000325	0.000975
10	30	2.0	0.0000255	0.000765
11	30	1.5	0.0000165	0.000495
12	30	1.5	0.0000165	0.000495

Table C6: Small Core Linear Flow Run #6

## Legend:

Glass Beads 4-6 mesh  
 Flow Rate = 8cc/min  
 Fines = Glass Beads < 45 $\mu$ m  
 Mass of Fines = 20.0 grams

Sample#	Volume, ml	Conc., NTU	Conc., G/ML	Mass, G
1	30	80.0	0.0011000	0.033000
2	15	35.0	0.0005200	0.007800
3	15	23.0	0.0003550	0.005325
4	15	20.0	0.0003000	0.004500
5	15	18.0	0.0002700	0.004050
6	20	7.5	0.0001020	0.002040
7	30	4.0	0.0000520	0.001560
8	30	3.0	0.0000385	0.001155
9	30	1.5	0.0000165	0.000495
10	30	1.5	0.0000165	0.000495
11	30	1.2	0.0000100	0.000300
12	30	1.0	0.0000050	0.000150

Table C7: Small Core Linear Flow Run #7**Legend:**

Glass Beads 4-6 mesh  
 Flow Rate = 8cc/min  
 Fines = Glass Beads < 45 $\mu$ m  
 Mass of Fines = 20.0 grams

Sample #	Volume, ml	Conc., NTU	Conc., G/ML	Mass, G
1	30	70.0	0.0010000	0.030000
2	15	67.0	0.0009700	0.014550
3	15	23.0	0.0003550	0.005325
4	15	12.0	0.0001630	0.002445
5	15	15.0	0.0002200	0.003300
6	20	10.0	0.0001350	0.007000
7	30	6.5	0.0000920	0.002760
8	30	5.0	0.0000700	0.002100
9	30	3.2	0.0000412	0.001236
10	30	4.0	0.0000520	0.001560
11	30	5.0	0.0000700	0.002100
12	30	4.5	0.0000615	0.001845

Table C8: Small Core Linear Flow Run #8**Legend:**

Glass Beads 50-100 mesh  
Flow Rate = 8cc/min  
No Fines Added

Sample#	Volume, ml	Conc., NTU	Conc., G/ML	Mass, G
1	30	5.50	0.0000785	0.0023550
2	15	1.50	0.0000165	0.0002475
3	15	2.40	0.0000310	0.0004650
4	15	2.00	0.0000255	0.0003825
5	15	1.20	0.0000100	0.0001500
6	20	0.80	0.0000050	0.0001000
7	30	0.55	0.0000050	0.0001500
8	30	0.64	0.0000050	0.0001500
9	30	0.50	0.0000050	0.0001500
10	30	0.45	0.0000050	0.0001500
11	30	0.45	0.0000050	0.0001500

Table C9: Small Core Linear Flow Run #9**Legend:**

Glass Beads 50-100 mesh  
 Flow Rate = 8cc/min  
 Fines = Glass Beads < 45 $\mu$ m  
 Mass of Fines = 20.0 grams  
 Dry Packing

Sample#	Volume, ml	Conc., NTU	Conc., G/ML	Mass, G
1	30	64.0	0.0009200	0.0276000
2	15	2.0	0.0000255	0.0003825
3	15	2.0	0.0000255	0.0003825
4	15	2.0	0.0000255	0.0003825
5	15	2.0	0.0000255	0.0003825
6	20	1.5	0.0000165	0.0003300
7	30	1.3	0.0000115	0.0003450
8	30	1.5	0.0000165	0.0004950
9	30	1.6	0.0000200	0.0006000
10	30	2.0	0.0000255	0.0007650
11	30	2.5	0.0000325	0.0009750

Table C10: Small Core Linear Flow Run #10**Legend:**

Glass Beads 50-100 mesh  
 Flow Rate = 8cc/min  
 Fines = Glass Beads < 45 $\mu$ m  
 Mass of Fines = 20.0 grams  
 Dry Packing

Sample#	Volume, ml	Conc., NTU	Conc., G/ML	Mass, G
1	30	65.0	0.0009350	0.0280500
2	15	7.5	0.0001020	0.0015300
3	15	2.0	0.0000255	0.0003825
4	15	2.0	0.0000255	0.0003825
5	15	2.0	0.0000255	0.0003825
6	20	1.2	0.0000100	0.002000
7	30	1.0	0.0000050	0.0001500
8	30	1.1	0.0000050	0.0001500
9	30	1.0	0.0000050	0.0001500
10	30	1.0	0.0000050	0.0001500
11	30	1.5	0.0000165	0.0004950

Table C11: Large Core Linear Flow Run #1**Legend:**

Ottawa Sand 50-100 mesh  
 Flow Rate = 8cc/min  
 No Fines Added

Sample#	Pressure Drop, PSI	Conc., NTU	Conc., G/ML	Mass, G
1	0.68	1.5	0.0000165	0.00033
2	0.72	0.8	0.0000050	0.00010
3	0.71	0.6	0.0000050	0.00010
4	0.70	0.6	0.0000050	0.00010
5	0.70	1.0	0.0000050	0.00010
6	0.69	0.7	0.0000050	0.00010
7	0.68	0.8	0.0000050	0.00010
8	0.68	0.7	0.0000050	0.00010
9	0.68	1.8	0.0000220	0.00044
10	0.68	4.0	0.0000520	0.00104
11	0.69	7.0	0.0000980	0.00196
12	0.69	6.7	0.0000950	0.00190
13	0.69	2.6	0.0000335	0.00069
14	0.71	1.5	0.0000165	0.00033
15	0.68	1.2	0.0000100	0.00020

Sample Volume = 20 ml



Table C12: Large Core Linear Flow Run #2**Legend:**

Ottawa Sand 50-100 mesh  
 Flow Rate = 8cc/min  
 Fines = Glass Beads < 45 $\mu$ m  
 Mass of Fines = 103.130 grams

Sample#	Pressure Drop, PSI	Conc., NTU	Conc., G/ML	Mass, G
1	1.02	4.0	0.000052	0.00104
2	1.27	3.5	0.000045	0.00090
3	2.05	21.0	0.000320	0.00640
4	2.26	71.0	0.001010	0.02020
5	1.75	85.0	0.001190	0.02380
6	1.19	78.0	0.001088	0.02176
7	1.45	75.0	0.001050	0.02100
8	1.23	75.0	0.001050	0.02100
9	1.23	100.0	0.001300	0.02600
10	1.22	130.0	0.001700	0.03400
11	1.22	120.0	0.001540	0.03080
12	1.20	74.0	0.001040	0.02080
13	1.22	39.0	0.000575	0.01150
14	1.23	20.0	0.000300	0.00600
15	1.23	13.0	0.000185	0.00370

Sample Volume = 20 ml

Table C13: Large Core Linear Flow Run #3**Legend:**

Ottawa Sand 50-100 mesh  
 Flow Rate = 8cc/min  
 Fines = Glass Beads < 45 $\mu$ m  
 Mass of Fines = 103.130 grams

Sample#	Pressure Drop, PSI	Conc., NTU	Conc., G/ML	Mass, G
1	1.84	1.5	0.0000165	0.000330
2	1.76	1.5	0.0000165	0.000330
3	1.65	3.6	0.0000464	0.000928
4	1.59	7.8	0.0001038	0.002076
5	1.60	36.0	0.0005338	0.010676
6	1.58	55.0	0.0007864	0.015728
7	1.57	100.0	0.0013000	0.026000
8	1.56	100.0	0.0013000	0.026000
9	1.53	77.0	0.0010770	0.021540
10	1.53	58.0	0.0008400	0.016800
11	1.53	42.0	0.0006150	0.012300
12	1.51	35.0	0.0005200	0.010400
13	1.49	29.0	0.0004420	0.008840
14	1.48	21.0	0.0003200	0.006400
15	1.49	17.0	0.0002550	0.005100

Sample Volume = 20 ml

Table C14: Large Core Linear Flow Run #4**Legend:**

Ottawa Sand 50-100 mesh  
 Flow Rate = 8cc/min  
 Fines = Glass Beads < 45µm  
 Mass of Fines = 183.218 grams

Sample#	Pressure Drop, PSI	Conc., NTU	Conc., G/ML	Mass, G
1	3.82	9.2	0.0001230	0.002460
2	3.64	58.0	0.0008400	0.016800
3	3.48	120.0	0.0015400	0.030800
4	3.51	300.0	0.0036000	0.072000
5	3.50	460.0	0.0054000	0.108000
6	3.51	500.0	0.0058700	0.117400
7	3.46	490.0	0.0058000	0.116000
8	3.43	560.0	0.0066000	0.132000
9	3.43	520.0	0.0061300	0.122600
10	3.44	360.0	0.0044000	0.088000
11	3.38	140.0	0.0017800	0.035600
12	3.32	42.0	0.0006150	0.012300
13	3.35	14.0	0.0002100	0.004200
14	3.32	6.0	0.0000860	0.001720
15	3.29	3.2	0.0000412	0.000824

Sample Volume = 20 ml

Table C15: Large Core Linear Flow Run #5

## Legend:

Ottawa Sand 50-100 mesh  
 Flow Rate = 8cc/min  
 Fines = Glass Beads < 325  $\mu$ m  
 Mass of Fines = 209.068 grams

Sample#	Pressure Drop, PSI	Conc., NTU	Conc., G/ML	Mass, G
1	4.66	270.0	0.0031700	0.063400
2	4.54	730.0	0.0089500	0.179000
3	4.38	730.0	0.0089500	0.179000
4	4.33	* 680.0	0.0164400	0.328800
5	4.28	** 610.0	0.0218100	0.436200
6	4.31	*** 510.0	0.0240000	0.480000
7	4.31	** 570.0	0.0201900	0.403800
8	4.40	** 600.0	0.0214200	0.428400
9	4.26	590.0	0.0070000	0.140000
10	4.20	410.0	0.0048800	0.097600
11	4.20	110.0	0.0013800	0.027600
12	4.14	36.0	0.0005338	0.010676
13	4.10	11.0	0.0001500	0.003000
14	4.11	5.2	0.0000736	0.001472
15	4.15	2.9	0.0000374	0.000748

Sample Volume = 20 ml

\* Diluted with 20 ml distilled water

\*\* Diluted with 40 ml distilled water

\*\*\* Diluted with 60 ml distilled water

Table C16: Large Core Linear Flow Run #6**Legend:**

Ottawa Sand 50-100 mesh  
 Flow Rate = 13.3cc/min  
 Fines = Glass Beads < 45µm  
 Mass of Fines = 114.344 grams

Sample#	Pressure Drop, PSI	Conc., NTU	Conc., G/ML	Mass, G
1	1.64	49.0	0.000705	0.01410
2	1.63	64.0	0.000920	0.01840
3	1.61,	110.0	0.001380	0.02760
4	1.66	95.0	0.001250	0.02500
5	1.65	94.0	0.001246	0.02492
6	1.67	130.0	0.001700	0.03400
7	1.67	200.0	0.002600	0.05200
8	1.63	200.0	0.002600	0.05200
9	1.66	170.0	0.002200	0.04400
10	1.66	170.0	0.002200	0.04400
11	1.67	150.0	0.001850	0.03700
12	1.67	95.0	0.001250	0.02500
13	1.67	45.0	0.000650	0.01300
14	1.67	22.0	0.000343	0.00686
15	1.67	15.0	0.000220	0.00440

Sample Volume = 20 ml

Table C17: Large Core Linear Flow Run #7

## Legend:

Ottawa Sand 100-325 mesh  
 Flow Rate = 8cc/min  
 No Fines Added

Sample#	Pressure Drop, PSI	Conc., NTU	Conc., G/ML	Mass, G
1	1.77	17.0	0.0002550	0.005100
2	1.63	7.4	0.0001015	0.002030
3	1.54	1.8	0.0000220	0.000440
4	1.52	1.0	0.0000050	0.000100
5	1.50	4.5	0.0000615	0.001230
6	1.53	23.0	0.0003550	0.007100
7	1.53	34.0	0.0005100	0.010200
8	1.52	65.0	0.0009350	0.018700
9	1.52	83.0	0.0011500	0.023000
10	1.52	50.0	0.0007183	0.014366
11	1.51	19.0	0.0002850	0.005700
12	1.53	10.0	0.0001350	0.002700
13	1.53	9.5	0.0001275	0.002550
14	1.55	8.6	0.0001160	0.002320
15	1.58	7.0	0.0000980	0.001960

Sample Volume = 20 ml

Table C18: Large Core Linear Flow Run #8**Legend:**

Ottawa sand 100-325 mesh  
Flow Rate = 8cc/min  
Fines = Glass Beads < 45 $\mu$ m  
Mass of Fines = 107.740 grams

Sample#	Pressure Drop, PSI	Conc., NTU	Conc., G/ML	Mass, G
1	2.73	10.0	0.0001350	0.002700
2	2.72	2.7	0.0000348	0.000696
3	2.72	11.0	0.0001500	0.003000
4	2.63	73.0	0.0010300	0.020600
5	2.61	130.0	0.0017000	0.034000
6	2.58	130.0	0.0017000	0.034000
7	2.60	120.0	0.0015400	0.030800
8	2.55	35.0	0.0005200	0.010400
9	2.58	30.0	0.0004560	0.009120
10	2.51	21.0	0.0003200	0.006400
11	2.55	30.0	0.0004560	0.009120
12	2.57	23.0	0.0003550	0.007100
13	2.60	9.5	0.0001275	0.002550
14	2.60	3.4	0.0000438	0.000876
15	2.56	1.0	0.0000050	0.000100

Sample Volume = 20 ml

Table C19: Large Core Linear Flow Run #9**Legend:**

Silica 40-70 mesh  
Flow Rate = 18cc/min  
No Fines Added

Sample#	Pressure Drop, PSI	Conc., NTU	Conc., G/ML	Mass, G
1	0.49	66	0.0009525	0.019050
2	0.51	110	0.0013800	0.027600
3	0.50	140	0.0017800	0.035600
4	0.47	210	0.0027000	0.054000
5	0.47	260	0.0031000	0.062000
6	0.47	250	0.0030250	0.060500
7	0.45	250	0.0030250	0.060500
8	0.43	250	0.0030250	0.060500
9	0.42	270	0.0031700	0.063400
10	0.41	250	0.0030250	0.060500
11	0.37	180	0.0023500	0.047000
12	0.38	94	0.0012460	0.024920
13	0.31	36	0.0005338	0.010676
14	0.30	13	0.0001850	0.003700
15	0.27	8	0.0000950	0.001900

Sample Volume = 20 ml



Table C20: Large Core Linear Flow Run #10**Legend:**

Silica 40-70 mesh  
Flow Rate = 8cc/min  
No Fines Added

Sample#	Pressure Drop, PSI	Conc., NTU	Conc., G/ML	Mass, G
1	0.25	65	0.0009350	0.018700
2	0.29	94	0.0012460	0.024920
3	0.37	110	0.0013800	0.027600
4	0.28	120	0.0015400	0.030800
5	0.22	140	0.0017800	0.035600
6	0.28	170	0.0022000	0.044000
7	0.33	210	0.0027000	0.054000
8	0.30	230	0.0028630	0.057260
9	0.32	250	0.0030250	0.060500
10	0.24	260	0.0031000	0.062000
11	0.33	170	0.0022000	0.044000
12	0.29	95	0.0012500	0.025000
13	0.35	64	0.0009200	0.018400
14	0.35	37	0.0005476	0.010952
15	0.31	16	0.0002400	0.004800

Sample Volume = 20 ml

Table C21: Large Core Linear Flow Run #11

## Legend:

Silica 40-70 mesh  
 Flow Rate = 8cc/min  
 Fines = Glass Beads < 45  $\mu$ m  
 Mass of Fines = 107.740 g

Sample#	Pressure Drop, PSI	Conc., NTU	Conc., G/ML	Mass, G
1	1.07	12.0	0.000163	0.00326
2	0.94	29.0	0.000442	0.00884
3	0.94	250.0	0.003025	0.06050
4	0.85	310.0	0.003750	0.07500
5	0.77	* 110.0	0.004140	0.08280
6	0.73	* 150.0	0.005550	0.11100
7	0.69	* 140.0	0.005340	0.10680
8	0.65	390.0	0.004760	0.09520
9	0.65	270.0	0.003170	0.06340
10	0.65	120.0	0.001540	0.03080
11	0.62	100.0	0.001300	0.02600
12	0.62	120.0	0.001540	0.03080
13	0.62	120.0	0.001540	0.03080
14	0.65	120.0	0.001540	0.03080
15	0.65	93.0	0.001242	0.02484

Sample Volume = 20 ml

\* Diluted with 40 ml distilled water

Table C22: Large Core Linear Flow Run #12**Legend:**

Glass Beads 100-325 mesh  
Flow Rate = 8cc/min  
No Fines Added

Sample#	Pressure Drop, PSI	Conc., NTU	Conc., G/ML	Mass, G
1	5.23	73.0	0.0010300	0.020600
2	5.18	170.0	0.0022000	0.044000
3	5.14	210.0	0.0027000	0.054000
4	5.17	190.0	0.0025000	0.050000
5	5.12	220.0	0.0027813	0.055626
6	5.17	250.0	0.0030250	0.060500
7	5.14	230.0	0.0028630	0.057260
8	5.15	250.0	0.0030250	0.060500
9	5.10	250.0	0.0030250	0.060500
10	5.14	240.0	0.0029440	0.058880
11	5.14	120.0	0.0015400	0.030800
12	5.11	48.0	0.0006900	0.013800
13	5.10	20.0	0.0003000	0.006000
14	5.13	9.4	0.0001260	0.002520
15	5.13	4.3	0.0000578	0.001156

Sample Volume = 20 ml

Table C23: Large Core Linear Flow Run #13**Legend:**

Glass Beads 100-325 mesh  
 Flow Rate = 8cc/min  
 Fines = Glass Beads < 45  $\mu$ m  
 Mass of Fines = 86.941 grams

Sample#	Pressure Drop, PSI	Conc., NTU	Conc., G/ML	Mass, G
1	5.58	47.0	0.0006750	0.013500
2	5.54	1.0	0.0000050	0.000100
3	5.56	30.0	0.0004560	0.009120
4	5.55	200.0	0.0026000	0.052000
5	5.55	270.0	0.0031700	0.063400
6	5.54	270.0	0.0031700	0.063400
7	5.52	300.0	0.0036000	0.072000
8	5.48	340.0	0.0041500	0.083000
9	5.45	220.0	0.0027813	0.055626
10	5.43	150.0	0.0018500	0.037000
11	5.39	240.0	0.0029440	0.058880
12	5.39	130.0	0.0017000	0.034000
13	5.35	61.0	0.0008700	0.017400
14	5.42	36.0	0.0005338	0.010676
15	5.50	26.0	0.0004000	0.008000

Sample Volume = 20 ml

Table C24: Large Core Linear Flow Run #14

Legend:

Ottawa Sand 50-100 mesh  
Flow Rate = 8cc/min  
Fines = Barite < 20 μm  
Mass of Fines = 104.667 grams

Sample#	Pressure Drop,PSI	Conc.,NTU	Conc.,G/ML	Mass,G
1	0.64	13.0	0.0000355	0.000710
2	0.92	1.0	0.0000050	0.000100
3	0.87	1.0	0.0000050	0.000100
4	0.84	0.6	0.0000050	0.000100
5	0.80	0.8	0.0000050	0.000100
6	0.90	3.0	0.0000100	0.000200
7	0.92	1.0	0.0000050	0.000100
8	0.91	0.4	0.0000050	0.000100
9	0.96	0.6	0.0000050	0.000100
10	0.98	1.2	0.0000050	0.000100
11	0.95	2.3	0.0000050	0.000100
12	0.87	3.4	0.0000170	0.000340
13	0.89	1.8	0.0000050	0.000100
14	0.85	1.5	0.0000050	0.000100
15	0.79	1.0	0.0000050	0.000100

Sample Volume = 20 ml

Table C25: Large Core Linear Flow Run #15Legend:

Ottawa Sand 50-100 mesh  
 Flow Rate = 8cc/min  
 Fines = Barite < 20  $\mu$ m  
 Mass of Fines = 231.949 grams

Sample#	Pressure Drop, PSI	Conc., NTU	Conc., G/ML	Mass, G
1	4.77	39.00	0.0001250	0.002500
2	5.31	1.40	0.0000050	0.000100
3	5.32	0.74	0.0000050	0.000100
4	5.30	0.80	0.0000050	0.000100
5	5.30	0.80	0.0000050	0.000100
6	5.35	0.60	0.0000050	0.000100
7	5.32	0.40	0.0000050	0.000100
8	5.39	0.55	0.0000050	0.000100
9	5.43	1.20	0.0000050	0.000100
10	5.46	1.60	0.0000050	0.000100
11	5.47	2.50	0.0000050	0.000100
12	5.49	3.00	0.0000100	0.000200
13	5.52	4.00	0.0000117	0.000234
14	5.51	4.20	0.0000121	0.000242
15	5.48	6.00	0.0000153	0.000306

Sample Volume = 20 ml

Table C26: Large Core Linear Flow Run #16

## Legend:

Silica 40-70 mesh  
 Flow Rate = 8cc/min  
 Fines = Calcium Carbonate < 1µm  
 Mass of Fines = 67.728 grams

Sample#	Pressure Drop, PSI	Conc., NTU	Conc., G/ML	Mass, G
1	1.18	* 750.0	0.0037800	0.075600
2	1.25	* 760.0	0.0038150	0.076300
3	1.15	** 480.0	0.0019350	0.038700
4	1.15	14.0	0.0000517	0.001034
5	1.16	6.8	0.0000365	0.000730
6	1.16	6.4	0.0000340	0.000680
7	1.16	4.3	0.0000287	0.000574
8	1.18	18.0	0.0000600	0.001200
9	1.18	21.0	0.0000665	0.001330
10	1.20	6.9	0.0000369	0.000738
11	1.16	7.3	0.0000370	0.000740
12	1.16	4.4	0.0000291	0.000582
13	1.18	4.2	0.0000283	0.000566
14	1.18	7.3	0.0000370	0.000740
15	1.01	7.5	0.0000372	0.000744

Sample Volume = 20 ml

\* Diluted with 120 ml distilled water

\*\* Diluted with 80 ml distilled water

Table C27: Radial Flow Run #1**Legend:**

Ottawa Sand 70-140 mesh  
 Flow Rate = 8cc/min  
 Pressure = 0.0 kPa  
 Well #1

Loading Pressure, KPA	Time, MIN	Sand volume, ML	Total Volume, ML
0.0	3.40	30.00	50
0.0	3.88	19.00	50
0.0	5.92	2.00	50
0.0	6.17	0.05	50
0.0	6.10	0.00	50
0.0	6.20	0.00	50
0.0	6.17	0.00	50
0.0	6.18	0.00	50



Table C28: Radial Flow Run #2

## Legend:

Ottawa Sand 70-140 mesh  
Flow Rate = 8cc/min  
Pressure = 0.0 kPa  
Well #1

Loading Pressure, KPA	Time, MIN	Sand volume, ML	Total Volume, ML
0.0	4.73	25.00	50
0.0	3.80	23.00	50
0.0	3.70	19.00	50
0.0	5.75	4.50	50
0.0	6.07	0.50	50
0.0	6.00	1.00	50
0.0	6.00	0.05	50
0.0	6.15	0.00	50

Table C29: Radial Flow Run #3

## Legend:

Ottawa Sand 70-140 mesh  
 Flow Rate = 8cc/min  
 Pressure = 611.0 kPa  
 Well #1

Loading Pressure, KPA	Time, MIN	Sand volume, ML	Total Volume, ML
611.0	4.62	27.0	50
611.0	4.28	23.0	50
611.0	4.88	22.0	50
611.0	3.72	25.0	50
611.0	4.55	17.0	50
611.0	5.60	9.0	50
611.0	4.88	16.0	50
611.0	5.25	9.0	50
611.0	5.88	6.5	50
611.0	5.82	5.0	50
611.0	5.82	7.5	50

Table C30: Radial Flow Run #4

## Legend:

Ottawa Sand 70-140 mesh  
Flow Rate = 8cc/min  
Pressure = 1018.4 kPa  
Well #1

Loading Pressure, KPA	Time, MIN	Sand volume, ML	Total Volume, ML
1018.4	5.93	26	50
1018.4	4.32	25	50
1018.4	4.65	24	50
1018.4	5.20	28	50
1018.4	4.10	32	50
1018.4	3.75	31	50
1018.4	2.82	30	50
1018.4	4.00	26	50
1018.4	3.53	26	50
1018.4	3.83	25	50
1018.4	4.10	24	50
1018.4	4.13	23	50
1018.4	3.03	26	50

Table C31: Radial Flow Run #5**Legend:**

Ottawa Sand 70-140 mesh  
 Flow Rate = 8cc/min  
 Pressure = 1731.3 kPa  
 Well #1

Loading Pressure, KPA	Time, MIN	Sand volume, ML	Total Volume, ML
1731.3	4.92	33	50
1731.3	3.65	35	50
1731.3	3.83	35	50
1731.3	3.47	35	50
1731.3	3.67	35	50
1731.3	3.08	35	50
1731.3	3.28	35	50
1731.3	2.47	35	50
1731.3	3.33	35	50
1731.3	2.75	36	50
1731.3	2.43	36	50
1731.3	2.88	35	50
1731.3	2.33	35	50
1731.3	2.30	36	50
1731.3	2.37	36	50

Table C32: Radial Flow Run #6

## Legend:

Ottawa Sand 70-140 mesh  
Flow Rate = 8cc/min  
Pressure = 1731.3 kPa  
Well #1

Loading Pressure, KPA	Time, MIN	Sand volume, ML	Total Volume, ML
1731.3	4.35	33	50
1731.3	3.65	34	50
1731.3	3.40	33	50
1731.3	2.85	35	50
1731.3	3.13	34	50
1731.3	2.82	35	50
1731.3	2.95	35	50
1731.3	2.80	34	50
1731.3	2.80	35	50
1731.3	2.63	35	50
1731.3	2.48	35	50
1731.3	2.50	35	50
1731.3	2.30	35	50

Table C33: Radial Flow Run #7**Legend:**

Glass Beads 80-120 mesh  
 Flow Rate = 8cc/min  
 Pressure = 1018.4 kPa  
 Well #1

Loading Pressure, KPA	Time, MIN	Sand volume, ML	Total Volume, ML
1018.4	6.12	37	50
1018.4	4.87	38	50
1018.4	3.93	38	50
1018.4	3.10	38	50
1018.4	2.53	38	50
1018.4	2.30	38	50
1018.4	2.17	38	50
1018.4	2.08	38	50
1018.4	2.02	39	50
1018.4	2.10	39	50

Table C34: Radial Flow Run #8**Legend:**

Glass Beads 80-120 mesh  
 Flow Rate = 8cc/min  
 Pressure = 0.0 kPa  
 Well #1

Loading Pressure, KPA	Time, MIN	Sand volume, ML	Total Volume, ML
0.0	6.77	34	50
0.0	6.27	34	50
0.0	6.37	35	50
0.0	6.27	35	50
0.0	3.07	37	50
0.0	3.03	37	50
0.0	3.58	35	50
0.0	6.03	29	50
0.0	7.38	25	50
0.0	2.62	37	50
0.0	1.55	38	50
0.0	1.72	38	50
0.0	1.93	35	50

Table C35: Radial Flow Run #9

## Legend:

Glass Beads 80-120 mesh  
Flow Rate = 8cc/min  
Pressure = 0.0 kPa  
Well #1

Loading Pressure, KPA	Time, MIN	Sand volume, ML	Total Volume, ML
0.0	5.63	35	50
0.0	4.50	35	50
0.0	3.22	37	50
0.0	3.57	36	50
0.0	5.37	32	50
0.0	7.58	30	50
0.0	0.97	39	50
0.0	1.02	39	50
0.0	1.10	39	50
0.0	1.20	39	50
0.0	1.40	39	50



Table C36: Radial Flow Run #10**Legend:**

Ottawa Sand 70-140 mesh  
Flow Rate = 2cc/min  
Pressure = 0,0 kPa  
Well #1

Loading Pressure, KPA	Time, MIN	Sand volume, ML	Total Volume, ML
0.0	20.47	21.00	50
0.0	22.82	7.00	50
0.0	21.55	4.50	50
0.0	23.68	2.50	50
0.0	23.92	1.00	50
0.0	24.72	0.75	50
0.0	24.03	1.00	50
0.0	24.93	0.40	50
0.0	24.87	0.20	50

Table C37: Radial Flow Run #11**Legend:**

Ottawa Sand 70-140 mesh  
 Flow Rate = 13.3cc/min  
 Pressure = 0.0 kPa  
 Well #1

Loading Pressure, KPA	Time, MIN	Sand volume, ML	Total Volume, ML
0.0	1.17	35.00	50
0.0	1.37	22.00	50
0.0	3.03	17.00	50
0.0	3.03	9.00	50
0.0	3.58	0.90	50
0.0	3.58	0.05	50
0.0	3.72	0.00	50
0.0	3.77	0.00	50
0.0	3.65	0.00	50
0.0	3.72	0.00	50
0.0	3.68	0.25	50

Table C38: Radial Flow Run #12**Legend:**

Ottawa Sand 70-140 mesh  
 Flow Rate = 2cc/min  
 Pressure = 1731.3 kPa  
 Well #1

Loading Pressure, KPA	Time, MIN.	Sand volume, ML	Total Volume, ML
1731.3	18.65	20.0	50
1731.3	20.50	15.0	50
1731.3	20.50	10.0	50
1731.3	23.77	6.0	50
1731.3	21.72	7.5	50
1731.3	22.72	6.0	50
1731.3	22.82	4.5	50
1731.3	23.88	5.0	50
1731.3	23.20	6.5	50
1731.3	23.08	6.5	50

Table C39: Radial Flow Run #13**Legend:**

Ottawa Sand 70-140 mesh  
 Flow Rate = 13.3cc/min  
 Pressure = 1731.3 kPa  
 Well #1

Loading Pressure, KPA	Time, MIN	Sand volume, ML	Total Volume, ML
1731.3	2.85	31	50
1731.3	2.92	31	50
1731.3	2.50	35	50
1731.3	2.37	37	50
1731.3	2.33	38	50
1731.3	1.82	37	50
1731.3	1.75	39	50
1731.3	1.63	38	50
1731.3	1.43	38	50
1731.3	1.43	38	50
1731.3	1.50	39	50
1731.3	0.25	34	50
1731.3	1.20	32	50
1731.3	2.10	37	50
1731.3	1.68	37	50
1731.3	1.43	37	50
1731.3	1.47	40	53
1731.3	1.33	39	52
1731.3	0.67	32	54
1731.3	0.33	43	53

Table C40: Radial Flow Run #14**Legend:**

Silica 40-70 mesh  
Flow Rate = 8cc/min  
Pressure = 0.0 kPa  
Well #1

Loading Pressure, KPA	Time, MIN	Sand volume, ML	Total Volume, ML
0.0	6.62	16.50	50
0.0	4.03	17.00	50
0.0	6.20	0.75	50
0.0	6.28	0.75	50
0.0	6.20	0.00	50
0.0	6.20	0.00	50
0.0	6.17	0.00	50
0.0	6.20	0.00	50
0.0	6.17	0.00	50
0.0	6.20	0.00	50
0.0	6.17	0.00	50
0.0	4.28	0.00	50

Table C41: Radial Flow Run #15

## Legend:

Silica 40-70 mesh  
Flow Rate = 8cc/min  
Pressure = 0.0 kPa  
Well #1

Loading Pressure, KPA	Time, MIN	Sand volume, ML	Total Volume, ML
0.0	4.72	15.0	50
0.0	6.52	1.5	50
0.0	6.13	0.0	50
0.0	6.23	0.0	50
0.0	6.20	0.0	50
0.0	6.15	0.0	50
0.0	6.22	0.0	50
0.0	6.25	0.0	50

Table C42: Radial Flow Run #16

## Legend:

Silica 40-70 mesh  
Flow Rate = 8cc/min  
Pressure = 1731.3 kPa  
Well #1

Loading Pressure, KPA	Time, MIN	Sand volume, ML	Total Volume, ML
1731.3	5.00	25	50
1731.3	3.83	23	50
1731.3	3.43	22	50
1731.3	3.72	23	50
1731.3	3.50	21	50
1731.3	4.17	18	50
1731.3	3.80	21	50
1731.3	4.62	15	50
1731.3	4.35	18	50
1731.3	3.78	19	50
1731.3	5.20	10	50
1731.3	4.03	19	50

Table C43: Radial Flow Run #17**Legend:**

Glass Beads 80-120 mesh  
Flow Rate = 8cc/min  
Pressure = 1018.4 kPa  
Well #3

Loading Pressure, KPA	Time, MIN	Sand volume, ML	Total Volume, ML
1018.4	8.77	23	50
1018.4	6.52	26	50
1018.4	5.00	25	50
1018.4	5.27	25	50
1018.4	4.50	26	50
1018.4	4.25	25	50
1018.4	4.30	28	50
1018.4	5.20	28	50
1018.4	4.30	25	50
1018.4	3.47	22	50



Table C44: Radial Flow Run #18**Legend:**

Glass Beads 170-325 mesh  
Flow Rate = 8cc/min  
Pressure = 1018.4 kPa  
Well #3

Loading Pressure, KPA	Time, MIN	Sand volume, ML	Total Volume, ML
1018.4	5.52	39	50
1018.4	4.63	43	50
1018.4	3.25	42	50
1018.4	3.13	43	50
1018.4	2.30	44	50
1018.4	2.20	43	50
1018.4	1.88	47	50
1018.4	1.92	43	50
1018.4	1.75	44	50
1018.4	1.03	43	50
1018.4	1.02	43	50
1018.4	1.65	46	50
1018.4	1.58	46	50

Table C45: Radial Flow Run #19**Legend:**

Ottawa Sand 70-140 mesh  
Flow Rate = 8cc/min  
Pressure = 1018.4 kPa  
Well #3

Loading Pressure, KPA	Time, MIN	Sand volume, ML	Total Volume, ML
1018.4	6.30	0	50
1018.4	6.13	0	50
1018.4	6.18	0	50
1018.4	5.08	0	50
1018.4	6.17	0	50
1018.4	6.13	0	50

Table C46: Radial Flow Run #20**Legend:**

Ottawa Sand 70-140 mesh  
Flow Rate = 8cc/min  
Pressure = 1018.4 kPa  
Well #2

Loading Pressure, KPA	Time, MIN	Sand volume, ML	Total Volume, ML
1018.4	5.87	0	50
1018.4	5.88	0	50
1018.4	5.95	0	50
1018.4	6.00	0	50
1018.4	5.88	0	50
1018.4	6.03	0	50

Table C47: Radial Flow Run #21**Legend:**

Glass Beads 80-120 mesh  
Flow Rate = 8cc/min  
Pressure = 1018.4 kPa  
Well #2

Loading Pressure, KPA	Time, MIN	Sand volume, ML	Total Volume, ML
1018.4	5.62	27	50
1018.4	5.40	28	50
1018.4	4.48	27	50
1018.4	4.03	29	50
1018.4	3.90	28	50
1018.4	3.33	29	50
1018.4	3.23	28	50
1018.4	3.23	28	50
1018.4	3.23	27	50
1018.4	3.33	27	50

Table C48: Two-Phase Flow Step #1

## Legend:

Berea Sandstone Core  
 Saturated with 2% Brine  
 Oil Flooded with Hamilton Lake Crude  
 Waterflooded with 2% Brine  
 Initial Oil Saturation = 77.87%  
 Residual Oil Saturation = 31.52%

Sample#	Water Vol.,ml	Oil Vol.,ml	Pres.,kPa	krw	kro
1	0.00	20.00	350	0.000	0.815
2	0.00	20.00	353	0.000	0.810
3	0.00	20.00	355	0.000	0.817
4	0.00	20.00	358	0.000	0.808
5	0.00	20.00	360	0.024	0.704
6	2.50	7.50	354	0.068	0.304
7	7.00	3.00	348	0.078	0.087
8	9.00	1.00	346	0.078	0.065
9	9.25	0.75	345	0.085	0.045
10	9.50	0.50	343	0.082	0.043
11	9.50	0.50	342	0.083	0.043
12	19.00	1.00	341	0.083	0.017
13	19.50	0.50	340	0.081	0.017
14	49.00	1.00	340	0.082	0.017

Table C49: Two-Phase Flow Step #2**Legend:**

Berea Sandstone Core  
 Oil Flooded with Hamilton Lake Crude  
 Waterflooded with 30% Brine  
 Initial Oil Saturation = 71.84%  
 Residual Oil Saturation = 29.94%

Sample#	Water Vol.,ml	Oil Vol.,ml	Pres.,kPa	krw	kro
1	0.0	50.0	510	0.000	0.271
2	0.0	25.0	550	0.000	0.266
3	0.0	20.0	580	0.037	0.102
4	9.0	6.0	600	0.054	0.034
5	13.0	2.0	620	0.071	0.022
6	14.0	1.0	650	0.063	0.019
7	14.0	1.0	675	0.057	0.013
8	14.5	0.5	695	0.047	0.004

Table C50: Two-Phase Flow Step #3**Legend:**

Berea Sandstone Core  
 Saturated with 2% Brine  
 Oil Flooded with Hamilton Lake Crude  
 Waterflooded with 2% Brine  
 Initial Oil Saturation = 67.49%  
 Residual Oil Saturation = 24.41%

Sample#	Water Vol.,ml	Oil Vol.,ml	Pres.,kPa	krw	kro
1	0.0	50.0	480	0.000	0.655
2	0.0	25.0	465	0.000	0.674
3	0.0	24.0	450	0.042	0.215
4	6.5	3.5	448	0.058	0.147
5	8.0	2.0	445	0.063	0.044
6	14.0	1.0	443	0.063	0.021
7	30.0	1.0	441	0.064	0.013
8	49.0	1.0	440	0.064	0.013

Table C51: Two-Phase Flow Step #4**Legend:**

Berea Sandstone Core  
 Oil Flooded with Hamilton Lake Crude  
 Waterflooded with 30% Brine  
 Initial Oil Saturation = 63.93%  
 Residual Oil Saturation = 22.63%

Sample#	Water Vol.,ml	Oil Vol.,ml	Pres.,kPa	krw	kro
1	0.0	50.0	985	0.000	0.133
2	0.0	40.0	1075	0.005	0.114
3	2.5	7.5	1095	0.025	0.026
4	8.0	2.0	1115	0.027	0.020
5	8.5	1.5	1135	0.032	0.015
6	9.0	1.0	1165	0.034	0.008
7	19.0	1.0	1220	0.025	0.002



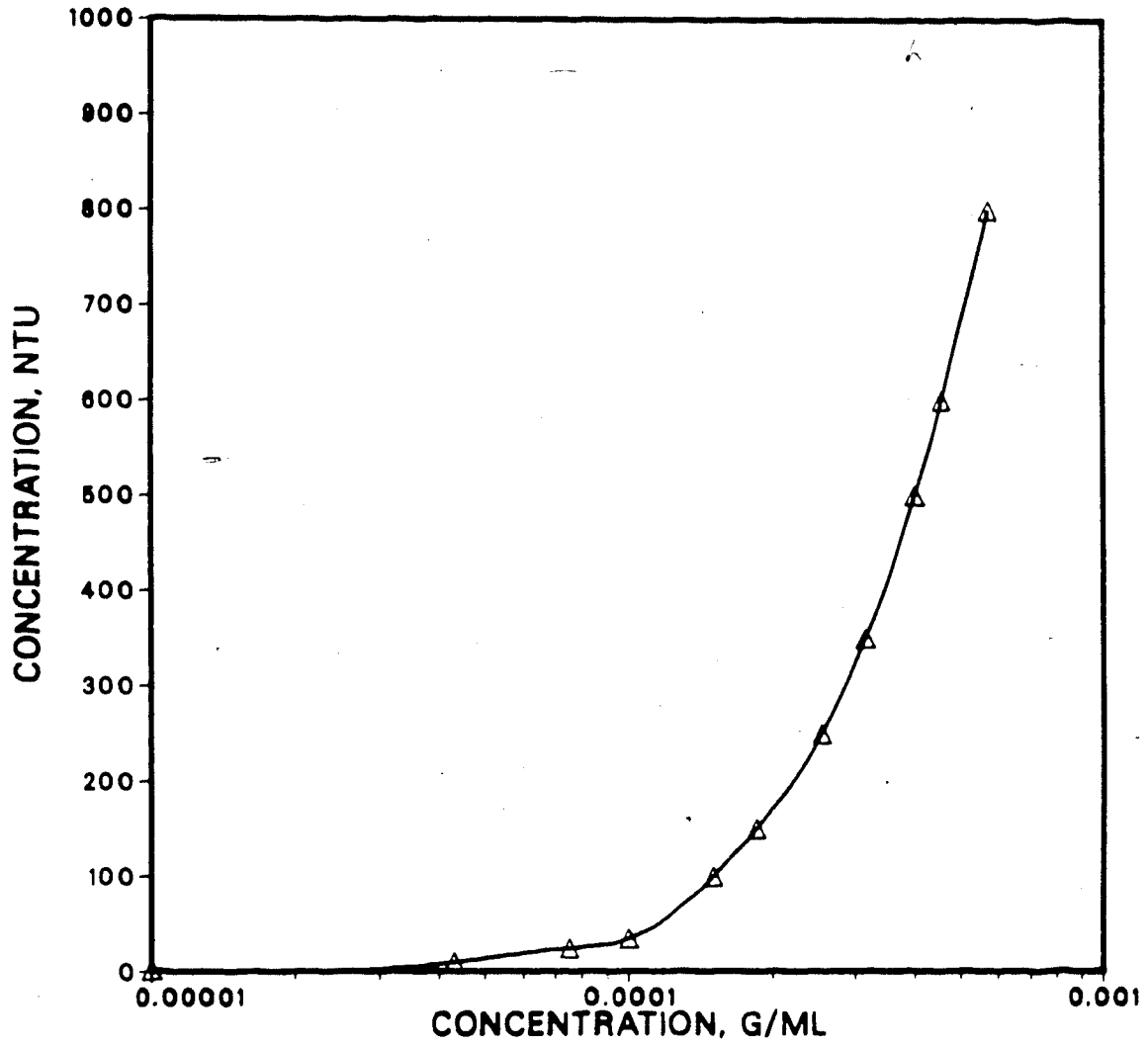


FIGURE C1: Conversion Chart of Calcium Carbonate Fines

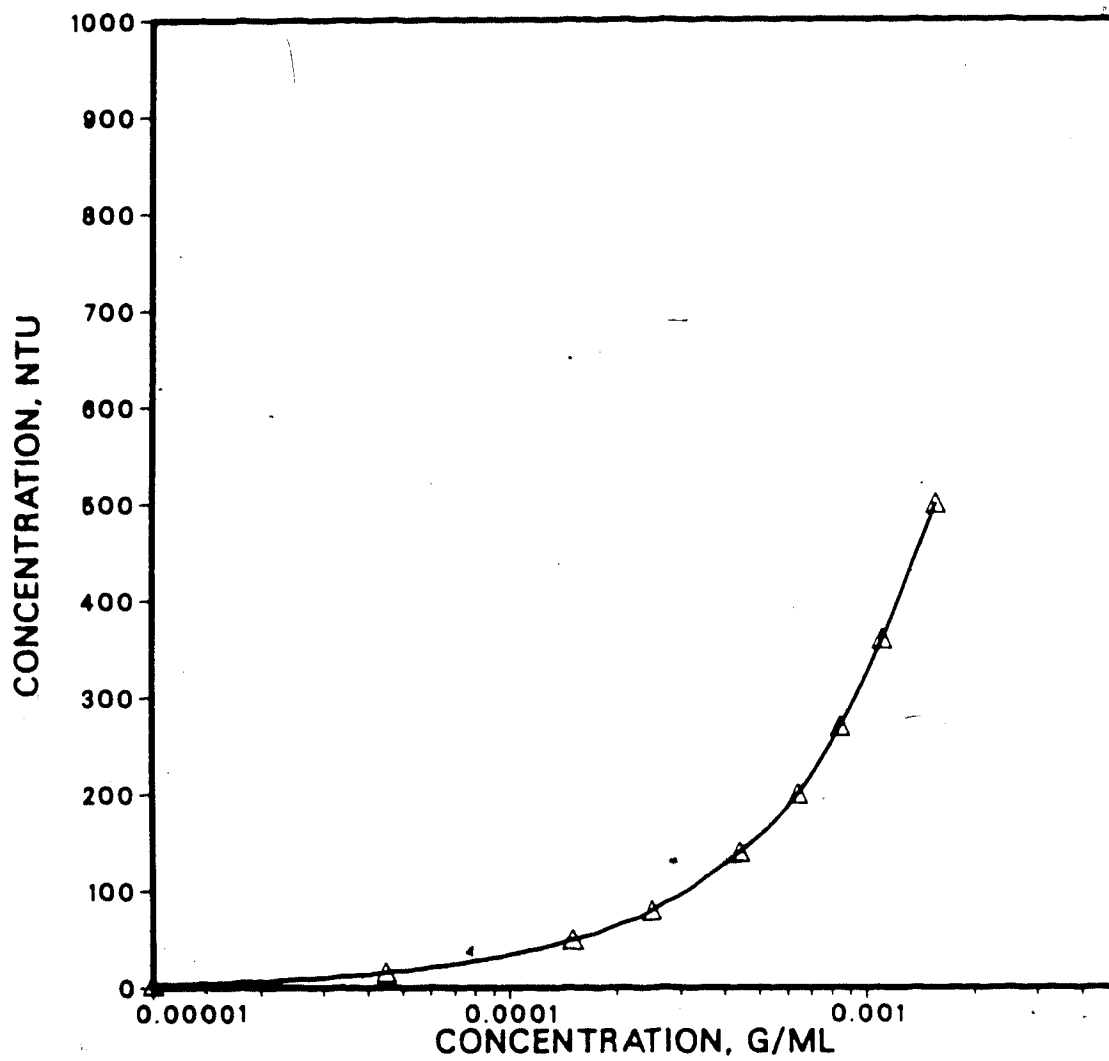


FIGURE C2 : Conversion Chart of Barite Fines

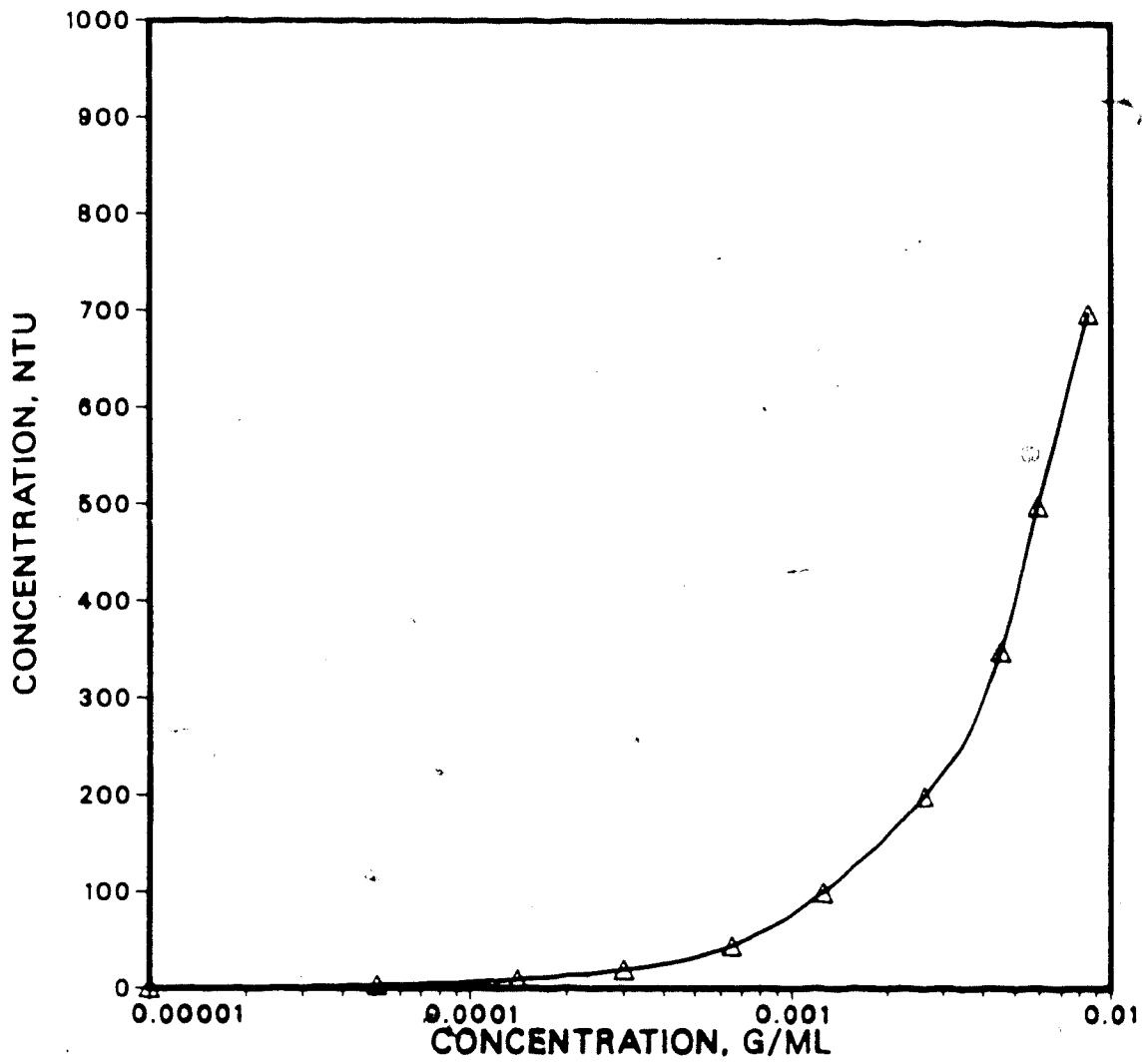


FIGURE C3 : Conversion Chart of Glass Bead Fines